

ผลของน้ำหนัโมเลกุลของซินติโอแทกติกพอลิสไตรีนต่อการเป็นเนื้อเดียวกันของพอลิเมอร์ผสม



นางสาวอำไพพรรณ ศิวะวิชชกิจ

สถาบันวิทยบริการ

จุฬาลงกรณ์มหาวิทยาลัย

วิทยานิพนธ์นี้เป็นส่วนหนึ่งของการศึกษาตามหลักสูตรปริญญาวิศวกรรมศาสตรมหาบัณฑิต

สาขาวิชาวิศวกรรมเคมี ภาควิชาวิศวกรรมเคมี


คณะวิศวกรรมศาสตร์ จุฬาลงกรณ์มหาวิทยาลัย

ปีการศึกษา 2547

ISBN 974-53-1383-1

ลิขสิทธิ์ของจุฬาลงกรณ์มหาวิทยาลัย

EFFECTS OF MOLECULAR WEIGHT OF SYNDIOTACTIC POLYSTYRENE
ON THE MISCIBILITY OF THE POLYMER BLENDS



Miss Ampaipun Sivavichchakij

สถาบันวิทยบริการ

จุฬาลงกรณ์มหาวิทยาลัย
A Thesis Submitted in Partial Fulfillment of the Requirements
for the Degree of Master of Engineering in Chemical Engineering

Department of Chemical Engineering

Faculty of Engineering

Chulalongkorn University

Academic Year 2004

ISBN 974-53-1383-1

Thesis Title EFFECTS OF MOLECULAR WEIGHT OF SYNDIOTACTIC
POLYSTYRENE ON THE MISCIBILITY OF THE
POLYMER BLENDS
By Miss Ampaipun Sivavichchakij
Field of Study Chemical Engineering
Thesis Advisor Assistant Professor ML. Supakanok Thongyai, Ph.D.

Accepted by the Faculty of Engineering, Chulalongkorn University in
Partial Fulfillment of the Requirements for the Master's Degree.

..... Dean of the Faculty of Engineering
(Professor Direk Lavansiri, Ph.D.)

THESIS COMMITTEE

..... Chairman
(Associate Professor Suttichai Assabumrungrat, Ph.D.)

..... Thesis Advisor
(Assistant Professor ML. Supakanok Thongyai, Ph.D.)

..... Member
(Assistant Professor Seeroong Prichanont, Ph.D.)

..... Member
(Joongjai Panpranot, Ph.D.)

อำไพพรรณ ศิวะวิชชกิจ : ผลของน้ำหนักโมเลกุลของซินดิโอแทกติกพอลิสไตรีนต่อการเป็นเนื้อเดียวกันของพอลิเมอร์ผสม (EFFECTS OF MOLECULAR WEIGHT OF SYNDIOTACTIC POLYSTYRENE ON THE MISCIBILITY OF THE POLYMER BLENDS). อาจารย์ที่ปรึกษา : ผศ. ดร. มล. ศุภกนก ทองใหญ่, 118 หน้า, ISBN 974-53-1383-1.

งานวิจัยนี้มุ่งเน้นที่จะศึกษาเกี่ยวกับลักษณะโครงสร้างผลึกของซินดิโอแทกติกพอลิสไตรีนและพอลิเมอร์ผสม เริ่มจากสังเคราะห์พอลิสไตรีนด้วยระบบตัวเร่งปฏิกิริยาเพนทาเมทิลไซโคลเพนทาไดอีนิลโทเทเนียมไตรคลอไรด์ร่วมกับเมทิลอะลูมิเนียมออกเซนที่ปรับปรุงแล้วเป็นตัวเร่งปฏิกิริยาร่วมที่อุณหภูมิการเกิดปฏิกิริยาต่างๆ กัน 3 ค่า เพื่อให้ได้พอลิเมอร์ที่มีน้ำหนักโมเลกุลต่างๆ กัน มีชื่อว่า sPS1, sPS2 และ sPS3 ตามลำดับเมื่อเรียงตามน้ำหนักโมเลกุล ทำการผสมซินดิโอแทกติกพอลิสไตรีนกับพอลิเมอร์อสังฐานต่างๆ ได้แก่ พอลิโนมอลบิวทิลเมทาคริเลต (PBMA) พอลิไซโคลเฮกซิลอะคริเลต (PCHA) พอลิเอทิลเมทาคริเลต (PEMA) พอลิแอลฟาเมทิลสไตรีน และพอลิไอโซพรีน พอลิเมอร์ผสมทุกตัวยกเว้นพอลิเมอร์ผสมของซินดิโอแทกติกพอลิสไตรีนกับ PVME แสดงอุณหภูมิกลาสทรานซิชัน 1 ค่า แสดงถึงการเป็นเนื้อเดียวกันของพอลิเมอร์ผสม ซึ่งจะมีค่าสูงขึ้นเมื่อมีปริมาณของซินดิโอแทกติกพอลิสไตรีนเพิ่มขึ้นและน้ำหนักโมเลกุลที่เพิ่มขึ้น ส่วนพอลิเมอร์ผสมของปริมาณของซินดิโอแทกติกพอลิสไตรีนกับ PVME ที่มีปริมาณของ PVME เกิน 20 เปอร์เซ็นต์โดยน้ำหนัก จะแสดงอุณหภูมิกลาสทรานซิชัน 2 ค่า แสดงถึงการแยกเฟสของพอลิเมอร์ผสม และเมื่อปริมาณของ PVME เกิน 20 เปอร์เซ็นต์โดยน้ำหนัก จะแสดงอุณหภูมิกลาสทรานซิชัน 1 ค่า อุณหภูมิหลอมเหลวของพอลิเมอร์ผสมมีค่าต่ำกว่าของซินดิโอแทกติกพอลิสไตรีน อุณหภูมิหลอมเหลวของพอลิเมอร์ผสมมีค่าสอดคล้องกับเปอร์เซ็นต์ความเป็นผลึกของพอลิเมอร์ผสมคือมีแนวโน้มในทิศทางเดียวกัน เมื่อผสมพอลิเมอร์อสังฐาน 10 เปอร์เซ็นต์โดยน้ำหนัก ลงไปในซินดิโอแทกติกพอลิสไตรีน จะทำให้กับเปอร์เซ็นต์ความเป็นผลึกของซินดิโอแทกติกพอลิสไตรีนลดลงซึ่งสอดคล้องกับอุณหภูมิกลาสทรานซิชันซึ่งลดลงอย่างเห็นได้ชัด ยกเว้นพอลิเมอร์ผสมของซินดิโอแทกติกพอลิสไตรีนกับพอลิแอลฟาเมทิลสไตรีน

ภาควิชา.....วิศวกรรมเคมี.....
สาขาวิชา.....วิศวกรรมเคมี.....
ปีการศึกษา.....2547.....

ลายมือชื่อนิสิต.....
ลายมือชื่ออาจารย์ที่ปรึกษา.....

4670607121 : MAJOR CHEMICAL ENGINEERING

KEY WORD : SYNDIOTACTIC POLYSTYRENE / POLYMER BLENDS /
MOLECULAR WEIGHT / MISCIBILITY.

AMPAIPUN SIVAVICHCHAKIJ : EFFECTS OF MOLECULAR WEIGHT
OF SYNDIOTACTIC POLYSTYRENE ON THE MISCIBILITY OF THE
POLYMER BLENDS. THESIS ADVISOR: ASST. PROF. ML. SUPAKANOK
THONGYAI, Ph.D., 118 pp. ISBN 974-53-1383-1.

This research is concerned with studying the crystallization and the morphologies of syndiotactic polystyrenes and their blends. Synthesize the syndiotactic polystyrene by using $Cp^*TiCl_3/MMAO$ catalyst system at three polymerization temperatures to obtain three different molecular weights of syndiotactic polystyrene. The three samples of sPS that ordered by the number average molecular weight (M_n) are named sPS1, sPS2 and sPS3, respectively. Blend syndiotactic polystyrene of different molecular weights with Poly(n-butyl methacrylate); (PBMA), Poly(cyclohexyl acrylate); (PCHA), Poly(ethyl methacrylate); (PEMA), Poly(α -methylstyrene), Polyisoprene and Poly(vinyl methyl ether); (PVME) by using solvent casting method. All of the blends except sPS/PVME blends at various compositions exhibit single glass transition temperature (T_g), indicating the miscibility of the blends, which shifts to a higher temperature with increasing the sPS content and the increase M_n . sPS/PVME blends with PVME contents higher than 20 wt% show two T_g , indicates that the sPS/PVME blends are phase separated. The crystalline melting temperature (T_m) of sPS blends are lower than pure sPS. The crystalline melting temperature in the first scan (T_{m1}) from the DSC results correspond to % crystallinity from the XRD results, which have the same trend in all blends. When the amorphous polymer were added, they affect to % crystallinity of all pure sPS decrease, that correspond to the T_g which T_g of sPS blends at the amorphous polymer content 10 wt% obviously decrease except sPS/Poly(α -methylstyrene) blends.

Department.....Chemical Engineering

Field of study.....Chemical Engineering

Academic Year.....2004.....

Student's signature.....

Advisor's signature

ACKNOWLEDGEMENTS

I would like to express my deeply gratitude to my advisor, Assistant Professor Dr. ML. Supakanok Thongyai, Ph.D. to his continuous guidance, enormous number of invaluable discussions, helpful suggestions, and warm encouragement. I am grateful to Associate Professor Suttichai Assabumrungrat, Ph.D., Assistant Professor Seeroong Prichanont, Ph.D. and Joongjai Panpranot, Ph.D. for serving as chairman and thesis committees, respectively, whose comments were constructively and especially helpful. I would like to thank Dr. Nigel Clarke for the kind discussions.

Sincere thanks are made to the Mektec Manufacturing Corporation (Thailand) Ltd. for using Differential Scanning Calorimetry (DSC), Thai Petrochemical Industry Public Co., Ltd. for Gel Permeation Chromatography (GPC) characterization and Polymer Engineering Research Laboratory (PEL), Chulalongkorn University for using digital hot plate stirrer.

Sincere thanks to all my friends and all members of the Center of Excellence on Catalysis and Catalytic Reaction Engineering Research Laboratory, Department of Chemical Engineering, Chulalongkorn University for their assistance and friendly encouragement.

Finally, I would like to dedicate this thesis to my parents and my families, who generously supported and encouraged me through the year spent on this study.

สถาบันวิทยบริการ
จุฬาลงกรณ์มหาวิทยาลัย

Contents

	Page
ABSTRACT (IN THAI).....	iv
ABSTRACT (IN ENGLISH).....	v
ACKNOWLEDGEMENTS.....	vi
CONTENTS.....	vii
LIST OF FIGURES.....	xi
LIST OF TABLES.....	xvii
CHAPTERS	
I INTRODUCTION.....	1
1.1 The Objective of This Thesis.....	3
1.2 The Scope of This Thesis.....	3
II LITERATURE REVIEWS.....	4
III THEORY.....	13
3.1 Metallocene Catalyst.....	13
3.2 Aluminoxane.....	14
3.3 Styrene Polymerization.....	14
3.4 Molecular-Weight Control in Polymerization : Need for Stoichiometric Control.....	15
3.5 Polymer Blends.....	16
3.5.1 Melt Mixing.....	16
3.5.2 Solvent Casting.....	16
3.5.3 Freeze Drying.....	17
3.5.4 Emulsions.....	17
3.5.5 Reactive Blend.....	18
3.6 Polymer Morphology.....	18
3.6.1 The Amorphous State.....	18
3.6.2 The Glass Transition.....	19
3.6.3 The Crystalline Polymer.....	20
3.6.4 Thermal Transitions.....	21

	viii
3.6.5 Structure of Polymer Crystals	23
3.6.5.1 The Fringed Micelle Model	23
3.6.5.2 The Folded-Chain Model	25
3.6.6 Crystallization From the Melt	27
3.6.6.1 Spherulitic Morphology	27
3.6.6.2 Mechanism of Spherulite Formation	29
3.6.6.3 Spherulites in Polymer Blends	29
3.6.6.4 Effect of Crystallinity on T_g	29
3.7 Crystal forms in thermally-processed sPS	29
3.7.1 α -Crystal	30
3.7.2 β -Crystal	32
3.8 Crystal forms in solvent-treated sPS	33
3.9 Crystal Morphology and thermal behavior of thermally- processed sPS	36
3.9.1 Crystal melting behavior	36
3.9.2 Effect of miscibility on polymorphism	36
3.9.3 Effects of tacticity and molecular weight	37
3.10 Crystal structure	37
 IV EXPERIMENT	 39
4.1 Chemicals	39
4.2 Equipments	40
4.2.1 Cooling System	40
4.2.2 Glove Box	41
4.2.3 Schlenk Line	41
4.2.4 Schlenk Tube	42
4.2.5 Glass Reactor	43
4.2.6 Vacuum Pump	43
4.2.7 Inert Gas Supply	44
4.2.8 Magnetic Stirrer and Hot Plate	44
4.2.9 Digital Hot Plate Stirrer	44
4.2.10 Syringe, Needle and Septum	45

4.3 Polymerization Procedure	45
4.3.1 Preparation of Catalyst.....	45
4.3.2 Preparation of Styrene Monomer.....	45
4.3.3 Styrene Polymerization.....	45
4.4 Blend Polymer between Syndiotactic Polystyrene and Selected Polymers.....	46
4.5 Polymer Characterization.....	47
4.5.1 Soxhlet Extractor.....	47
4.5.2 Differential Scanning Calorimetry (DSC).....	47
4.5.3 Gel Permeation Chromatography (GPC).....	47
4.5.4 X-ray Diffraction (XRD).....	48
V RESULTS AND DISCUSSION.....	49
5.1 Polymerization of Styrene.....	49
5.1.1 The Effect of Polymerization Temperature on Catalytic Activity.....	49
5.1.2 The Effect of Polymerization Temperature on Stereospecificity.....	50
5.1.3 The Effect of Polymerization Temperature on Molecular Weight.....	51
5.2 Differential Scanning Calorimetry (DSC).....	52
5.3 X-ray Diffraction (XRD).....	61
5.4 The Comparison of the DSC and XRD Results.....	73
5.4.1 Conformation of DSC and XRD on Crystalline Melting Temperature (T_m), Glass Transition Temperature (T_g) and % Crystallinity of Polymer Blends.....	73
5.4.2 Conformation of DSC and XRD on Glass Transition Temperature (T_g) and Weight Fraction of sPS in amorphous of Polymer Blends.....	73
5.4.3 Conformation of DSC and XRD on Glass Transition Temperature (T_g), % Crystallinity and Number Average Molecular Weight (M_n) of sPS in amorphous of Polymer Blends.....	76

5.5 The Comparison between the Acrylate Polymers.....	x 77
5.6 Crystal Structure.....	77
VI CONCLUSIONS AND RECOMMENDATIONS.....	78
6.1 Conclusions.....	78
6.2 Recommendations for Further Studies.....	79
REFERENCES.....	81
APPENDICES.....	83
APPENDIX A.....	84
APPENDIX B.....	117
VITA.....	118



สถาบันวิทยบริการ
จุฬาลงกรณ์มหาวิทยาลัย

List of Figures

	Page
Figure 3.1 Structures of two metallocenes.....	13
Figure 3.2 Three different configurations of a polypropylene.....	21
Figure 3.3 The fringed micelle model : (a) unoriented; (b) chains oriented by applied stress.....	24
Figure 3.4 Adjacent-reentry model of single crystal.....	25
Figure 3.5 Switchboard model of single crystal.....	26
Figure 3.6 Model of spherulitic structure.....	28
Figure 3.7 Hexagonal model proposed by Greis <i>et al.</i> , space group $P62c$ ($a = b = 26.25 \text{ \AA}$, $c = 5.04 \text{ \AA}$).....	30
Figure 3.8 Trigonal model proposed by De Rosa <i>et al.</i> , space group $P3c1$ ($a = b = 26.26 \text{ \AA}$, $c = 5.04 \text{ \AA}$).....	31
Figure 3.9 Model for α'' -modification.....	31
Figure 3.10 Model for α' -modification.....	32
Figure 3.11 Model for β'' -modification.....	32
Figure 3.12 Model for β' -modification.....	33
Figure 3.13 A proposed model for the crystal structure of the solvent-induced δ -form of sPS swelled by toluene molecules in the space $P2_1/a$	33
Figure 3.14 Solvent-induced clathrate δ -form of sPS swelled by dichloroethane (DCE) molecules in the space $P2_1/a$	34
Figure 3.15 A model for the crystal structure of the emptied δ -form (δ_e -form) of sPS in the space $P2_1/a$	35
Figure 3.16 WAXD spectra of sPS and sPS/poly(styrene-co- α -methyl styrene) blends: melt-crystallized with $10 \text{ }^\circ\text{C}/\text{min}$	38
Figure 4.1 Glove box.....	41
Figure 4.2 Schlenk line.....	42
Figure 4.3 Schlenk tube.....	42
Figure 4.4 Glass reactor.....	43
Figure 4.5 Vacuum pump.....	43
Figure 4.6 Inert gas supply system.....	44
Figure 5.1 X-ray diffractogram of syndiotactic polystyrenes.....	62
Figure 5.2 X-ray diffractogram of sPS1/PBMA blends at various compositions.....	63

Figure 5.3	X-ray diffractogram of sPS2/PBMA blends at various compositions	63
Figure 5.4	X-ray diffractogram of sPS3/PBMA blends at various compositions	64
Figure 5.5	X-ray diffractogram of sPS1/PCHA blends at various compositions	65
Figure 5.6	X-ray diffractogram of sPS2/PCHA blends at various compositions	65
Figure 5.7	X-ray diffractogram of sPS3/PCHA blends at various compositions	66
Figure 5.8	X-ray diffractogram of sPS1/PEMA blends at various compositions	67
Figure 5.9	X-ray diffractogram of sPS2/PEMA blends at various compositions	67
Figure 5.10	X-ray diffractogram of sPS3/PEMA blends at various compositions	68
Figure 5.11	X-ray diffractogram of sPS1/Poly(α -methylstyrene) blends at various compositions	69
Figure 5.12	X-ray diffractogram of sPS2/Poly(α -methylstyrene) blends at various compositions	69
Figure 5.13	X-ray diffractogram of sPS3/Poly(α -methylstyrene) blends at various compositions	70
Figure 5.14	X-ray diffractogram of sPS2/Polyisoprene blends at various compositions	71
Figure 5.15	X-ray diffractogram of sPS2/Polyisoprene blends at various compositions	71
Figure 5.16	X-ray diffractogram of sPS3/Polyisoprene blends at various compositions	72
Figure A.1	DSC curve of PBMA	84
Figure A.2	DSC curve of PCHA	84
Figure A.3	DSC curve of PEMA	84
Figure A.4	DSC curve of Poly(α -methylstyrene)	85
Figure A.5	DSC curve of Polyisoprene	85
Figure A.6	DSC curve of PVME	85
Figure A.7	DSC curve of sPS1	86
Figure A.8	DSC curve of sPS2	86
Figure A.9	DSC curve of sPS3	86
Figure A.10	DSC curve of sPS1/PBMA blends at composition 50/50 wt%	87
Figure A.11	DSC curve of sPS2/PBMA blends at composition 50/50 wt%	87
Figure A.12	DSC curve of sPS2/PBMA blends at composition 50/50 wt%	87
Figure A.13	DSC curve of sPS1/PBMA blends at composition 60/40 wt%	88

Figure A.14 DSC curve of sPS2/PBMA blends at composition 60/40 wt%	88
Figure A.15 DSC curve of sPS3/PBMA blends at composition 60/40 wt%	88
Figure A.16 DSC curve of sPS1/PBMA blends at composition 70/30 wt%	89
Figure A.17 DSC curve of sPS2/PBMA blends at composition 70/30 wt%	89
Figure A.18 DSC curve of sPS3/PBMA blends at composition 70/30 wt%	89
Figure A.19 DSC curve of sPS1/PBMA blends at composition 80/20 wt%	90
Figure A.20 DSC curve of sPS2/PBMA blends at composition 80/20 wt%	90
Figure A.21 DSC curve of sPS3/PBMA blends at composition 80/20 wt%	90
Figure A.22 DSC curve of sPS1/PBMA blends at composition 90/10 wt%	91
Figure A.23 DSC curve of sPS2/PBMA blends at composition 90/10 wt%	91
Figure A.24 DSC curve of sPS3/PBMA blends at composition 90/10 wt%	91
Figure A.25 DSC curve of sPS1/PCHA blends at composition 50/50 wt%	92
Figure A.26 DSC curve of sPS2/PCHA blends at composition 50/50 wt%	92
Figure A.27 DSC curve of sPS3/PCHA blends at composition 50/50 wt%	92
Figure A.28 DSC curve of sPS1/PCHA blends at composition 60/40 wt%	93
Figure A.29 DSC curve of sPS2/PCHA blends at composition 60/40 wt%	93
Figure A.30 DSC curve of sPS3/PCHA blends at composition 60/40 wt%	93
Figure A.31 DSC curve of sPS1/PCHA blends at composition 70/30 wt%	94
Figure A.32 DSC curve of sPS2/PCHA blends at composition 70/30 wt%	94
Figure A.33 DSC curve of sPS3/PCHA blends at composition 70/30 wt%	94
Figure A.34 DSC curve of sPS1/PCHA blends at composition 80/20 wt%	95
Figure A.35 DSC curve of sPS2/PCHA blends at composition 80/20 wt%	95
Figure A.36 DSC curve of sPS3/PCHA blends at composition 80/20 wt%	95
Figure A.37 DSC curve of sPS1/PCHA blends at composition 90/10 wt%	96
Figure A.38 DSC curve of sPS2/PCHA blends at composition 90/10 wt%	96
Figure A.39 DSC curve of sPS3/PCHA blends at composition 90/10 wt%	96
Figure A.40 DSC curve of sPS1/PEMA blends at composition 50/50 wt%	97
Figure A.41 DSC curve of sPS2/PEMA blends at composition 50/50 wt%	97
Figure A.42 DSC curve of sPS3/PEMA blends at composition 50/50 wt%	97
Figure A.43 DSC curve of sPS1/PEMA blends at composition 60/40 wt%	98
Figure A.44 DSC curve of sPS2/PEMA blends at composition 60/40 wt%	98
Figure A.45 DSC curve of sPS3/PEMA blends at composition 60/40 wt%	98
Figure A.46 DSC curve of sPS1/PEMA blends at composition 70/30 wt%	99

Figure A.47 DSC curve of sPS2/PEMA blends at composition 70/30 wt%	99
Figure A.48 DSC curve of sPS3/PEMA blends at composition 70/30 wt%	99
Figure A.49 DSC curve of sPS1/PEMA blends at composition 80/20 wt%	100
Figure A.50 DSC curve of sPS2/PEMA blends at composition 80/20 wt%	100
Figure A.51 DSC curve of sPS3/PEMA blends at composition 80/20 wt%	100
Figure A.52 DSC curve of sPS1/PEMA blends at composition 90/10 wt%	101
Figure A.53 DSC curve of sPS2/PEMA blends at composition 90/10 wt%	101
Figure A.54 DSC curve of sPS3/PEMA blends at composition 90/10 wt%	101
Figure A.55 DSC curve of sPS1/Poly(α -methylstyrene) blends at composition 50/50 wt%	102
Figure A.56 DSC curve of sPS2/Poly(α -methylstyrene) blends at composition 50/50 wt%	102
Figure A.57 DSC curve of sPS3/Poly(α -methylstyrene) blends at composition 50/50 wt%	102
Figure A.58 DSC curve of sPS1/Poly(α -methylstyrene) blends at composition 60/40 wt%	103
Figure A.59 DSC curve of sPS2/Poly(α -methylstyrene) blends at composition 60/40 wt%	103
Figure A.60 DSC curve of sPS3/Poly(α -methylstyrene) blends at composition 60/40 wt%	103
Figure A.61 DSC curve of sPS1/Poly(α -methylstyrene) blends at composition 70/30 wt%	104
Figure A.62 DSC curve of sPS2/Poly(α -methylstyrene) blends at composition 70/30 wt%	104
Figure A.63 DSC curve of sPS3/Poly(α -methylstyrene) blends at composition 70/30 wt%	104
Figure A.64 DSC curve of sPS1/Poly(α -methylstyrene) blends at composition 80/20 wt%	105
Figure A.65 DSC curve of sPS2/Poly(α -methylstyrene) blends at composition 80/20 wt%	105
Figure A.66 DSC curve of sPS3/Poly(α -methylstyrene) blends at composition 80/20 wt%	105

Figure A.67 DSC curve of sPS1/Poly(α -methylstyrene) blends at composition 90/10 wt%.....	106
Figure A.68 DSC curve of sPS2/Poly(α -methylstyrene) blends at composition 90/10 wt%.....	106
Figure A.69 DSC curve of sPS3/Poly(α -methylstyrene) blends at composition 90/10 wt%.....	106
Figure A.70 DSC curve of sPS1/Polyisoprene blends at composition 50/50 wt% ...	107
Figure A.71 DSC curve of sPS2/Polyisoprene blends at composition 50/50 wt% ...	107
Figure A.72 DSC curve of sPS3/Polyisoprene blends at composition 50/50 wt% ...	107
Figure A.73 DSC curve of sPS1/Polyisoprene blends at composition 60/40 wt% ...	108
Figure A.74 DSC curve of sPS2/Polyisoprene blends at composition 60/40 wt% ...	108
Figure A.75 DSC curve of sPS3/Polyisoprene blends at composition 60/40 wt% ...	108
Figure A.76 DSC curve of sPS1/Polyisoprene blends at composition 70/30 wt% ...	109
Figure A.77 DSC curve of sPS2/Polyisoprene blends at composition 70/30 wt% ...	109
Figure A.78 DSC curve of sPS3/Polyisoprene blends at composition 70/30 wt% ...	109
Figure A.79 DSC curve of sPS1/Polyisoprene blends at composition 80/20 wt% ...	110
Figure A.80 DSC curve of sPS2/Polyisoprene blends at composition 80/20 wt% ...	110
Figure A.81 DSC curve of sPS3/Polyisoprene blends at composition 80/20 wt% ...	110
Figure A.82 DSC curve of sPS1/Polyisoprene blends at composition 90/10 wt% ...	111
Figure A.83 DSC curve of sPS2/Polyisoprene blends at composition 90/10 wt% ...	111
Figure A.84 DSC curve of sPS3/Polyisoprene blends at composition 90/10 wt% ...	111
Figure A.85 DSC curve of sPS1/PVME blends at composition 50/50 wt%	112
Figure A.86 DSC curve of sPS2/PVME blends at composition 50/50 wt%	112
Figure A.87 DSC curve of sPS3/PVME blends at composition 50/50 wt%	112
Figure A.88 DSC curve of sPS1/PVME blends at composition 60/40 wt%	113
Figure A.89 DSC curve of sPS2/PVME blends at composition 60/40 wt%	113
Figure A.90 DSC curve of sPS3/PVME blends at composition 60/40 wt%	113
Figure A.91 DSC curve of sPS1/PVME blends at composition 70/30 wt%	114
Figure A.92 DSC curve of sPS2/PVME blends at composition 70/30 wt%	114
Figure A.93 DSC curve of sPS3/PVME blends at composition 70/30 wt%	114
Figure A.94 DSC curve of sPS1/PVME blends at composition 80/20 wt%	115
Figure A.95 DSC curve of sPS2/PVME blends at composition 80/20 wt%	115
Figure A.96 DSC curve of sPS3/PVME blends at composition 80/20 wt%	115

Figure A.97 DSC curve of sPS1/PVME blends at composition 90/10 wt%	116
Figure A.98 DSC curve of sPS2/PVME blends at composition 90/10 wt%	116
Figure A.99 DSC curve of sPS3/PVME blends at composition 90/10 wt%	116
Figure B.1 The chromatogram of sPS1	117
Figure B.2 The chromatogram of sPS2	117
Figure B.3 The chromatogram of sPS3	117



สถาบันวิทยบริการ
จุฬาลงกรณ์มหาวิทยาลัย

List of Tables

	Page
Table 5.1 Yield and catalytic activity of polystyrene produced at various polymerization temperatures.....	49
Table 5.2 % Syndiotactic index (% S.I.) of polystyrene products at various polymerization temperatures.....	50
Table 5.3 Molecular weights and molecular weight distributions of syndiotactic polystyrene at various polymerization temperatures.....	51
Table 5.4 Glass transition temperature (T_g), crystalline temperature (T_c) and crystalline melting temperature (T_m) of syndiotactic polystyrenes.....	52
Table 5.5 Glass transition temperature (T_g), crystalline temperature (T_c) and crystalline melting temperature (T_m) of sPS/PBMA blends at various compositions.....	53
Table 5.6 Glass transition temperature (T_g), crystalline temperature (T_c) and crystalline melting temperature (T_m) of sPS/PCHA blends at various compositions.....	55
Table 5.7 Glass transition temperature (T_g), crystalline temperature (T_c) and crystalline melting temperature (T_m) of sPS/PEMA blends at various compositions.....	56
Table 5.8 Glass transition temperature (T_g), crystalline temperature (T_c) and crystalline melting temperature (T_m) of sPS/Poly(α -methylstyrene) blends at various compositions.....	57
Table 5.9 Glass transition temperature (T_g), crystalline temperature (T_c) and crystalline melting temperature (T_m) of sPS/Polyisoprene blends at various compositions.....	58
Table 5.10 Glass transition temperature (T_g), crystalline temperature (T_c) and crystalline melting temperature (T_m) of sPS/PVME blends at various compositions.....	59
Table 5.11 % Crystallinity of syndiotactic polystyrenes.....	62
Table 5.12 % Crystallinity of sPS/PBMA blends at various compositions.....	64
Table 5.13 % Crystallinity of sPS/PCHA blends at various compositions.....	66
Table 5.14 % Crystallinity of sPS/PEMA blends at various compositions.....	68

Table 5.15 % Crystallinity of sPS/Poly(α -methylstyrene) blends at various compositions.....	70
Table 5.16 % Crystallinity of sPS/Polyisoprene blends at various compositions.....	72
Table 5.17 % Weight fraction of sPS in amorphous from XRD and Flory-Fox equation of sPS/PBMA blends at various compositions.....	74
Table 5.18 % Weight fraction of sPS in amorphous from XRD and Flory-Fox equation of sPS/PCHA blends at various compositions.....	74
Table 5.19 % Weight fraction of sPS in amorphous from XRD and Flory-Fox equation of sPS/PEMA blends at various compositions.....	75
Table 5.20 % Weight fraction of sPS in amorphous from XRD and Flory-Fox equation of sPS/Poly(α -methylstyrene) blends at various compositions.....	75
Table 5.21 % Weight fraction of sPS in amorphous from XRD and Flory-Fox equation of sPS/Polyisoprene blends at various compositions.....	76

CHAPTER I

INTRODUCTION

Polymers are the groups of macromolecules that built up by the linkages of large numbers of much smaller molecules called monomers. The reactions by which they combined are termed polymerizations.

Polymers are one of the most popular materials encountered in our daily life. For example, polymers are the major component of plastics, films, fibers, foods, biomaterials or others. Polymers are used extensively in the chemical, electronics, optical, pharmaceutical and medical industries as important components of highly functional materials.

Polystyrenes are among the most important polymers in terms of production. The outstanding growth rate of the four major commodity polymers, polyethylene (PE), polypropylene (PP), polyvinylchloride (PVC) and polystyrene (PS) is based strictly on economics. Polymerizations of commodity polymer are usually general, and in addition to the four major products, a wide variety of other forms of commodity polymers are commercially available. In all commodity polymers, the repeating unit in the macromolecules is identical with their monomer.

Polystyrene (PS) was commercialized and utilized as a commodity plastic similar to polyolefins. Some special properties are rare in other commodity plastics such as clarity but its amorphous nature limits the utilizations in some areas. Polystyrene can have special arrangement of the benzene rings which can be classified as atactic, isotactic and syndiotactic. Atactic polystyrene (aPS) is an amorphous (non-crystalline) polymer with a glass transition temperature (T_g) of about 100 °C. Its application at high temperature is limited and it has low organic solvent resistance. Syndiotactic polystyrene (sPS) is a semi-crystalline polymer with a T_g similar to aPS but it also has a melting temperature (T_m) of 270 °C. sPS has exceptional heat and solvent resistance. Isotactic polystyrene (iPS) is also classified as crystalline PS with a T_m of 240 °C, but it has not been commercialized because of it

has slow crystallization rate compared to sPS (roughly 100 times slower). [Takebe T. *et al.*, 1992]

The sPS was first synthesized by Ishihara *et al.* in 1985 by using a homogeneous metallocene catalyst of titanium compounds activated with methylaluminoxane (MAO) [Ishihara N. *et al.*, 1986]. Because of the crystalline ability, the sPS displays entirely different properties to conventional atactic polystyrene such as high chemical resistance and excellent environmental stress cracking resistance. The sPS does share one major property with conventional polystyrene, however, namely inherent brittleness. For this reason, blending of sPS with other polymers is another strategy for improving its performances at room conditions.

Blending Polymers are the commonly applied techniques to improve the ultimate properties. There are many methods to blend each polymer together such as by using heat (melt mixing), solvent (solution casting, freeze-drying) or others. The miscibility of the blends share parts in the special interactions between molecules and the molecular weights. The blends can be synergistic or having better properties than either polymer pairs. In this research, the selected polymers that have been reported to be miscible with aPS were chosen as a conjugation pair of sPS. The differences in M_w of sPS can also play the major role in the properties of their blends.

สถาบันวิทยบริการ
จุฬาลงกรณ์มหาวิทยาลัย

1.1 The Objective of This Thesis

Study the effects of molecular weight of syndiotactic polystyrene on the miscibility of the polymer blends with various polymers in order to verify the degree of miscibility among the blends.

1.2 The Scope of This Thesis

1. Synthesize the syndiotactic polystyrene by using $Cp^*TiCl_3/MMAO$ catalyst system at three polymerization temperatures to obtain three different molecular weights of syndiotactic polystyrene.

2. Blend syndiotactic polystyrene of different molecular weights in conjugate with each various polymers as follows,

Poly(n-butyl methacrylate), (PBMA)

Poly(cyclohexyl acrylate), (PCHA)

Poly(ethyl methacrylate), (PEMA)

Poly(α -methylstyrene)

Polyisoprene, cis

Poly(vinyl methyl ether), (PVME)

by using solvent casting method.

3. Characterize syndiotactic polystyrenes and their blends by using differential scanning calorimetry (DSC), X-ray diffraction (XRD) and gel permeation chromatography (GPC) techniques.

สถาบันวิทยบริการ
จุฬาลงกรณ์มหาวิทยาลัย

CHAPTER II

LITERATURE REVIEWS

Ishihara N. *et al.* [1986] succeeded in obtaining a new polystyrene which has a syndiotactic structure and a high degree of crystallinity. They described the determination of the stereoregularity and some other properties of the newly obtained polystyrene. They polymerized the styrene with their novel catalyst system, containing a titanium compound and an organoaluminum compound, for 2 h at 50 °C, and 20.3 g of polymer was obtained. The crude product was extracted with methyl ethyl ketone (MEK) under reflux for 4 h. A total of 98 wt % of the polymer was insoluble in MEK and its weight-average molecular weight was 82000.

Ishihara N., Kuramoto M. and Voi M. [1988] found that a mixture of titanium compounds [TiCl₄, Ti(OEt)₄ or (η-C₅H₅)TiCl₃] with methylaluminoxane catalyzed the polymerization of styrene, even above room temperature, to the pure syndiotactic polystyrene, which had a narrow molecular weight distribution ($M_w/M_n = 2$). Pure syndiotactic polymers were also obtained with ring-substituted styrenes. Monomer reactivity was enhanced by electron-releasing substituents on the aromatic ring.

Kucht A. *et al.* [1993] synthesized and characterized (η⁵-Tetramethylcyclopentadienyl)-, (η⁵-tetraphenylcyclopentadienyl)-, (η⁵-(diphenylphosphino) tetramethylcyclopentadienyl)- and (η⁵-(trimethylsilyl) tetramethylcyclopentadienyl) titanium triisopropoxide. Their catalytic activities for syndiotactic styrene polymerization have been compared with the reference compound (η⁵-cyclopentadienyl) titanium triisopropoxide. (η⁵-tetramethylcyclopentadienyl) titanium triisopropoxide was the best catalyst precursor, giving rise to catalysts having the highest activity to produce polystyrene with the highest syndiotactic yield and molecular weight.

Ready T. E., Chein J. C. W., and Rausch M. D. [1996] discovered that a variety of 1- and 3-substituted alkylindines (R = H, Me, Et, tert-butyl, Me₃Si) as well as 2-methylindine have been prepared in good yields. The substituted indenenes were

converted into trimethylsilyl derivatives via reactions of intermediate organolithium complexes with chlorotrimethylsilane. The corresponding titanium complexes, (R-Ind)TiCl₃, were synthesized in excellent yield from reactions of the trimethylsilyl derivatives with TiCl₄. The titanium complexes were evaluated as styrene polymerization catalysts in toluene solution when activated by methylaluminoxane. Activities increased in the order: Cp < H₄Ind < Ind < 1-(Me)Ind < 2-(Me)Ind. A steep drop in activity was observed when R = Et, tert-butyl and Me₃Si, corresponding to an increase in the steric bulk of substituent in the catalyst precursor. 1-(Me₃S)IndTiCl₃ was found to be ineffective as a styrene polymerization catalyst. Syndiospecificities of the titanium complexes were generally very good (65-98 %).

Kaminsky W. *et al.* [1997] investigated fluorinated half-sandwich complexes catalysts in syndiospecific styrene polymerization. It was found that fluorinated half-sandwich complexes of titanium, such as CpTiF₃, showed an increase in activity of up to a factor of 50 compared to chlorinated compounds. In a temperature range of 10-70 °C the methylaluminoxane could be reduced to an Al:Ti ratio of 300. If the cyclopentadienyl ligand in the metallocene is changed to a pentamethylcyclopentadienyl ligand (Cp*) that is a stronger electron donor and exerts a greater steric hindrance, the polymerization activity is lowered. But the pentamethylcyclopentadienyltitanium fluoride (Cp*TiF₃) could be produced the polystyrene with highest melting point of 277 °C.

Qing Wu, Zhong Ye and Shangan Lin [1997] investigated syndiotactic polymerization of styrene with cyclopentadienyltribenzyloxytitanium/methylaluminoxane catalyst. The reaction conditions e.g., [Ti], [MAO], [St], temperature and the content of retained trimethylaluminium (TMA) in MAO effected on the catalytic activity, syndiotacticity and molecular weight of the polymer. With [MAO] = 0.17 mol/l, the catalyst exhibits higher activities. The catalytic activity increased with increase of [MAO], and reaches a maximum value at [MAO] of 0.5 mol/l. The molecular weight of the polymer decreased and the molecular weight distribution became narrow with increasing the [MAO]. The [MAO] was necessary for activating the titanocene molecules and scavenging of impurities. Additionally, the MAO acted as a chain transfer agent, so that the higher the [MAO] used, the lower is

the molecular weight of the polystyrene produced. The catalytic activity was directly proportional to the monomer concentration.

Kim Y., Koo B. H. and Do Y. [1997] synthesized five substituted indenyltrichlorotitanium compounds with spectroscopic methods. Their catalytic behavior for the polymerization of styrene was studied in the presence of methylaluminoxane as a cocatalyst. Substituted indenyl ligands include 1,3-dimethyl, 1-methyl, 1-ethyl, 1-isopropyl and 1-(trimethylsilyl) indenyl groups. All five compounds gave extremely pure syndiotactic polystyrene and conversion rates of at least 95 %. The UV-visible and $^{47,49}\text{Ti}$ NMR Spectra provided a consistent measure of the electron densities at the metal centers of five substituted indenyltrichlorotitanium compounds. The catalytic activity was enhanced by less bulky and better electron-releasing substituents of the indenyl ligand.

Schneider N., Propenc M. H. and Brintzinger H. H. [1997] synthesized cyclopentaphenanthrenetitanium trichloride and its 2-methyl and phenyl derivatives. The crystal structure of 2-methyl-substituted complex was determined by X-ray diffraction analysis. In the presence of methylaluminoxane, these complexes give highly active catalysts for the syndiotactic polymerization of styrene. The 2-phenyl-substituted complex exceeded all previously described catalysts in its catalytic activity.

Fan R. *et al.* [2001] synthesized the powdery syndiotactic polystyrene in a bulk process with the homogeneous metallocene catalyst system, mono(η^5 -pentamethylcyclopentadienyl) trichloride titanium/ methylaluminoxane/ triisobutylaluminum. The morphology of the nascent polymer particles were investigated and an interesting splaying morphology was observed when the conversion ranged from 0.9% to 1.7%. The crystallinities of the as-polymerized polymer samples at different conversion were studied also. The experimental results suggested that manipulating the relative crystallizing rate to exceed the relative polymerizing rate in the initial stage of the polymerization is feasible to prepare the powdery product.

Kim Y. and Do Y. [2002] prepared a new type of the half-metallocene catalysts for the syndiospecific polymerization of styrene by the reaction of various kinds of trialkanolamine with Cp^*TiCl_3 in the presence of triethylamine. All seven compounds have a highly thermal stability and they show fairly good activities in the presence of cocatalyst MMAO in styrene polymerization. Especially, highly bulky and electronically deficient modified catalyst system affords syndiotactic polystyrene with very high molecular weight.

Nomura K. and Fudo A. [2003] studied $(^i\text{BuC}_5\text{H}_4)\text{TiCl}_2(\text{O}-2,6-^i\text{Pr}_2\text{C}_6\text{H}_3)$ exhibited relatively high catalytic activity for syndiospecific polymerization of styrene at 25 °C if both $[\text{PhMe}_2\text{NH}]\text{B}(\text{C}_6\text{F}_5)_4$ and a mixture of $\text{Al}^i\text{Bu}_3/\text{Al}(\text{n-C}_8\text{H}_{17})_3$ were used as the cocatalyst. Effects of both organoaluminum and organoboron compounds were explored, and the effect of cocatalyst was different from that observed in 1-hexene polymerization catalyzed by $\text{Cp}^*\text{TiCl}_2(\text{O}-2,6-^i\text{Pr}_2\text{C}_6\text{H}_3)$. Resultant syndiotactic polystyrene possessed narrow molecular weight distribution under the optimized conditions, and the M_w values were unchanged during the time course.

Lyu Y. *et al.* [2004] prepared a series of new half-metallocene complexes of titanium containing siloxy ligands and a new bimetallic titanocene complex with a crystallographically determined structure. When activated with methylaluminoxane (MAO), they showed high activities toward polymerization of styrene with high syndiotacticity. Origin of the high activity and syndiotacticity found in this work was investigated systematically by comparison with polymerization results using other known complexes.

Wang C. *et al.* [2004] investigated the lamellar morphologies of melt-crystallized blends of syndiotactic polystyrene (sPS, weight-average molecular weight $M_w = 200 \text{ k}$) and atactic polystyrene (aPS, $M_w = 100\text{k}$) using small-angle X-ray scattering (SAXS) and transmission electron microscopy (TEM). sPS/aPS blends with various compositions were prepared and crystallized isothermally at 250 °C prior to morphological studies. Due to the proximity in the densities of the crystal and amorphous phases, a weak SAXS reflection associated with lamellar microstructure at

room temperature. In addition, strong diffuse scattering at low scattering vectors was evidently observed and its appearance may obscure the intensity maximum associated with the lamellar features, leading to the difficulties in determining the microstructure of the blends. To enhance the density contrast, SAXS intensities at an elevated temperature of 150 °C were measured as well to deduce the morphological results with better precision. Based on the Debye–Bueche theory, the intensities of the diffuse scattering were estimated and subtracted from the observed intensities to obtain the scattering contribution exclusively from the lamellar microstructure. Morphological parameters of the sPS/aPS blends were derived from the one-dimensional correlation function. On addition of aPS, no significant changes in the lamellar thickness have been found and the derived lamellar thicknesses are in good agreement with TEM measurements. Segregation of rejected aPS components during sPS crystallization was evidently observed from TEM images which showed aPS pockets located between sPS lamellar stacks and distributed uniformly in the bulk samples, leading to the interfibrillar segregation.

Guerra G. *et al.* [1990] found that both the crystalline forms containing zigzag planar conformations (pure or mixed) can be obtained by melt crystallization of syndiotactic polystyrene. Some of the factors that influence the polymorphic behavior in samples crystallized on cooling from the melt are described: the cooling rate from the melt, the crystalline form of the starting material, the maximum temperature of the melt, the time of residence in the melt at that temperature, and, in some cases, also the heating rate to reach melting. A possible interpretation of the observed polymorphic behavior in melt crystallizations for moderate cooling rates is that when a memory of α -form crystals remains in the melt, the acquisition of the α form is favored, otherwise the β form is obtained. The formation of the α form, also by quenching from the melt or by annealing from the amorphous phase, could be a kinetically controlled process.

Guerra G. *et al.* [1991] studied the polymorphic behavior of syndiotactic polystyrene (sPS) blending with poly(2,6-dimethyl-1,4-phenylene oxide) (PPO) when the former is crystallized from the quenched amorphous phase. In particular, while for pure sPS samples disordered modifications of the α form (closer to the limiting disordered α' modification) are obtained, more perfect modifications of the α form

(closer to the limiting ordered α'' modification) and the thermodynamically more stable β form are obtained, for low and high PPO content of the blend respectively. On the basis of the present results, it is suggested that these substantial changes in the polymorphic behavior of sPS can be related to the large increases of the crystallization temperatures which are observed in the presence of PPO.

Chatani Y. *et al.* [1992] studied structural of syndiotactic polystyrene. sPS exhibits polymorphism : there are principally four distinct crystalline phases. Melt-crystallization yields a planar zigzag form. As-cast samples from solutions with a variety of solvents are molecular compounds with the solvents used, in which the polymer chains assume a twofold helical conformation of type $(TTGG)_2$. On annealing the molecular compounds at moderate temperatures below ~ 130 °C, they are transformed in common, by removal of the solvent molecules, to a $(TTGG)_2$ twofold helical form free from solvents. On annealing at higher temperatures, the helical form is transformed to a planar zigzag form, which is distinguished from the melt-crystallized planar zigzag form in terms of the mode of molecular arrangement.

Cimmino S. *et al.* [1993] investigated the dependence of miscibility on blend composition and temperature for polystyrene/poly(vinyl methyl ether) (sPS/PVME) blends by solid state n.m.r. spectroscopy and differential scanning calorimetry (d.s.c.) and compared with that of the blend containing atactic polystyrene (aPS). The temperature dependence of ^{13}C cross polarization/magic angle spinning intensities for the resonance of sPS/PVME blends indicates that these blends are phase separated, whereas for the aPS/PVME blends, there is evidence of extensive mixing. These results are supported by the presence of one and two glass transition temperatures for the aPS/PVME and sPS/PVME blends, respectively, on d.s.c. thermograms.

Cimmino S. *et al.* [1993] studied the crystallization from the melt, the morphology and the miscibility of syndiotactic polystyrene/poly(vinyl methyl ether) (sPS/PVME) blends and syndiotactic polystyrene/poly(2,6-dimethyl-1,4-phenylene oxide) (sPS/PPO) blends by differential scanning calorimetry (d.s.c.) and optical microscopy. It was found that the kinetic parameters are strongly altered by blending and by crystallization conditions. In particular, the spherulite growth rate of sPS

decreases if PPO is added, whereas it increases in the case of sPS/PVME blends. The half-time of crystallization is drastically increased by the presence of both PPO and PVME. The PVME segregated into spherical domains in the sPS intraspherulitic region, whereas there is no microscopic evidence that the PPO forms segregated domains. These results were correlated to the viscosity of the melt and the degree of miscibility of the blends. It was concluded that the sPS/PPO system is completely miscible in the amorphous phase, whereas PVME forms with sPS a two-phase separated system. This conclusion results in agreement with the present of one T_g , composition-dependent, for the sPS/PPO blends, and of two T_g for the sPS/PVME blends.

Hong B. K. *et al.* [1998] studied the melting behaviour and the polymorphism of syndiotactic polystyrene (sPS) and its blend with poly(2,6-dimethyl-1,4-phenylene oxide) (PPO). Both pure sPS and sPS/PPO blends showed three melting endotherms under their crystallization conditions. When the differential scanning calorimetry (d.s.c.) results are compared with the X-ray patterns, it is suggested that the lowest and middle melting endotherms are due to the melting of β - and α -forms of sPS, respectively, whereas the highest melting endotherm comes from the melting of recrystallized sPS crystals formed during the d.s.c. scan. It is also noted that pure sPS recrystallizes more easily than sPS/PPO blends, indicating that the PPO disturbs the recrystallization of sPS.

Bhoje Gowd E. *et al.* [2002] found that the structural changes occurring during heating in a syndiotactic polystyrene (sPS)-solvent complex were monitored in situ by X-ray diffraction. The room temperature δ form transformed into the γ form on heating above the glass transition temperature of the sPS. The transition temperature showed a linear dependency on the amount of solvent absorbed; the higher the solvent molecules absorbed, the higher the transition temperature. However, the transition temperature does not depend on the nature of the solvent. The emptied clathrate form transformed into the γ form at the glass transition temperature. The γ form transformed into the α'' form at ~ 200 °C on heating and is independent of the δ to γ form transition. Calorimetric studies showed an endotherm followed by an exotherm

during these transitions and indicated that the transitions are first order in nature. The studies provided information on the stability of various crystalline forms of sPS.

Fang-Chyou Chiu and Chi-Gong Peng [2002] examined how the molecular weight of atactic polystyrene (aPS) affects the thermal properties and crystal structure of syndiotactic polystyrene (sPS)/aPS blends using differential scanning calorimetry, polarized light microscopy and wide angle X-ray diffraction (WAXD) technique. For comparative purposes, the structure and properties of the parent sPS was also investigated. The experimental results indicated that these blends showed single glass transition temperatures (T_g s), implying the miscibility of these blends in the amorphous state regardless of the aPS molecular weight. The non-isothermal and isothermal melt crystallization of sPS were hindered with the incorporation of aPSs. Moreover, aPS with a lower molecular weight caused a further decrease in the crystallization rate of sPS. Complex melting behavior was observed for parent sPS and its blends as well. The melting temperatures of these blends were lower than those of the parent sPS, and they decreased as the molecular weight of aPS decreased. Compared with the results of the WAXD study, the observed complex melting behavior resulted from the mixed polymorphs (i.e. the α and β forms) along with the melting–recrystallization–remelting of the β form crystals during the heating scans. The degree of melting–recrystallization–remelting phenomenon for each specimen was dependent primarily on how fast the sPS crystals were formed instead of the incorporation of aPSs. Furthermore, the existence of aPS in the blends, especially the lower molecular weight aPS, apparently reduced the possibility of forming the less stable α form in the sPS crystals.

Fang-Chyou Chiu and Ming-Te Li [2003] studied the miscibility, crystallization kinetics, melting behavior and crystal structure of syndiotactic polystyrene (sPS)/poly(styrene-co- α -methyl styrene) blends. Differential scanning calorimetry, polarized light microscopy and wide angle X-ray diffraction technique were used to approach the goals. The single composition-dependent T_g s of the blends and the melting temperature (T_m) depression of sPS in the blends indicated the miscible characteristic of the blend system at all compositions. Furthermore, the T_g s of the blends could be predicted by either of the Gordon–Taylor equation (with $K =$

0.99) or the Fox equation with a slightly higher deviation. The dynamic and isothermal crystallization abilities of sPS were hindered with the incorporation of the miscible copolymer. Complex melting behavior was observed for melt-crystallized pure sPS and its blends as well. Nevertheless, the blends showed relatively simpler melting curves. Comparing with melt-crystallized samples, the cold-crystallized samples exhibited simpler melting behavior. The equilibrium melting temperature (T_m^0) of β form sPS crystal determined from the conventional extrapolative method is 295.2 °C. The Flory–Huggins interaction parameter; χ , of the blends was estimated to be -0.27. The crystal morphology of sPS was disturbed in the blends. Only underdeveloped granular-like crystalline superstructure of sPS exhibited in cold-crystallized blends. Moreover, the existence of the copolymer in the blends apparently reduced the possibility of forming the less stable α form sPS crystals.



CHAPTER III

THEORY

3.1 Metallocene Catalyst

The main component of homogeneous catalyst systems, the catalyst precursor, is the Group 4B transition metallocenes (titanocenes, zirconocenes and hafnocenes), which are characterized by two bulky cyclopentadienyl (Cp) or substituted cyclopentadienyl ligands (Cp'). Two simple examples of these metallocenes are shown in Figure 3.1.

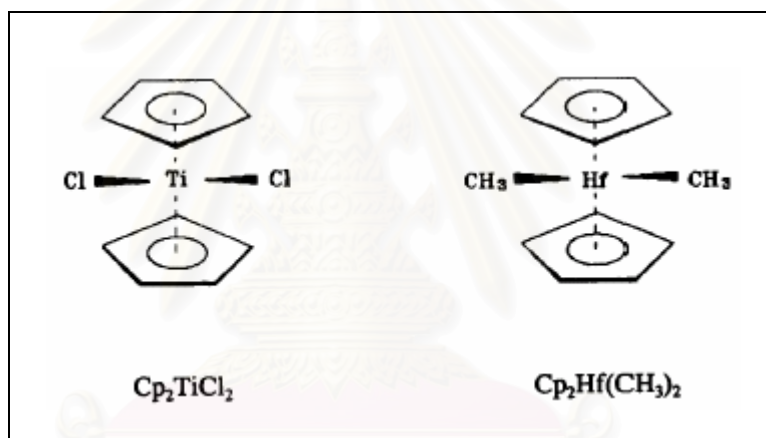


Figure 3.1 Structures of two metallocenes

The discovery of group 4 metallocene/aluminoxane systems as catalysts for polymerization reactions has opened up a new frontier in the area of organometallic chemistry and polymer synthesis. Metallocene systems are comprised of (1) bicomponents consisting of a metallocene and an aluminoxane and (2) a single component such as $[\text{Cp}_2\text{MR}]^+[\text{B}(\text{C}_6\text{F}_5)_4]^-$. The polymerization of monoolefins by metallocene in comparison to conventional Ziegler-Natta systems offers a versatile possibility to polymer synthesis. The broader flexibility of electronic and steric variations in the cyclopentadienyl (Cp) type ligands allow greater maneuvering in the

design of catalyst systems. Such modifications govern the polyinsertion reaction leading to regioregular and stereoregular polyolefins.

3.2 Aluminoxane

Methylaluminoxane (MAO) is produced by the reaction between trimethylaluminum (TMA) and water. The reaction is controlled by the reaction temperature. Small amount of TMA always exist in MAO.

MAO is the most important cocatalyst which activates the group 4B metallocenes in homogeneous Ziegler-Natta polymerization. Before the discovery of the MAO cocatalyst, the homogeneous Ziegler-Natta catalyst Cp_2TiCl_2 was activated with alkylaluminum chloride which led to poor catalyst activity. The use of MAO cocatalyst raised the catalyst activity by several orders of magnitude. There are some other alumoxanes which can also activate the metallocenes, such as ethylalumoxane (EAO) and isobutylalumoxane (*i*BAO), but MAO is much more effective than its ethyl and isobutyl analogous and is most preferred in practice.[Giannetti E. *et al.*, 1985]

3.3 Styrene Polymerization [Kricheldorf H. R., 1992]

Styrene is slightly polar compared to ethylene and α -olefins. The lack of a strongly polar functional group allow styrene to undergo highly isospecific polymerization (> 95-98 %) with many of heterogeneous Ziegler-Natta initiators effective for α -olefins [by Soga *et al.* in 1988, Pasquon *et al.* in 1989 and Longo *et al.* in 1990]. Highly syndiotactic polystyrene (sPS) is obtained using soluble Ziegler-Natta initiators, such as tetrabenzyltitanium, tetrabenzylzirconium and tetraethoxytitanium or cyclopentadienyltitanium trichloride (CpTiCl_3) with methylaluminoxane [by Pellecchia *et al.* in 1987, Ishihara *et al.* in 1988 and Zambelli *et al.* in 1989]. Further, there are recent reports of highly syndiospecific polymerization of styrene with heterogeneous initiators based on tetra-*n*-butoxytitanium and methylaluminoxane supported on silica or magnesium hydroxide

(by Soga and Monoi in 1990 and Soga and Nakatani in 1990). Styrene can also be homogeneous polymerized. The C-C double bond of styrene can act either as electron-donating or as electron-withdrawing center. Therefore, not only radicals can polymerize styrene but also by anionically, or cationically Ziegler-Natta initiators.

3.4 Molecular-Weight Control in Polymerization : Need for Stoichiometric Control [Odián G., 1991]

There are two important aspects with regard to the control of molecular weight in polymerizations. In the synthesis of polymers, one is usually interested in obtaining a product of very specific molecular weight, since the properties of the polymer will usually be highly depended on molecular weight. Molecular weights higher or lower than the desired molecular weights are equally undesirable. Since the degree of polymerization is a function of reaction time, the desired molecular weight can be obtained by quenching the reaction (e.g., by cooling) at the appropriate time. However, the polymer obtained in this manner is unstable in that subsequent heating leads to change in molecular weight because the ends of the polymer molecules contain functional groups that can react further with each other.

สถาบันวิทยบริการ
จุฬาลงกรณ์มหาวิทยาลัย

3.5 Polymer Blends

Polymer blends are the mixtures of at least two polymers or copolymers. The product of blending of two or more existing polymers may have the new properties instead of obtained from synthesizing the new polymers. In the plastic industry, polymer blends are more advantageous than the synthesis of new polymers because of their lower production cost.

There are many methods to blend polymers together such as by using heat (melt mixing), solvent (solution casting, freeze-drying) or others. Some methods will be mention as follows,

3.5.1 Melt Mixing

Melt mixing of thermoplastics polymer is performed by mixing the polymers in the molten state under shear in various mixing equipments. The method is popular in the preparation of polymer blends on the large commercial scale because of its simplicity, speed of mixing and the advantage of being free from foreign components (e.g. solvents) in the resulted blends. A number of equipments are available for laboratory scale mixing such as internal mixer, electrically heated two roll mill, extruder and rotational rheometer.

The advantages of this method are the most similar to the industrial practice. The commercial compounding or adding additives into base polymers are applied by melt mixing. So the investigations of polymer blends by melt mixing method are the most practical methods in industrial applications.

3.5.2 Solvent Casting

This method group is performed by dissolving polymers in the same solvent. The solution is then cast on a glass plate into thin films and the removal of solvent from the films is performed by evaporating the solvent out at ambient or elevated temperature. To remove traces of solvents from the casting polymer films, the

condition of high temperature is invariably needed and protection of polymer in case of degradation is essential. The evaporation of solvent in inert gas or low pressure (vacuum) is typically used. In the vacuum conditions, the vapor pressure can be reduced and thus allows the solvents to evaporate more easily. However, too fast evaporation rate of solvent will create the bubble in the final films produced.

Solvent casting is the simplest mixing method available and is widely practiced in academic studies, usually when having very small quantity of polymers.

3.5.3 Freeze Drying

In the freeze drying processes, the solution of the two polymers is quenched down immediately to a very low temperature and the solution is frozen. Solvent is then removed from the frozen solution by sublimation under vacuum at a very low temperature. Dilute solutions must be used and the solution volume must have as large surface area as possible for good heat transfer.

An Advantage of this method is that the resulted blend will be independent of the solvent, if the single phase solution is frozen rapidly enough. However, there are many limitations of this method. Freeze drying method seems to work best with solvents having high symmetry, i.e. benzene, naphthalene, etc. The powdery form of the blend after solvent removal is usually not very useful and further shaping must be performed. While not complex, freeze drying does require a good vacuum system for low – boiling solvents and it is not a fast blending method. After solvent removal, the blend is in the powdery form, which usually needs further shaping. The advantage of this method is the simplicity. However, this method needs a good fume trap, vacuum line for the sublimation solvent and it takes times to complete the sublimation process.

3.5.4. Emulsions

The advantages of the emulsion polymer mixing are the easy handling and all the other advantages of the solvent casting. The mixing or casting of the film requires

neither expensive equipment nor high temperature. However, emulsions of polymers are an advantage technique and not always applicable to all monomers.

3.5.5. Reactive Blend

Co-crosslinking and interpenetrating polymer networks (IPN) formations are the special methods for forming blends. The idea of these methods is to enforce degree of miscibility by reactions between the polymer chains. Other methods involve the polymerization of a monomer in the presence of other polymer and the introduction of interface graft copolymer onto the polymer chains.

3.6 Polymer Morphology

Solid polymers differ from ordinary, low-molecular-weight compounds in the nature of their physical state or morphology. Most polymers show simultaneously the characteristics of both crystalline solids and highly viscous liquids. X-ray and electron diffraction patterns of polymer often show the sharp features typical of three-dimensionally ordered, crystalline material as well as the diffuse features characteristic of liquids. The terms crystalline and amorphous are used to indicate the ordered and unordered polymer regions, respectively. Different polymers show different degrees of crystalline behavior. The known polymers constitute a spectrum of materials from those that are completely amorphous to others that possess low to moderate to high crystallinity. The term semicrystalline is used to refer to polymers that are partially crystalline. Completely crystalline polymers are rarely encountered.

3.6.1 The Amorphous State

The amorphous state is a characteristic of polymers in the solid state that shows no traces of crystallinity. A common analogy is a bowl of cooked spaghetti. The major difference between the solid and liquid amorphous states is that with the former, molecular motion is restricted to very short-range vibrations and rotations, whereas in the molten state there is considerable segmental motion or conformational freedom arising from rotation about chemical bonds.

At the glass transition temperature, the polymer continuously changes from the glassy state (hard) to the rubbery state (soft). This transition corresponds to the onset of chain motion; below T_g the polymer chains are unable to move and are 'frozen' in position.

3.6.2 The Glass Transition

If the melted non-crystallizable polymer is cooled, it becomes more viscous and flows less readily. If the temperature is reduced low enough it becomes rubbery and if the temperature is reduced further, the polymer becomes a relatively hard and low-elastic polymer glass. The temperature at which the polymer undergoes the transformation from a rubber to a glass is known as the glass transition temperature, T_g . The ability to form glasses is not confined to non-crystallizable polymers. Any material which can be cooled sufficiently below its melting temperature without crystallizing will have a glass transition temperature.

There is a dramatic change in the properties of a polymer at the glass transition temperature. For example, there is a sharp increase in the stiffness of an amorphous polymer when its temperature is reduced below T_g . There are also abrupt changes in other physical properties such as heat capacity and thermal expansion coefficient at the glass transition. One of the most widely used methods of demonstrating the glass transition and determining T_g is by measuring the specific volume of a polymer sample as a function of the temperature.

Another characteristic of the T_g is that the exact temperature depends upon the rate at which the temperature is changed. It is found that lower the cooling rate the lower the value of T_g that is obtained. It is still a matter of some debate as to whether a limiting value of T_g would eventually be reached if the cooling rate were low enough. It is also possible to detect a glass transition in a semi-crystalline polymer, but the change in properties at T_g is usually less marked than for a fully amorphous polymer.

3.6.3 The Crystalline Polymer

Polymers crystallized in the bulk states are never completely crystalline, because of a consequence of their long – chain nature and subsequent entanglements of the long molecules. The melting temperature of the polymer (T_m) is always higher than the glass transition temperature (T_g). Thus the polymer may be either hard and rigid or flexible at room temperature depended on the T_g and T_m ranges. For example , polypropylene which has a glass transition temperature of about $-5\text{ }^\circ\text{C}$ and a melting temperature of about $175\text{ }^\circ\text{C}$. At room temperature it forms a leathery product as a result.

The development of crystallinity in polymers depends on the regularity of their structures in the polymer, the tacticity of the polymer. The different possible spatial arrangements are called the tacticity of the polymer. If the R groups on successive pseudo-chiral carbons all have the same configuration , the polymer is called isotactic. When the pseudo-chiral centers alternate in configuration from one repeating unit to the next , the polymer is called syndiotactic. If the pseudo-chiral centers do not have any particular order , but in fact are statistical arrangements , the polymer is said to be atactic.

Thus isotactic and syndiotactic structure are both crystallizable , because of their special regularity along the chain but their ability to crystalline are not the same and they usually have different crystalline melting temperature. On the other hand , atactic polymers are usually completely amorphous unless the side group is so small or so polar which can permit some crystallinity.

Nonregularity of structure first decreases the melting temperature and finally prevents crystallinity. Monomers of incorrect tacticities tend to destroy crystallinity. Thus statistical copolymers are generally amorphous. Blends of isotactic and atactic polymers show a reduction in crystallinity , because only the isotactic portion can be crystallizing. Furthermore, the long – chain nature and the subsequent entanglements prevent complete crystallization.

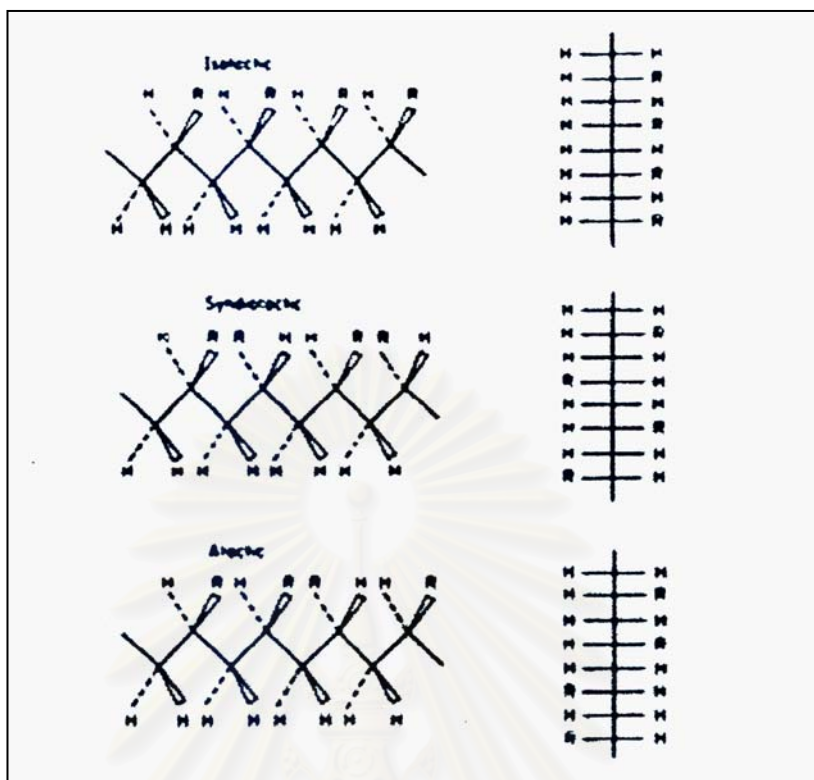


Figure 3.2 Three different configurations of a polypropylene [Sperling L. H., 2001]

3.6.4 Thermal Transitions

Polymeric materials are characterized by two major types of transition temperatures—the crystalline melting temperature, T_m and the glass transition temperature, T_g . The crystalline melting temperature is the melting temperature of the crystalline domains of a polymer sample. The glass transition temperature is the temperature at which the amorphous domains of a polymer take on the characteristic properties of the glassy state—brittleness, stiffness, and rigidity. The difference between the two thermal transitions can be understood more clearly by considering the changes that occur in a liquid polymer as it is cooled. The translational, rotational, and vibrational energies of the polymer molecules decrease on cooling. When the total energies of the molecules have fallen to the point where the translational and rotational energies are essentially zero, crystallization is possible. If certain symmetry requirements are met, the molecules are able to pack into an ordered, lattice

arrangement and crystallization occurs. The temperature at which this occurs is T_m . However, not all polymers meet the necessary symmetry requirements for crystallization. If the symmetry requirements are not met, crystallization does not take place, but the energies of the molecules continue to decrease as the temperature decreases. A temperature is finally reached—the T_g —at which long-range motions of the polymer chains stop. Long-range motion, also referred to as segmental motion, refers to the motion of a segment of a polymer chain by the concerted rotation of bonds at the ends of the segment.

Whether a polymer sample exhibits both or only one thermal transitions depends on its morphology. Completely amorphous polymers show only T_g . Semicrystalline polymers exhibit both the crystalline melting and glass transition temperature. Changes in properties such as specific volume and heat capacity occur as a polymer undergoes each of thermal transitions.

Some polymers undergo other thermal transitions in addition to T_g and T_m . These include crystal-crystal transitions (i.e. transition from one crystalline form to another) and crystalline-liquid crystal transitions.

The values of T_g and T_m for a polymer affect its mechanical properties at any particular temperature and determine the temperature range in which that polymer can be employed. Consider the manner in which T_g and T_m vary from one polymer to another. One can discuss the two transition simultaneously since both are affected similarly by considerations of polymer structure. Polymer with low T_g values usually have low T_m values; high T_g and high T_m values are usually found together. Polymer chains that do not easily undergo bond rotation so as to pass through the glass transition would also be expected to melt with difficulty. This is reasonable, since similar considerations of polymer structure are operating in both instances. The two thermal transitions are generally affected in the same manner by the molecular symmetry, structural rigidity, and secondary forces of polymer chains. High secondary forces (due to high polarity or hydrogen bonding) lead to strong crystalline forces requiring high temperature for melting. High secondary forces also decrease the mobility of amorphous polymer chains, leading to high T_g . Decreased mobility of

polymer chains, increased chain rigidity, and high T_g are found where the chains are substituted with several substituents as in poly(methyl methacrylate) and polytetrafluoroethylene or with bulky substituents as in polystyrene. The T_m values of crystalline polymers produced from such rigid chains would also be high.

The rigidity of polymer chains is especially high when there are cyclic structures in the main polymer chains. Polymers such as cellulose have high T_g and T_m values. On the other hand, the highly flexible polysiloxane chain (a consequence of the large size of Si) results in very low values of T_g and T_m .

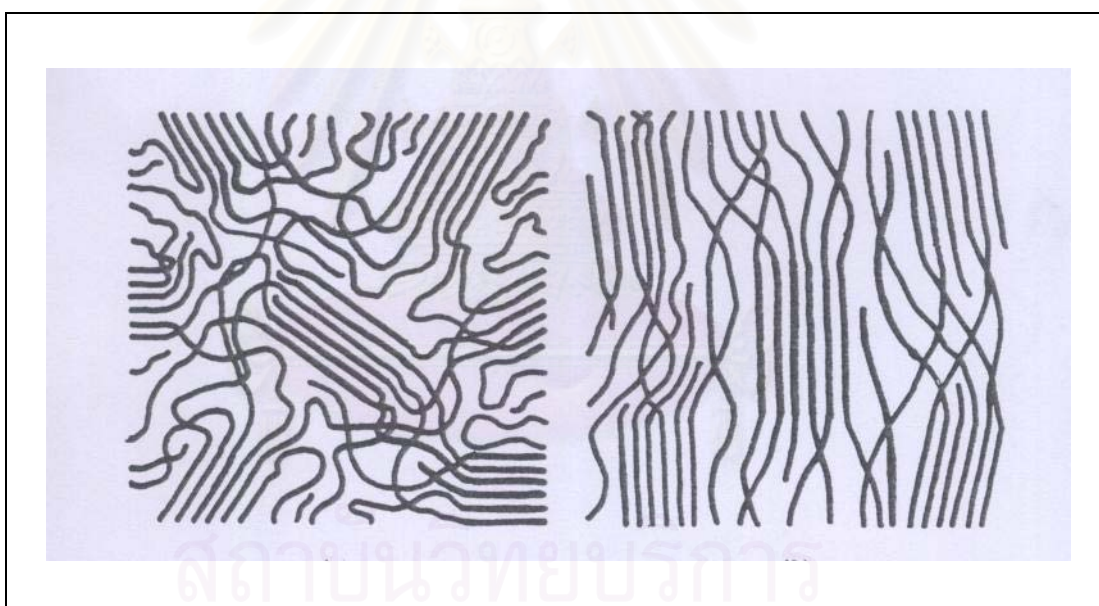
Although T_g and T_m depend similarly on molecular structure, the variation in the two transition temperatures do not always quantitatively parallel to each other. Molecular symmetry, chain rigidity, and secondary forces do not affect T_g and T_m in the same quantitative manner. An empirical consideration of the ratio T_g/T_m (Kelvin temperatures) for various polymers aids this discussion. The T_g/T_m ratio is approximately $\frac{1}{2}$ for symmetrical polymers [e.g. poly(vinylidene chloride)], but the ratio is closer to $\frac{3}{4}$ for unsymmetrical polymers [e.g. poly(vinyl chloride)]. This result indicates that T_m is more dependent on molecular symmetry while T_g is more dependent on secondary forces and chain flexibility.

3.6.5 Structure of Polymer Crystals

3.6.5.1 The Fringed Micelle Model

The first attempt to explain the observed properties of crystalline polymers was the fringed micelle model (Fig. 3.3). This model pictures crystalline regions known as fringed micelles or crystallites interspersed in an amorphous matrix. The crystallites, whose dimensions are on the order of tens of nanometers, are small volumes in which portions of the chains are regularly aligned parallel to one another, tightly packed into a crystal lattice. The individual chains, however, are many times longer than the dimensions of a crystallite, so they pass from one crystallite to another through amorphous areas.

This model explains nicely the coexistence of the crystalline and amorphous material in polymers, and also explains the increase in crystallinity that is observed when fibers are drawn (stretched). Stretching the polymer orients the chains in the direction of the stress, increasing the alignment in the amorphous areas and producing greater degrees of crystallinity (Fig. 3.3b). Since the chains pass randomly from one crystallite to another, it is easy to see why perfect crystallinity can never be achieved. This also explains why the effects of crystallinity on properties are in many ways similar to those of cross-linking, because, like crosslinks, the crystallites tie the individual chains together. Unlike crosslinks, though, the crystallites will generally melt before the polymer degrades and solvents that form strong secondary bonds with the chains can dissolve them.



(a)

(b)

Figure 3.3 The fringed micelle model:

(a) unoriented; (b) chains oriented by applied stress. [Rosen Stephen L., 1993]

3.6.5.2 The Folded-Chain Model

The folded-chain model has been well substantiated for single polymer crystals. The lamellae are about 50 to 60 carbon atoms thick, with about five carbon atoms in a direct reentry fold. The atoms in a fold, whether direct or indirect reentry, can never be part of a crystal lattice.

The folded-chain lamella theory arose when polymer single crystals in the form of thin platelets termed lamella, measuring about $10,000 \text{ \AA} \times 100 \text{ \AA}$, were grown from polymer solutions. Contrary to previous, X-ray diffraction patterns showed the polymer chain axes to be parallel to the smaller dimension of the platelet. Since polymer molecules are much longer than 100 \AA , the polymer molecules are presumed to fold back and forth on themselves in an accordion like manner in the process of crystallization. Chain folding was unexpected, since the most thermodynamically stable crystal is the one involving completely extended chains. The latter is kinetically difficult to achieve and chain folding is apparently the system's compromise for achieving a highly stable crystal structure under normal crystallization conditions. Two models of chain folding can be visualized. Chain folding is regular and sharp with a uniform fold period in the adjacent-reentry model (Fig. 3.4). In the nonadjacent-reentry or switchboard model (Fig.3.5) molecules wander through the nonregular surface of a lamella before reentering the lamella or a neighboring lamella.

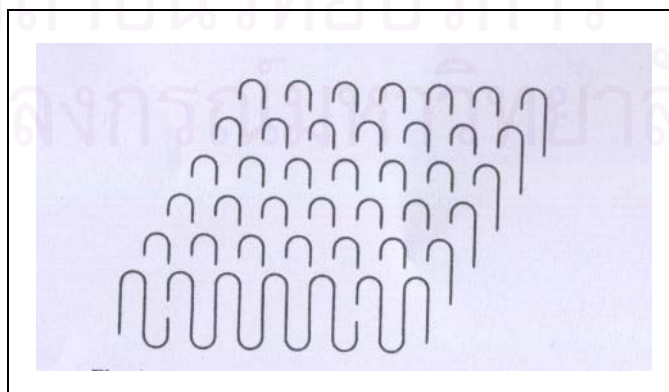


Figure 3.4 Adjacent-reentry model of single crystal.

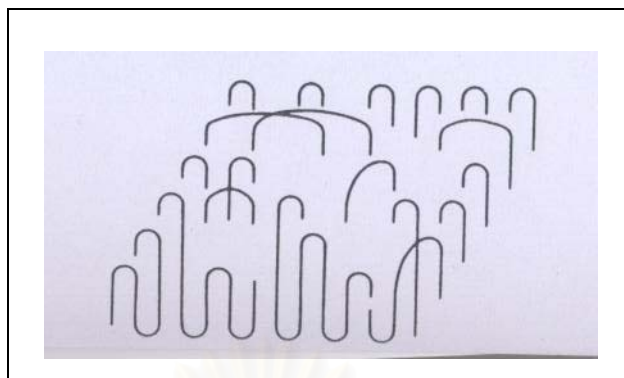


Figure 3.5 Switchboard model of single crystal.

In the chain-folded lamella picture of polymer crystallinity less than 100% crystallinity is attributed to defects in the chain-folding process. The defects maybe imperfect folds, irregularities in packing, chain entanglements, loose chain ends, dislocations, occluded impurities, or numerous other imperfections. The adjacent-reentry and switchboard model differ in the details of what constitutes the chain-folding defects. The switchboard model indicates that defects are located as much within the crystal as at the crystal surface.

Folded-chain lamella represent the morphology not only for single crystals grown from solution but also polymers crystallized from the melt—which is how almost all commercial and other synthetic polymer are obtained. Melt-crystallized polymers have the most prominent structural feature of polymer crystal—the chains are oriented perpendicular to the lamella face so that chain folding must occur. Chain folding maximum for polymers crystallized slowly near the crystalline melting temperature. Fast cooling (quenching) gives a more chaotic crystallization with less chain folding.

3.6.6 Crystallization from The Melt

3.6.6.1 Spherulitic Morphology

When polymer samples are crystallized from the bulk of an unstained melt, the most obvious of the observed structures are the spherulites are sphere – shaped crystalline structure that form in bulk. Usually the spherulites are really spherical in shape only during the initial stages of crystallization. During the latter stages of crystallization, the spherulites impinge on their neighbours. When the spherulites are nucleated simultaneously, the boundaries between them are straight. However, when the spherulites have been nucleated at different duration, they are different in impinging size on one another and they have hyperbolas boundaries. Finally, the spherulites form structures that pervade the entire mass of the material.

Electron microscopy examination of the spherulitic structure shows that the spherulites are composed of individual lamellar crystalline plates. The lamellar structures sometimes resemble staircases, being composed of nearly parallel lamellae of equal thickness.

The growth and structure of spherulites may also be studied by small-angle light scattering. The sample is placed between polarizers, a light beam is passed through, and the resultant scattered beam is photographed. Two types of scattering patterns are obtained, depending on polarization condition. When the polarization of the incident beam and that of the analyzer are both vertical, it is called a Vv type of pattern. When the incident polarization radiation is vertical but the polarization of analyzer is horizontal (polarizers crossed), an Hv pattern is obtained.

These patterns arise from the spherulitic structure of the polymer, which is optically anisotropic, with the radial and tangential refractive indices being different.

A model of the spherulite structure is illustrated in Figure 3.6.

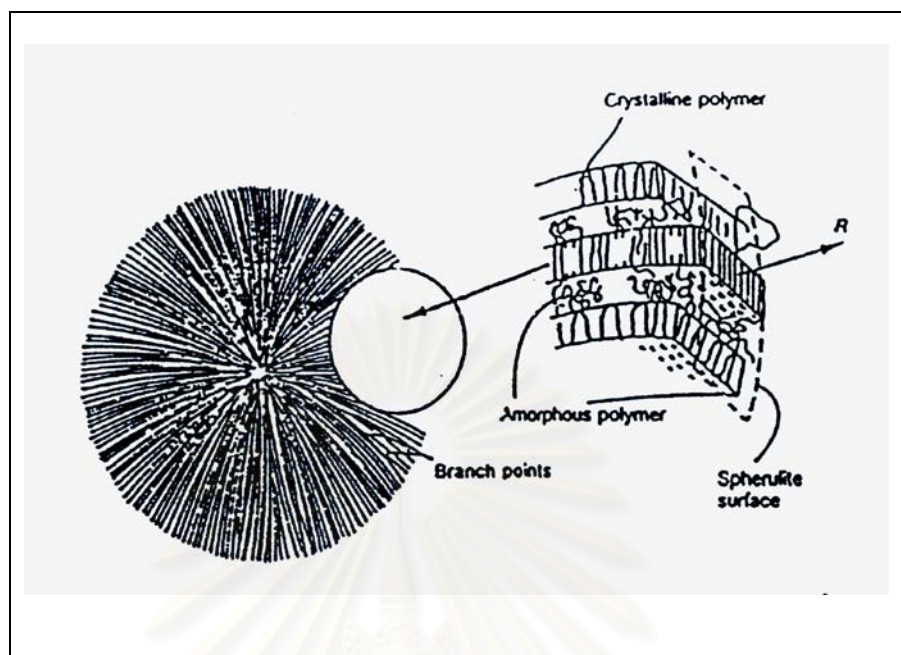


Figure 3.6: Model of spherulitic structure. [McCrum N. G. *et al.*, 1988]

The chain direction in the bulk crystallized lamellae is perpendicular to the broad plane of the structure, similar to the dilute solution crystallized material. The spherulite lamellae also contain low – angle branch points, where new lamellar structures are initiated. The new lamellae tend to keep the spacing between the crystallites equal. While the lamellar structures in the spherulites are the analogue of the single crystals. In between the lamellar structures, amorphous material is laid. This portion is rich in components such as atactic polymers, low – molecular – weight material, or impurities of various kinds.

The individual lamellae in the spherulites are bonded together by tie molecules, which lie partly in one crystallite and partly in the others. Sometimes these tie molecules are actually in the form of what are called intercrystalline links, which are long, threadlike crystalline structures. These intercrystalline links are thought to be important in the development of the great toughness characteristic of semi-crystalline polymers. They serve to tie the entire structure together by crystalline regions and/or primary chain bonds.

3.6.6.2 Mechanism of Spherulite Formation

On cooling from the melt, the first structure that forms is the single crystal. These rapidly degenerate into sheaflike structures during the early stages of the growth of polymer spherulites. These sheaflike structures have been variously called axialites or hedrites. These transitional, multilayered structures represent an intermediate stage in the formation of spherulites.

3.6.6.3 Spherulites in Polymer Blends

There are two cases to be considered. Either the two polymers composing the blend may be miscible and form one phase in the melt, or they are immiscible and form two phases. If the glass transition of the noncrystallizing component is lower than that of the crystallizing component (i.e., its melt viscosity will be lower, other things being equal), then the spherulites will actually grow faster, although the system is diluted. The crystallization behavior is quite different if the two polymers are immiscible in the melt. On spherulite formation, the droplets, which are non-crystallizing, become ordered within the growing arms of the crystallizing component.

3.6.6.4 Effect of Crystallinity on T_g

Semi-crystalline polymers such as polyethylene or polypropylene types also exhibit glass transitions, though only in the amorphous portions of these polymers. The T_g is often increased in temperature by the molecular – motion restricting crystallites. Sometimes T_g appears to be masked, especially for high crystalline polymers.

3.7 Crystal forms in thermally-processed sPS

Four different unit cell forms, which will be namely as α , β , γ and δ , can be obtained in sPS. Each type of crystal will exist depending on the thermal histories and/or solution treatments. The arrangements of the unit cells of these four forms are distinctly different. Normally, α - and β -forms crystal are co-existed in various relative

fractions in melt-processed sPS. The α - and β -forms are more common and associated with polymer chains in trans-planar (zig-zag) conformation while the γ - and δ -forms are of a helical conformation that are commonly associated with solvent-induced crystallization in sPS. Only two crystal forms, α - and β -crystals, are commonly found in sPS subjected to various thermal treatments. Each of the α -form (a hexagonal unit cell) and β -form (an orthorhombic unit cell) can be sub-classified as two different modifications characterized by differing degrees of structural order, which are described as α' and β' and the others are two limited-order modifications (α'' and β''). Two less common crystalline forms are γ and δ , which are characterized by their main chain in $s(2/1)_2$ helical conformation. It was shown that on annealing above T_g , the δ form transforms into the γ form. The γ form changes into the α form when heated in the temperature range 180-220 °C. On the other hand, the α crystals change to β form or vice versa achieved by melting and recrystallization under appropriate conditions.

3.7.1 α -Crystal

Two proposed packing models for the α - form crystal of sPS are shown in Figure 3.7-3.8.

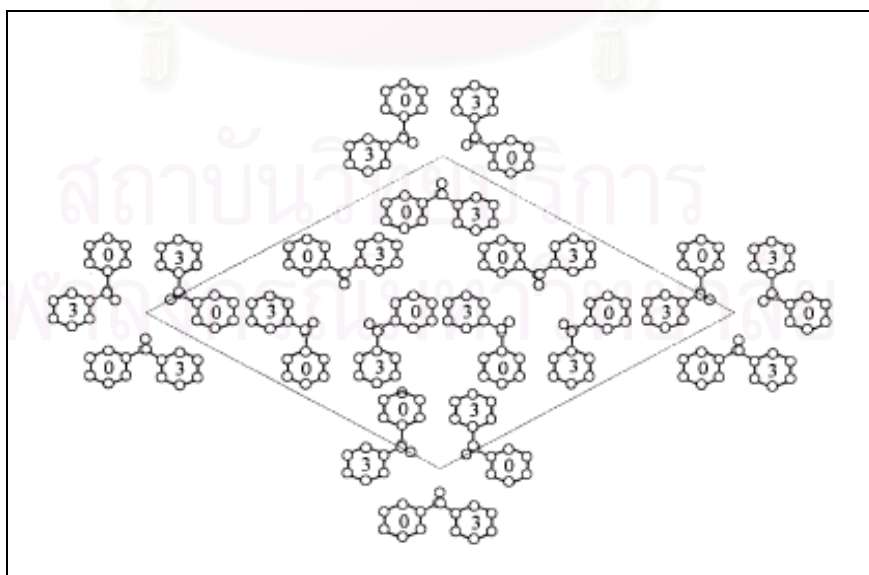


Figure 3.7 Hexagonal model proposed by Greis *et al.*, space group $P6_2c$ ($a = b = 26.25 \text{ \AA}$, $c = 5.04 \text{ \AA}$)

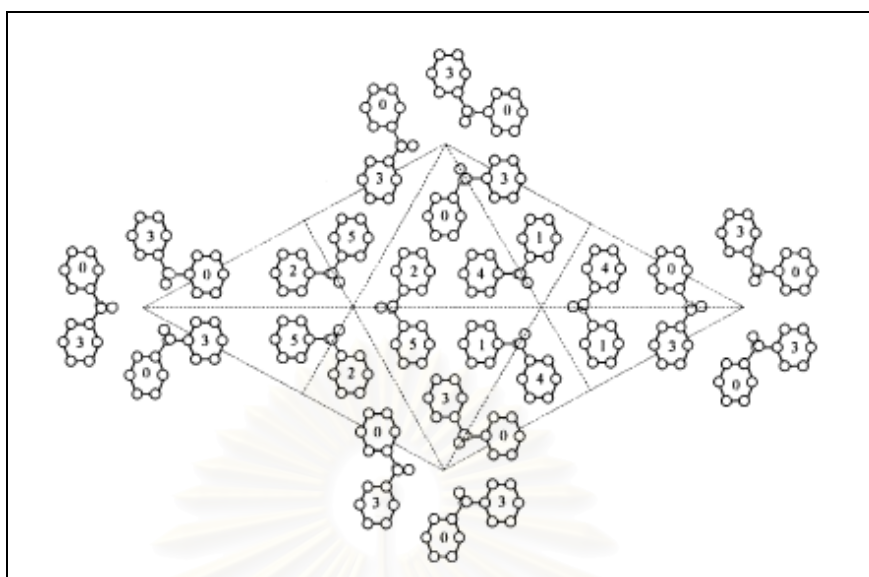


Figure 3.8 Trigonal model proposed by De Rosa *et al.*, space group $P3c1$ ($a = b = 26.26 \text{ \AA}$, $c = 5.04 \text{ \AA}$)^a

^a Relative heights of the center of phenyl rings are in units $c/6$. Dotted lines in Figure 3.8 indicate crystallographic glide planes c . In Figure 3.7, glide planes c contain the axes of the unit cell.

In addition, it is generally accepted that there are two sub-modifications for the α -crystal : a limit-ordered α'' -modification and a limit-ordered α' -modification.

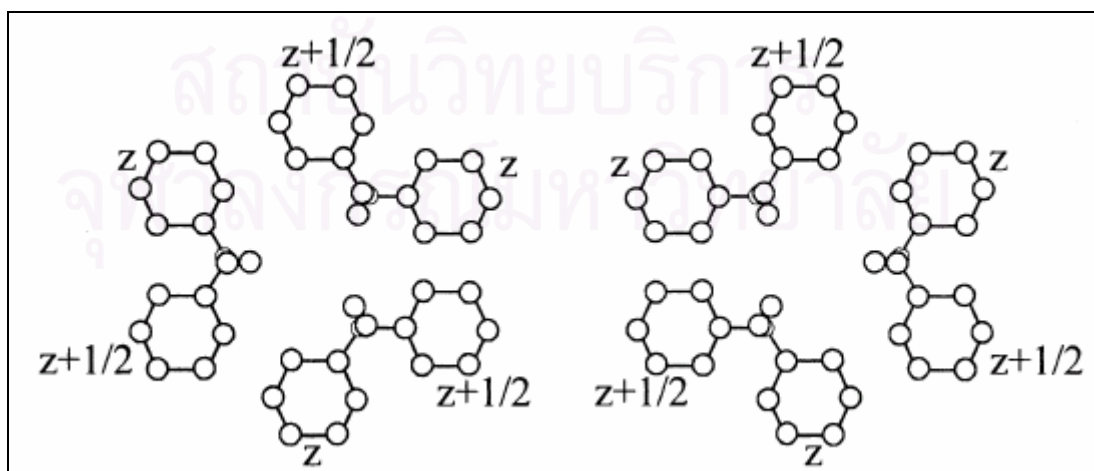


Figure 3.9 Model for α'' -modification

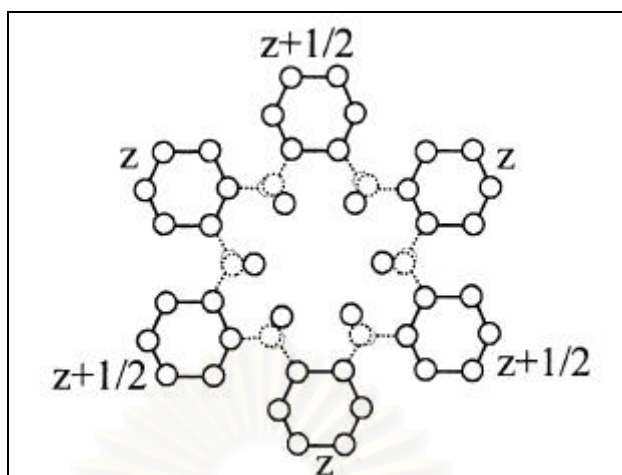


Figure 3.10 Model for α' -modification

3.7.2 β -Crystal

The β -form is an orthorhombic unit cell and the chain conformation is all-trans planar zig-zag. It is generally accepted that there are two sub-modifications for the β -crystal : a limit-ordered β'' -modification and a limit-ordered β' -modification. The β' - and β'' -forms are both orthorhombic, with a unit cell dimensions : $a = 8.81\text{\AA}$, $b = 28.82\text{\AA}$, $c = 5.51\text{\AA}$.

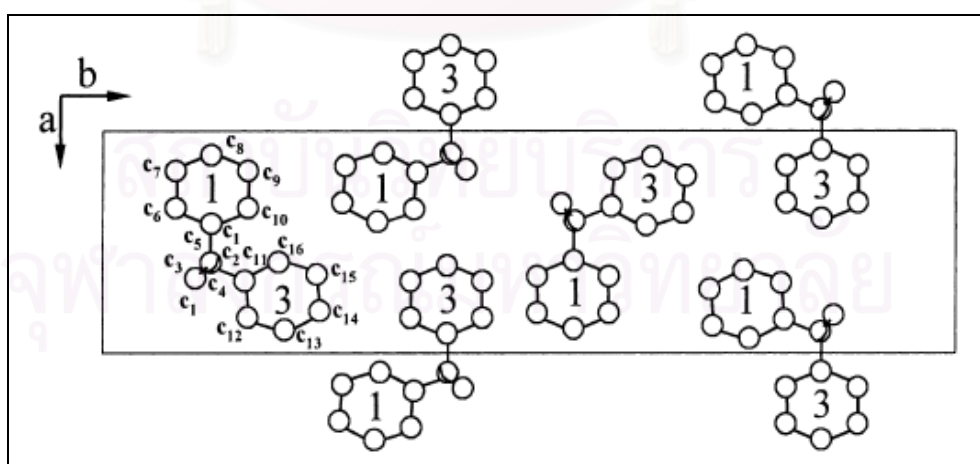


Figure 3.11 Model for β'' -modification^b

^b The carbon atoms of the asymmetric unit labeled with the number 1-16.

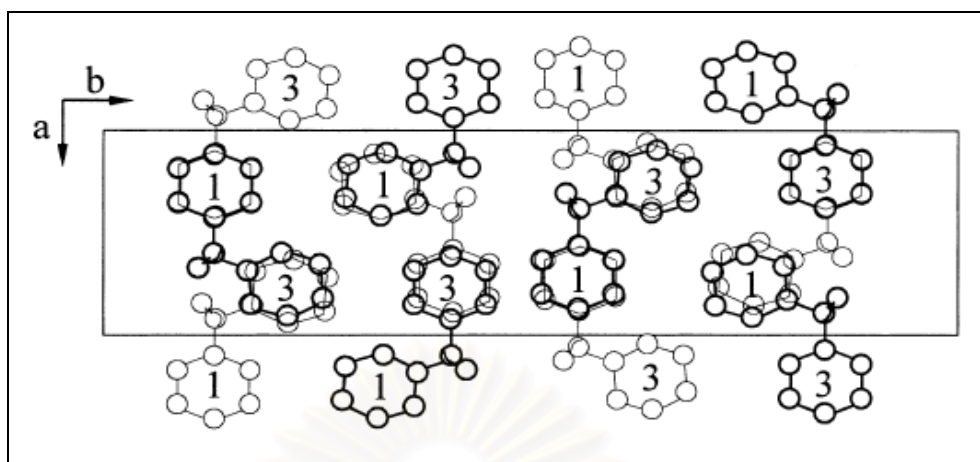


Figure 3.12 Model for β' -modification

3.8 Crystal forms in solvent-treated sPS

The γ - and δ -forms are not usually seen in melt-processed sPS and commonly associated with solvent-induced crystallization in sPS. The δ -form is monoclinic unit cell, and the chain conformation is helical. The γ -form is also of a helical conformation. The γ -form can only be obtained by heating a δ -form to higher temperature.

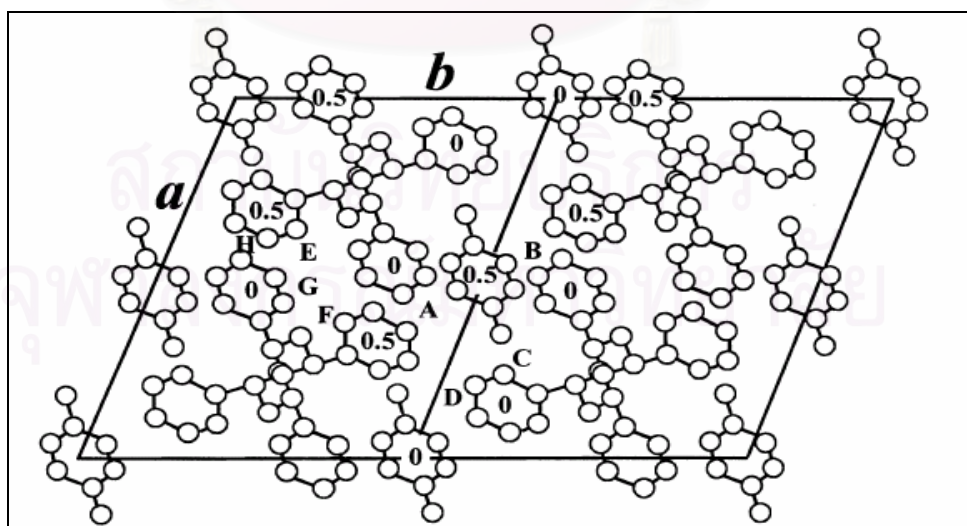


Figure 3.13 A proposed model for the crystal structure of the solvent-induced δ -form of sPS swelled by toluene molecules in the space $P2_1/a$.^c

^c The approximate z fractional coordinates of the barycenters of the phenyl rings are also shown. The carbon atoms which give the lowest intermolecular contact distances between and inside ac layers of macromolecules are labeled with letter A-H.

Dimensions : $a = 17.58 \text{ \AA}$, $b = 13.26 \text{ \AA}$, c (chain axis) = 7.71 \AA , monoclinic angle $\gamma = 121.2^\circ$.

Different solvents produce a similar δ -crystal form in sPS.

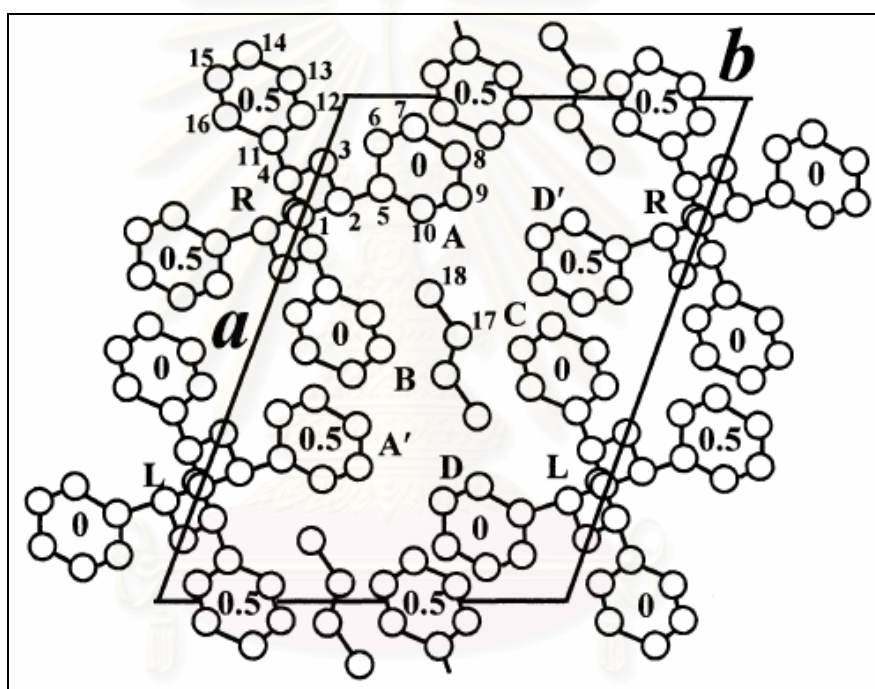


Figure 3.14 Solvent-induced clathrate δ -form of sPS swelled by dichloroethane (DCE) molecules in the space $P2_1/a$.^d

^d The atoms of the asymmetric unit (atom 1-18) are labeled. The approximate z fractional coordinates of the barycenters of the phenyl rings are also shown. R = right-, L = left-handed chain. The letters A-D, A', and B', indicate the phenyl rings with the surrounding DCE molecules.

Crystal dimensions : $a = 17.11 \text{ \AA}$, $b = 12.17 \text{ \AA}$, $c = 7.70 \text{ \AA}$, monoclinic angle $\gamma = 120^\circ$.

When solvents are driven off completely from the solvent-induced crystal, the packing remains the same, but the dimensions change slightly.

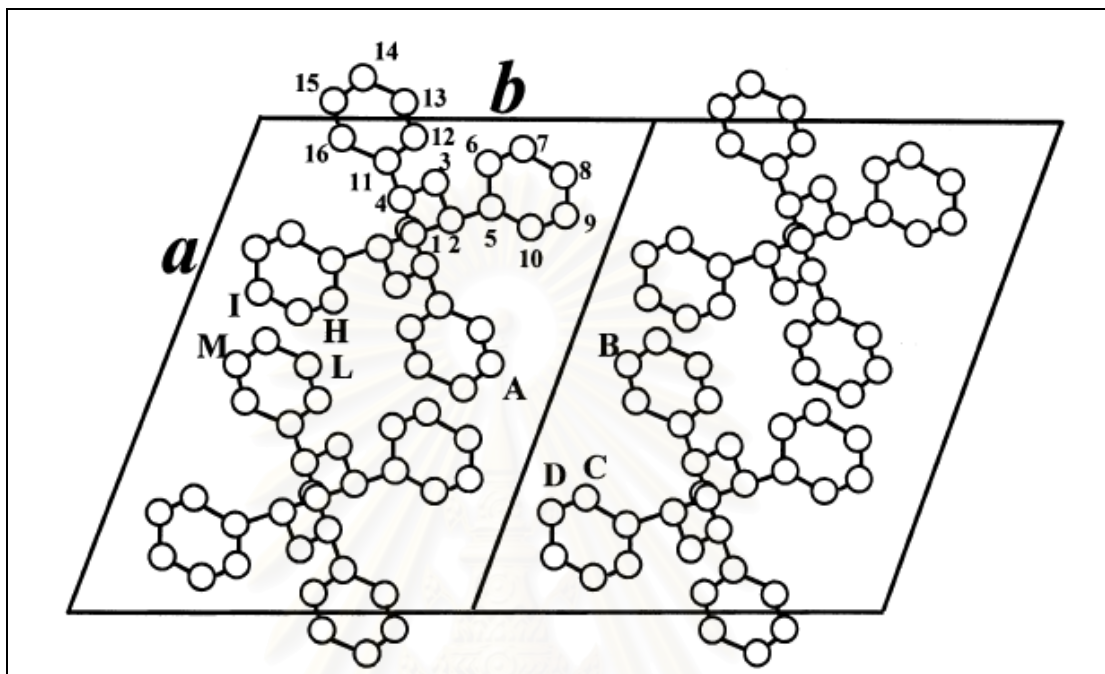


Figure 3.15 A model for the crystal structure of the emptied δ -form (δ_e -form) of sPS in the space $P2_1/a$.

This δ_e -form differs from the previous ones in the crystal dimensions. The δ_e -form has a reduced b -dimension in the unit cell.^e

^e The carbon atoms of the asymmetric unit are labeled with the numbers 1-16. The carbon atoms which give the lowest intermolecular contact distance between and inside ac layers of macromolecules are labeled with letters A-D, H-M.

Crystal dimensions : $a = 17.4 \text{ \AA}$, $b = 11.85 \text{ \AA}$, $c = 7.70 \text{ \AA}$, monoclinic angle $\gamma = 117^\circ$.

3.9 Crystal Morphology and thermal behavior of thermally-processed sPS

3.9.1 Crystal melting behavior

Upon melt crystallization of sPS at most accessible temperatures (230-260°C), it has been proven that sPS develops two major crystals (α and β) with four sharp discernible melting peaks (P-I, P-II, P-III, P-IV) associated with these two different crystal lamellae. In general, the α -crystal packing can become an alternative route in sPS crystallization under three conditions ; (1) slow cooling from molten state, (2) melt crystallization at low temperatures (e.g. 230 °C or lower), or (3) cold crystallization from quenched glass. As a matter of fact, cold-crystallized sPS samples contain only α -type crystal, which differs significantly from melt-crystallized sPS in crystal forms or the shapes of melting endotherms. By comparison, melt crystallization of sPS at most accessible temperatures produce both α -type (P-II, and P-IV) and β -type (P-I and P-III) crystals of various fractions. In general, the low to medium melt crystallization temperature always result in growth of β -crystal and α -type, but higher melt crystallization temperature tends to favor greater fractions of β -type. As a matter of fact, the β -type crystal became the only dominating species if sPS was melt-crystallized at temperature equal to or higher than 260 °C. Under conditions approaching equilibrium, only the β -crystal is present and is the favored type of packing.

3.9.2 Effect of miscibility on polymorphism

In contrast with the fact that both α' - and β' -types usually co-exist in melt-crystallized neat sPS, only the β -type is identified in miscible sPS/aPS or sPS/PPO blends. Actually, however, the α -crystal in addition to the β -crystal could also be grown in miscible blends of sPS; but the relative fractions of α - and β - crystals are quite different from those in a neat sPS when all were crystallized at the same conditions. Apparently, factors related to the miscibility might have influenced the polymorphism in sPS.

3.9.3 Effects of tacticity and molecular weight

It has been found that the sPS of lower molecular weights and/or lower tacticity ($M_w = 63,000$ g/mol) developed only β -crystal when held for melt crystallization at any temperatures. This is quite interesting and surprising. Usually, when sPS of high molecular weights and high tacticity is melt-crystallized at most medium temperature (230 ~ 250°C), the crystals are packed with both α - and β -crystals unit cells with various fractions, which depend on factors, such as temperature, cooling rate, or other thermal histories. Molecular weight apparently has an effect on relative fraction of α - vs. β -crystals in sPS upon melt crystallization. Nevertheless, cold crystallization of sPS of any molecular weight leads only to the α -crystals. By using the sPS model of a low molecular weight ($M_w = 63,000$ g/mol), relationships between the polymorphism and melting behavior in the melt-crystallized sPS, containing only the β -crystal.

3.10 Crystal Structure

The intensities of the diffraction peaks located at $2\theta = 11.6$ and 12.2° are employed to estimate the content of the α form in the crystals via the following relation :

$$P_\alpha(\%) = \frac{1.8A(11.6)/A(12.2)}{1 + 1.8A(11.6)/A(12.2)} \times 100\%$$

where 1.8 is the ratio between the intensities of the 2θ diffraction peak located at 11.6 and 12.2° , respectively, for specimens with the same thickness and crystallinity in the pure α and β forms. Meanwhile, $A(11.6)$ and $A(12.2)$ are the areas of the 2θ diffraction peaks located at 11.6 and 12.2° .

In Figure 3.16, both diffraction peaks with comparable intensity appear for pure sPS, indicating the crystals formed are mixtures of α form and β form. However, for the blends, the intensity ratio between peaks located at $2\theta = 11.6$ and 12.2° decreases with increasing copolymer content. Only one diffraction peak ($2\theta = 12.28$) is found for the blend with 80% of the copolymer. It is concluded that the addition of

the copolymer reduces the possibility of α form sPS crystal formation. The observation in this system is suspected to be attributed to the T_m^0 depression of sPS in the blends, which results in a so-called higher ‘premelting temperature’ effect on the resulting crystal structure of the samples.

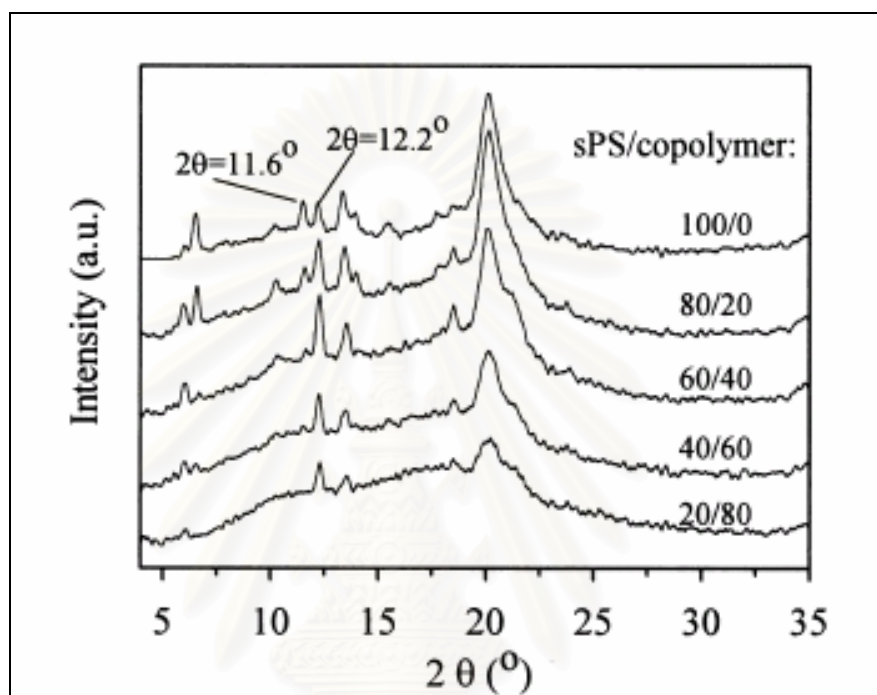


Figure 3.16 WAXD spectra of sPS and sPS/poly(styrene-*co*- α -methyl styrene) blends: melt-crystallized with 10 °C/min.

CHAPTER IV

EXPERIMENT

The experimental procedures used in this study were divided as follows:

1. Styrene monomer and materials preparations.
2. Syndiospecific styrene polymerization by a homogeneous half-metallocene catalyst system with modified-methylaluminoxane (MMAO).
3. Blending of syndiotactic polystyrene with selected polymers.
4. Characterize syndiotactic polystyrene and sPS blends.

4.1 Chemicals

The chemicals used in these experiments were analytical grade, but only critical materials were specified as follows:

1. Argon gas (Ultra High Purity, 99.999%) was purchased from Thai Industrial Gas Co., Ltd. (TIG) and was purified by passing through the column packed with molecular sieve 3 Å, BASF Catalyst R3-11G, sodium hydroxide (NaOH) and phosphorus pentoxide (P₂O₅) to remove traces of oxygen gas and moisture.
2. Styrene monomer was purchased from Fluka Chemie A.G., Switzerland was distilled from sodium under vacuum just before use.
3. Pentamethylcyclopentadienyltitanium trichloride (Cp*TiCl₃) was purchased from Aldrich chemical Company, Inc.
4. Modified-Methylaluminoxane (MMAO) 1.83 M in toluene was donated from Tosoh Akso, Japan.
5. Methanol (Commercial grade) was purchased from SR lab.
6. Methyl ethyl ketone (MEK) was purchased from Carlo Erba, Italy.
7. *o*-Dichlorobenzene (*o*-DCB) was purchased from Aldrich chemical Company, Inc.
8. Poly(ethyl methacrylate), (PEMA) was purchased from Scientific Polymer Products, Inc.
9. Poly(*n*-butyl methacrylate), (PBMA) was purchased from Scientific Polymer Products, Inc.

10. Poly(α -methylstyrene) was purchased from Aldrich chemical Company, Inc.
11. Polyisoprene, cis was purchased from Scientific Polymer Products, Inc.
12. Poly(vinyl methyl ether), (PVME) was purchased from Scientific Polymer Products, Inc.
13. Poly(cyclohexyl acrylate), (PCHA) was purchased from Scientific Polymer Products, Inc.
14. Toluene was donate from Exxon Chemical Ltd., Thailand. This solvent was dried over dehydrated CaCl_2 and distilled over sodium/benzophenone under argon atmosphere before use.
15. Calcium chloride (Dehydrated) was manufactured from Fluka Chemie A.G. Switzerland.
16. Sodium (lump in kerosene, 99.0%) was supplied from Aldrich chemical Company, Inc.
17. Benzophenone (purum 99.0%) was obtained from Fluka Chemie A.G. Switzerland.
18. Hydrochloric acid (Fuming 36.7%) was supplied from Sigma.

4.2 Equipments

All types of equipments used in syndiospecific styrene polymerization and polymer blends, were listed as follows:

4.2.1 Cooling System

There were two cooling systems, one was used for the solvent distillation for condensing the freshly evaporated solvent and the other one was for cooling the system of the polymerization reactor due to the rapid rate of exothermic polymerization reaction.

4.2.2 Glove Box

The glove box was used for preparing and storing the chemicals under inert gas atmosphere to avoid oxygen and moisture. The oxygen and moisture levels are normally below 2 ppm inside the glove box. The glove box is shown in Figure 4.1.

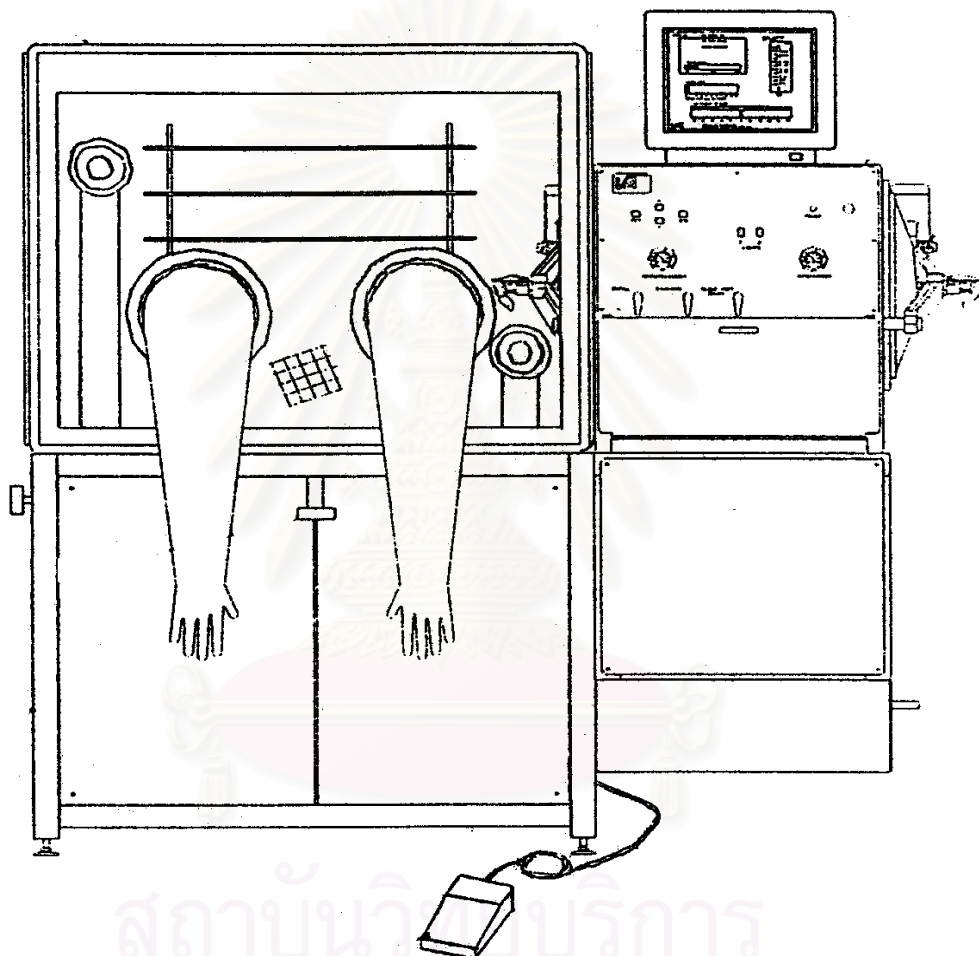


Figure 4.1 Glove box

4.2.3 Schlenk Line

The Schlenk line consists of vacuum and argon lines. The vacuum line was equipped with the solvent trap and vacuum pump, respectively. The argon line was connected with the trap and the mercury bubbler that was a manometer tube and

contained enough mercury to provide a seal from the atmosphere when argon line was evacuated. The Schlenk line is shown in Figure 4.2.

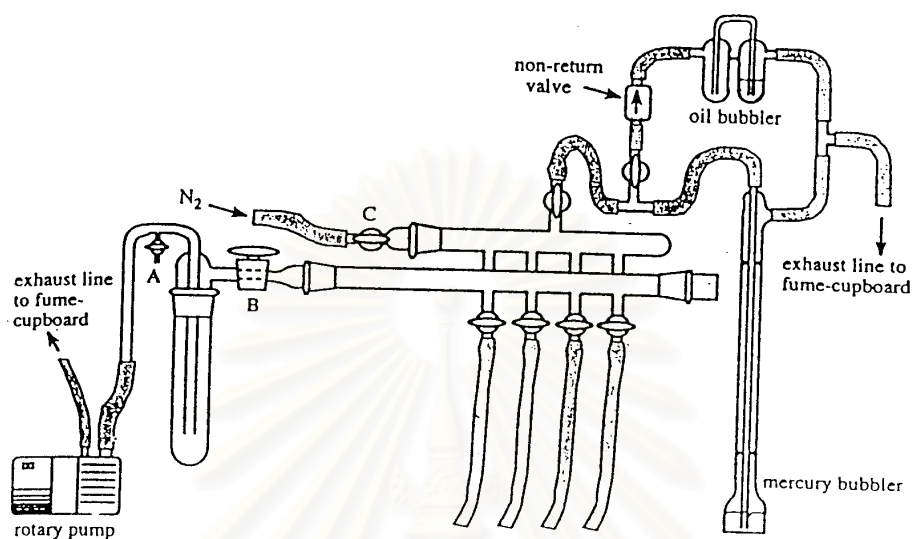


Figure 4.2. Schlenk line

4.2.4 Schlenk Tube

Schlenk tube is a tube with a ground glass joint and side arm, which is three-way glass valve as shown in Figure 4.3. Schlenk tube was used for keeping the reagents under argon atmosphere outside the glove box.

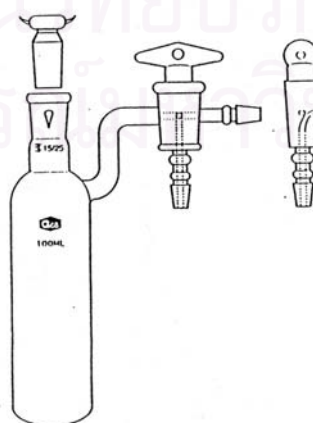


Figure 4.3 Schlenk tube

4.2.5 Glass Reactor

The polymerization reactor was a 250 ml three-neck flask. The reactor was equipped with several fittings for injecting the chemicals and purging with argon gas. The glass reactor is shown in Figure 4.4.



Figure 4.4. Glass reactor

4.2.6 Vacuum Pump

The vacuum pump model 195 from Labconco Corporation was used. A pressure of 10^{-1} to 10^{-3} mmHg was adequate for the vacuum supply to the vacuum line in the Schlenk line. The vacuum pump is shown in Figure 4.5.

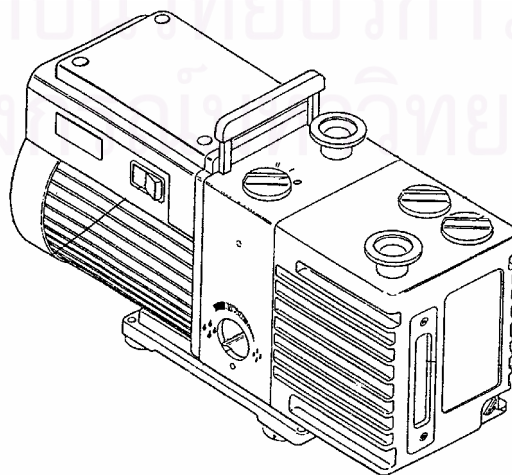


Figure 4.5. Vacuum pump

4.2.7 Inert Gas Supply

The inert gas (argon) was passed through columns of oxygen trap (BASF catalyst, R3-11G), moisture trap (molecular sieve), sodium hydroxide (NaOH) and phosphorus pentoxide (P_2O_5) for purifying ultra high purity argon before use in Schlenk line and solvent distillation column. The inert gas supply system is shown in Figure 4.6.

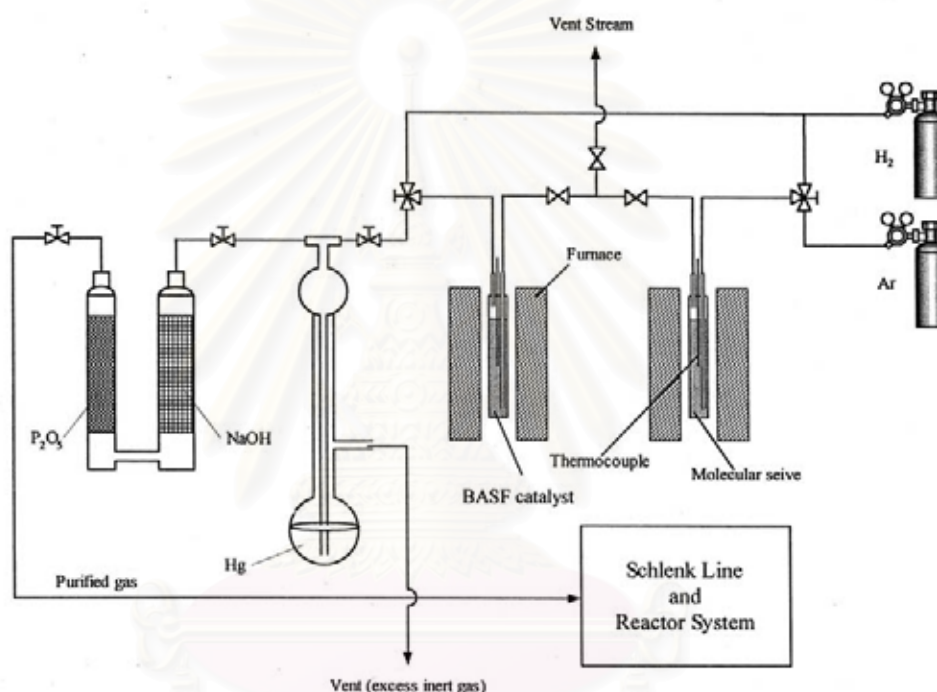


Figure 4.6. Inert gas supply system

4.2.8 Magnetic Stirrer and Hot Plate

The magnetic stirrer and hot plate model RCT basic from IKA Labor Technik were used.

4.2.9 Digital Hot Plate Stirrer

A Cole-Parmer digital hot plate stirrer was used for blending the polymers. The hot plate stirrer is programmable. All functions can be set from digital panel and

display their status on LCD. The plate temperature, stirrer speed and time are controllable.

4.2.10 Syringe, Needle and Septum

The syringe that were used in the experiment had a volume of 10 and 50 ml and the needle were No. 17 and 20, respectively. The septum was a silicone rod. They were used in order to prevent the surrounding air from entering into the glass bottle by blocking at the needle end. The solvent, catalyst, cocatalyst and monomer were introduced into a glass reactor by using needles.

4.3 Polymerization Procedure

4.3.1 Preparation of Catalyst

Cp^*TiCl_3 approximately 0.014 g was dissolved in 35 ml of toluene under argon atmosphere in glove box. The catalyst solution was stirred until the catalyst was completely soluble. The solution was used as a catalyst for styrene polymerization with modified-methylaluminoxane (MMAO) as a cocatalyst.

4.3.2 Preparation of Styrene Monomer

The styrene monomer was extracted with NaOH solution (5 % w/w) and distilled water, then distilled over sodium at 50 °C under vacuum atmosphere before use.

4.3.3 Styrene Polymerization

The styrene polymerization reaction was carried out in a 250 ml glass reactor with a magnetic stirrer. Polymerizations were carried out as follows: 46 ml of toluene, 32 ml of catalyst solution, 13.6 ml of cocatalyst solution and 28.4 ml of styrene monomer were injected into a 250 ml glass reactor with a magnetic stirrer at the

desired polymerization temperature under argon atmosphere. After the polymerization time was reached, the reaction was terminated by the addition of methanol and the addition of 10 % HCl in methanol was followed. The resulting precipitated polymer was washed with methanol and dried at room temperature.

The polymer was extracted with refluxing methyl ethyl ketone (MEK) for 12 hours in order to determine the syndiotactic index (S.I.) of the polymer obtained.

This study of styrene polymerization emphasized on the effect of polymerization temperatures, the conditions for styrene polymerization by using homogeneous half-metallocene catalyst system were specified as follows:

[Cp*TiCl ₃]	=	3.68×10 ⁻⁴ M
[MMAO]	=	1.83 M
[Styrene]	=	2.06 M
Al _{MMAO} /Ti mole ratio	=	563
Toluene	=	46 ml
Polymerization Time (t _p)	=	6 h, 1 h and 6 min
Polymerization Temperature (T _p)	=	0, 10 and 20 °C

4.4 Blend Polymer between Syndiotactic Polystyrene and Selected Polymers

The blend of syndiotactic polystyrene and selected polymers were prepared by using solvent casting method with various compositions. *o*-Dichlorobenzene (*o*-DCB) was used as a solvent. The solution was mixed together in order to have a uniform mixture and then cast on a glass slip into film and dried at room temperature. After that all the samples were preheated at 300 °C until the samples were completely melted and transparent, then immediately cooled to 200 °C and hold the temperature for 10 minutes and finally quenched to room temperature.

4.5 Polymer Characterization

The instruments used to characterize pure syndiotactic polystyrene and sPS blends were specified as follows:

4.5.1 Soxhlet Extractor

The Soxhlet extractor was used to determine the syndiotactic index (S.I.) of polystyrene. Polystyrene was weighed in the cellulose thimble and then was extracted in the Soxhlet extractor by using methyl ethyl ketone (MEK) as a solvent for 12 hours at the atmosphere. The syndiotactic polymer was isolated as MEK insoluble fraction. The resultant polymer was dried at room temperature. A % syndiotactic index (% S.I.) is computed from

$$\% \text{ S.I.} = (\text{Insoluble Weight of PS} / \text{Total Weight of PS}) \times 100$$

4.5.2 Differential Scanning Calorimetry (DSC)

The glass temperature (T_g), crystalline temperature (T_c) and crystalline melting temperature (T_m) of polymer were measured by using a Perkin-Elmer Diamond DSC. The heating rate of 20 °C/min in the temperature range 50 to 300 °C was employed. The heating cycle was run twice. The first scan, samples were heated and then cooled to room temperature. The second scan, samples were reheated at the same rate, both the results of the first and second scan were reported. In general, the first scan was influenced by the mechanical and thermal history (annealing) of samples but the second scan was influenced by the heat energy for endothermic and exothermic reaction within DSC instrument.

4.5.3 Gel Permeation Chromatography (GPC)

The weight average molecular weights (M_w), the number average molecular weights (M_n) and the molecular weight distributions (M_w/M_n) of syndiotactic

polystyrene were determined by GPC-220 at Thai Petrochemical Industry Public Co., Ltd. All of the samples were prepared accurately at a concentration of approximately 1.0-2.0 mg/ml in the mobile phase and dissolved by using PL-SP 260 at the temperature of 150 °C for approximately 3 hours. *o*-Dichlorobenzene (*o*-DCB) was used as a solvent. The dissolved samples were transferred into PL-GPC 220. The columns were calibrated with standard polystyrene.

4.5.4 X-ray Diffraction (XRD)

The crystallinity of polymer was analyzed by a Siemens D5000 X-ray diffractometer. The X-ray used was Ni filtered CuK α radiation. The XRD patterns of the crystallized polymer were obtained at room temperature and operated at 30 kV and 30 mA with a 2 θ scan of 0.04 °/s and the 2 θ range is 10-40 °.

CHAPTER V

RESULTS AND DISCUSSION

5.1 Polymerization of Styrene

5.1.1 The Effects of Polymerization Temperature on Catalytic Activity

The effects of various polymerization temperatures on styrene polymerization by using Cp^*TiCl_3 as a catalyst and modified-methylaluminoxane (MMAO) as a cocatalyst were investigated. The polymerization was operated in three different polymerization temperatures viz., 0, 10 and 20 °C. The experimental results indicated the relationship of polymerization temperatures, % yields and catalytic activities of polystyrene produced are shown in Table 5.1.

Table 5.1 % Yield and catalytic activity of polystyrene produced at various polymerization temperatures ^a

Polymerization Temperature (°C)	Yield (%)	Catalytic Activity (g PS / mmol Ti-hr)
0 ^b	11.47	11.13
10 ^c	13.95	79.48
20 ^d	15.22	885.42

^a Polymerization conditions : $[\text{Cp}^*\text{TiCl}_3] = 3.68 \times 10^{-4}$ M, $[\text{MMAO}] = 1.83$ M, $[\text{Styrene}] = 2.06$, Al/Ti = 563.

^{b, c, d} Polymerization time = 6 h, 1 h and 6 min, respectively.

Table 5.1 shows % yield of polystyrene increases as the polymerization temperature increases up to 20 °C. It may be attributed to the large equilibrium constant for monomer absorption (PO R. and Cardi N., 1996).

Similar to results of % yield, the catalytic activity increases as the polymerization temperature increases but it decreases with an increase in polymerization time. The decrease may be attributed to the deactivation of the active centers or to the occlusion of part of the catalyst in the precipitating polymer (Ishihara N., Kuramoto M. and Uoi M., 1988).

5.1.2 The Effects of Polymerization Temperature on Stereospecificity

The polystyrene products were extracted in the Soxhlet extraction by using methyl ethyl ketone (MEK) as a solvent for 12 hours at the atmosphere to determine the syndiotacticity. A % syndiotactic index (% S.I.) is calculated from the weight fraction of insoluble polystyrene. The syndiotacticity of polystyrene products with various polymerization temperatures are shown in Table 5.2.

Table 5.2 % Syndiotactic index (% S.I.) of polystyrene products at various polymerization temperatures ^a

Polymerization Temperature (°C)	Weight of Polystyrene Product		% Syndiotactic Index (% S.I.)
	Before Extracted (g)	After Extracted (g)	
0 ^b	2.9506	2.7589	93.50
10 ^c	3.5132	3.3148	94.35
20 ^d	3.9164	3.7209	95.01

^a Polymerization conditions : [Cp*TiCl₃] = 3.68×10⁻⁴ M, [MMAO] = 1.83 M, [Styrene] = 2.06, Al/Ti = 563.

^{b, c, d} Polymerization time = 6 h, 1 h and 6 min, respectively.

Table 5.2 shows the syndiotacticities of polystyrene produced with various polymerization temperatures. The increase in the polymerization temperature affords the polystyrene with slightly increasing syndiotacticity.

5.1.3 The Effects of Polymerization Temperature on Molecular Weight

The weight average molecular weights (M_w), the number average molecular weights (M_n) and the molecular weight distributions (M_w/M_n) of syndiotactic polystyrene were determined by gel permeation chromatography (GPC). The results can be shown in Table 5.3.

Table 5.3 Molecular weights and molecular weight distributions of syndiotactic polystyrene at various polymerization temperatures ^a

Polymerization Temperature (°C)	M_n	M_w	M_w/M_n
0 ^b (sPS3)	372,900	1,083,300	2.9
10 ^c (sPS1)	636,400	1,663,000	2.6
20 ^d (sPS2)	379,300	1,040,500	2.8

^a Polymerization conditions : $[Cp^*TiCl_3] = 3.68 \times 10^{-4}$ M, $[MMAO] = 1.83$ M, $[Styrene] = 2.06$, Al/Ti = 563.

^{b, c, d} Polymerization time = 6 h, 1 h and 6 min, respectively.

The three samples of sPS that ordered by the number average molecular weight (M_n) are named sPS1, sPS2 and sPS3, respectively.

5.2 Differential Scanning Calorimetry (DSC)

The glass transition temperatures (T_g), crystalline temperatures (T_c) and crystalline melting temperatures (T_m) of polymers were measured by using a DSC. The heating rate of 20 °C/min in the temperature range 50 to 300 °C was employed. The heating cycle was run twice. Before the first scan, the polymer blends were melted at 300°C and preheated at the isothermal crystallization condition at 200°C. Before the second scan, the polymer blends were cooling down at the constant cooling rate of 20 °C/min from 300°C to 50°C. T_c were detected and recorded during the cooling down circle. The second scan, samples were reheated at rate 20 °C/min from 50°C to 300°C, both the results of the first and second scan were reported. The results of syndiotactic polystyrenes are illustrated in Table 5.4 and sPS blends are illustrated in Table 5.5-5.10.

Table 5.4 Glass transition temperature (T_g), crystalline temperature (T_c) and crystalline melting temperature (T_m) of syndiotactic polystyrenes

Sample	T_{g1} (°C)	T_{g2} (°C)	T_c (°C)	T_{m1} (°C)	$T_{m2.1}$ (°C)	$T_{m2.2}$ (°C)
sPS1	97.28	97.41	243.25	268.88	263.53	271.21
sPS2	94.00	95.34	242.57	268.73	263.55	270.57
sPS3	93.48	94.19	240.78	268.69	263.14	270.17

From Table 5.4, T_g and T_m of all pure sPS increase with the increase M_n . sPS with higher M_n has much more phenyl groups in the chain, has a higher T_g and T_m (Ulrich H., 1993).

Table 5.5 Glass transition temperature (T_g), crystalline temperature (T_c) and crystalline melting temperature (T_m) of sPS/PBMA blends at various compositions (T_g of pure PBMA = 31.85 °C)

sPS1 (weight fraction)	T_{g1} (°C)	T_{g2} (°C)	T_c (°C)	T_{m1} (°C)	$T_{m2.1}$ (°C)	$T_{m2.2}$ (°C)
0.5	67.83	64.80	n.d.	n.d.	n.d.	n.d.
0.6	68.27	n.d.	210.10	254.43	249.58	n.d.
0.7	68.94	n.d.	213.69	255.21	250.34	n.d.
0.8	69.37	n.d.	214.77	255.58	251.07	n.d.
0.9	70.83	n.d.	234.25	265.30	262.90	n.d.
1.0	97.28	97.41	243.25	268.88	263.53	271.21

sPS2 (weight fraction)	T_{g1} (°C)	T_{g2} (°C)	T_c (°C)	T_{m1} (°C)	$T_{m2.1}$ (°C)	$T_{m2.2}$ (°C)
0.5	66.67	63.41	n.d.	n.d.	n.d.	n.d.
0.6	67.60	n.d.	n.d.	n.d.	n.d.	n.d.
0.7	67.73	n.d.	n.d.	n.d.	n.d.	n.d.
0.8	68.19	n.d.	n.d.	n.d.	n.d.	n.d.
0.9	69.29	n.d.	233.28	263.26	262.61	n.d.
1.0	94.00	95.34	242.57	268.73	263.55	270.57

sPS3 (weight fraction)	T_{g1} (°C)	T_{g2} (°C)	T_c (°C)	T_{m1} (°C)	$T_{m2.1}$ (°C)	$T_{m2.2}$ (°C)
0.5	64.56	61.72	n.d.	n.d.	n.d.	n.d.
0.6	65.75	n.d.	197.51	238.31	236.71	n.d.
0.7	66.12	n.d.	206.30	247.48	244.82	n.d.
0.8	66.98	n.d.	201.71	247.74	241.16	n.d.
0.9	67.64	n.d.	214.85	251.61	248.70	n.d.
1.0	93.48	94.19	240.78	268.69	263.14	270.17

From Table 5.5, all of the blends at various compositions exhibit single T_g , indicating the miscibility of the blends, which shifts to a higher temperature with increasing the sPS content and the increase M_n . T_m of these blends are lower than pure sPS.



สถาบันวิทยบริการ
จุฬาลงกรณ์มหาวิทยาลัย

Table 5.6 Glass transition temperature (T_g), crystalline temperature (T_c) and crystalline melting temperature (T_m) of sPS/PCHA blends at various compositions (T_g of pure PCHA = 25.81 °C)

sPS1 (weight fraction)	T_{g1} (°C)	T_{g2} (°C)	T_c (°C)	T_{m1} (°C)	$T_{m2.1}$ (°C)	$T_{m2.2}$ (°C)
0.5	63.61	64.14	n.d.	n.d.	n.d.	n.d.
0.6	69.52	72.02	223.84	261.90	261.49	n.d.
0.7	72.99	74.26	226.74	262.70	262.33	n.d.
0.8	76.18	77.42	230.97	261.89	261.92	n.d.
0.9	78.65	81.09	239.64	268.52	262.73	n.d.
1.0	97.28	97.41	243.25	268.88	263.53	271.21

sPS2 (weight fraction)	T_{g1} (°C)	T_{g2} (°C)	T_c (°C)	T_{m1} (°C)	$T_{m2.1}$ (°C)	$T_{m2.2}$ (°C)
0.5	59.05	60.89	n.d.	n.d.	n.d.	n.d.
0.6	60.64	63.08	223.94	263.88	263.48	n.d.
0.7	61.31	64.05	215.61	255.59	253.08	n.d.
0.8	62.12	65.15	215.39	262.69	249.87	n.d.
0.9	66.50	68.72	234.32	261.10	255.27	n.d.
1.0	94.00	95.34	242.57	268.73	263.55	270.57

sPS3 (weight fraction)	T_{g1} (°C)	T_{g2} (°C)	T_c (°C)	T_{m1} (°C)	$T_{m2.1}$ (°C)	$T_{m2.2}$ (°C)
0.5	53.68	56.69	n.d.	n.d.	n.d.	n.d.
0.6	55.18	58.80	223.87	261.09	261.5	n.d.
0.7	56.91	61.00	220.10	257.73	258.14	n.d.
0.8	58.57	61.96	216.89	258.70	255.76	n.d.
0.9	61.40	62.37	220.64	253.94	253.52	n.d.
1.0	93.48	94.19	240.78	268.69	263.14	270.17

From Table 5.6, all of the blends at various compositions exhibit single T_g , which increases with increasing the sPS content and the increase M_n .

Table 5.7 Glass transition temperature (T_g), crystalline temperature (T_c) and crystalline melting temperature (T_m) of sPS/PEMA blends at various compositions (T_g of pure PEMA = 65.54 °C)

sPS1 (weight fraction)	T_{g1} (°C)	T_{g2} (°C)	T_c (°C)	T_{m1} (°C)	$T_{m2.1}$ (°C)	$T_{m2.2}$ (°C)
0.5	73.12	73.90	216.60	255.05	256.48	n.d.
0.6	74.96	n.d.	203.94	228.19	245.44	n.d.
0.7	75.83	n.d.	203.23	247.16	243.70	n.d.
0.8	76.01	n.d.	207.10	246.83	246.52	n.d.
0.9	78.76	n.d.	225.79	260.77	258.13	n.d.
1.0	97.28	97.41	243.25	268.88	263.53	271.21

sPS2 (weight fraction)	T_{g1} (°C)	T_{g2} (°C)	T_c (°C)	T_{m1} (°C)	$T_{m2.1}$ (°C)	$T_{m2.2}$ (°C)
0.5	67.94	69.63	n.d.	n.d.	n.d.	n.d.
0.6	68.65	n.d.	195.46	228.12	235.55	n.d.
0.7	69.79	n.d.	199.36	245.38	240.51	n.d.
0.8	70.53	n.d.	213.94	249.86	247.81	n.d.
0.9	71.76	n.d.	212.97	252.02	247.86	n.d.
1.0	94.00	95.34	242.57	268.73	263.55	270.57

sPS3 (weight fraction)	T_{g1} (°C)	T_{g2} (°C)	T_c (°C)	T_{m1} (°C)	$T_{m2.1}$ (°C)	$T_{m2.2}$ (°C)
0.5	66.70	66.96	n.d.	n.d.	n.d.	n.d.
0.6	67.87	n.d.	204.01	250.44	246.31	n.d.
0.7	68.81	n.d.	199.66	240.62	238.66	n.d.
0.8	69.60	n.d.	216.81	255.53	251.02	n.d.
0.9	70.32	n.d.	199.21	245.61	236.55	n.d.
1.0	93.48	94.19	240.78	268.69	263.14	270.17

From Table 5.7, all of the blends at various compositions exhibit single T_g , which increases with increasing the sPS content and the increase M_n .

Table 5.8 Glass transition temperature (T_g), crystalline temperature (T_c) and crystalline melting temperature (T_m) of sPS/Poly(α -methylstyrene) blends at various compositions (T_g of pure Poly(α -methylstyrene) = 87.33 °C)

sPS1 (weight fraction)	T_{g1} (°C)	T_{g2} (°C)	T_c (°C)	T_{m1} (°C)	$T_{m2.1}$ (°C)	$T_{m2.2}$ (°C)
0.5	84.27	85.37	223.79	258.38	243.36	257.24
0.6	89.06	92.48	229.79	262.58	251.75	263.67
0.7	92.59	94.89	233.43	263.02	256.81	266.63
0.8	93.56	95.79	236.68	267.01	260.75	268.82
0.9	95.35	96.11	238.13	268.81	263.25	270.26
1.0	97.28	97.41	243.25	268.88	263.53	271.21

sPS2 (weight fraction)	T_{g1} (°C)	T_{g2} (°C)	T_c (°C)	T_{m1} (°C)	$T_{m2.1}$ (°C)	$T_{m2.2}$ (°C)
0.5	83.79	84.97	217.73	250.90	237.80	252.40
0.6	87.27	91.05	226.49	261.72	249.88	261.46
0.7	88.63	92.39	235.75	266.43	258.06	267.54
0.8	90.51	93.31	237.86	267.13	259.81	268.57
0.9	92.86	94.92	240.86	268.43	262.87	269.90
1.0	94.00	95.34	242.57	268.73	263.55	270.57

sPS3 (weight fraction)	T_{g1} (°C)	T_{g2} (°C)	T_c (°C)	T_{m1} (°C)	$T_{m2.1}$ (°C)	$T_{m2.2}$ (°C)
0.5	77.26	79.17	207.31	241.54	229.59	246.80
0.6	80.01	83.75	221.43	253.57	240.74	255.84
0.7	85.08	86.55	215.80	252.60	235.14	250.93
0.8	89.46	92.23	224.18	257.68	241.30	256.39
0.9	91.31	93.67	225.53	256.56	242.24	257.67
1.0	93.48	94.19	240.78	268.69	263.14	270.17

From Table 5.8, all of the blends at various compositions exhibit single T_g , which increases with increasing the sPS content and the increase M_n .

Table 5.9 Glass transition temperature (T_g), crystalline temperature (T_c) and crystalline melting temperature (T_m) of sPS/Polyisoprene blends at various compositions (T_g of pure Polyisoprene = -47.02 °C)

sPS1 (weight fraction)	T_{g1} (°C)	T_{g2} (°C)	T_c (°C)	T_{m1} (°C)	$T_{m2.1}$ (°C)	$T_{m2.2}$ (°C)
0.5	70.17	63.51	n.d.	n.d.	n.d.	n.d.
0.6	74.66	71.15	217.20	259.04	261.54	n.d.
0.7	76.85	73.10	221.37	263.16	264.87	n.d.
0.8	77.90	80.45	220.94	260.68	259.44	n.d.
0.9	78.83	82.23	225.12	258.83	257.51	n.d.
1.0	97.28	97.41	243.25	268.88	263.53	271.21

sPS2 (weight fraction)	T_{g1} (°C)	T_{g2} (°C)	T_c (°C)	T_{m1} (°C)	$T_{m2.1}$ (°C)	$T_{m2.2}$ (°C)
0.5	45.12	49.73	217.76	250.60	253.22	n.d.
0.6	58.83	63.28	217.16	259.82	263.96	n.d.
0.7	60.03	64.57	221.72	261.45	265.23	n.d.
0.8	70.14	71.12	223.84	262.27	262.67	n.d.
0.9	73.43	73.64	236.72	265.45	265.90	n.d.
1.0	94.00	95.34	242.57	268.73	263.55	270.57

sPS3 (weight fraction)	T_{g1} (°C)	T_{g2} (°C)	T_c (°C)	T_{m1} (°C)	$T_{m2.1}$ (°C)	$T_{m2.2}$ (°C)
0.5	44.18	45.75	220.94	255.86	257.91	n.d.
0.6	48.16	52.16	215.97	259.04	261.51	n.d.
0.7	56.82	53.38	218.90	261.53	262.38	n.d.
0.8	61.22	57.67	225.99	263.60	264.00	n.d.
0.9	69.28	73.99	225.95	256.89	256.91	n.d.
1.0	93.48	94.19	240.78	268.69	263.14	270.17

From Table 5.9, all of the blends at various compositions exhibit single T_g , which increases with increasing the sPS content and the increase M_n .

Table 5.10 Glass transition temperature (T_g), crystalline temperature (T_c) and crystalline melting temperature (T_m) of sPS/PVME blends at various compositions (T_g of pure PVME = -27.10 °C)

sPS1 (weight fraction)	$T_{g1.1}$ (°C)	$T_{g1.2}$ (°C)	T_{g2} (°C)	T_c (°C)	T_{m1} (°C)	$T_{m2.1}$ (°C)	$T_{m2.2}$ (°C)
0.5	-24.19	46.13	-20.10	218.15	265.00	267.19	n.d.
0.6	-23.73	47.84	-18.47	227.16	266.26	267.81	n.d.
0.7	-22.31	50.29	-17.82	223.49	262.08	264.66	n.d.
0.8	56.91	56.91	57.02	234.85	265.16	265.69	n.d.
0.9	57.14	57.14	57.51	237.13	268.19	268.17	n.d.
1.0	97.28	97.28	97.41	243.25	268.88	263.53	271.21

sPS2 (weight fraction)	$T_{g1.1}$ (°C)	$T_{g1.2}$ (°C)	T_{g2} (°C)	T_c (°C)	T_{m1} (°C)	$T_{m2.1}$ (°C)	$T_{m2.2}$ (°C)
0.5	-22.80	50.37	-17.13	215.86	262.69	267.12	n.d.
0.6	-22.10	53.49	-16.11	219.36	264.67	266.70	n.d.
0.7	-21.72	55.32	-15.97	223.96	263.58	266.71	n.d.
0.8	57.76	57.76	57.98	221.90	259.44	261.53	n.d.
0.9	58.22	58.22	58.90	236.32	269.70	269.73	n.d.
1.0	94.00	94.00	95.34	242.57	268.73	263.55	270.57

sPS3 (weight fraction)	$T_{g1.1}$ (°C)	$T_{g1.2}$ (°C)	T_{g2} (°C)	T_c (°C)	T_{m1} (°C)	$T_{m2.1}$ (°C)	$T_{m2.2}$ (°C)
0.5	-22.23	52.19	-15.79	228.63	265.13	265.64	n.d.
0.6	-21.53	56.60	-14.90	219.83	263.59	266.17	n.d.
0.7	-21.01	57.43	-14.26	221.36	262.53	265.12	n.d.
0.8	58.86	58.86	59.54	220.81	262.00	263.36	n.d.
0.9	59.37	59.37	60.15	228.63	265.13	265.64	n.d.
1.0	93.48	93.48	94.19	240.78	268.69	263.14	270.17

From Table 5.10, all of the blends with PVME contents higher than 20 wt% show two T_g , indicates that the sPS/PVME blends are phase separated. The highest T_g could be due to an sPS-rich phase and the other to a PVME-rich phase.



สถาบันวิทยบริการ
จุฬาลงกรณ์มหาวิทยาลัย

5.3 X-Ray Diffraction (XRD)

The crystallinity of polymers are estimated by X-ray diffractometer. X-ray diffractograms and % crystallinity of syndiotactic polystyrenes and sPS blends are as follow.

The % crystallinity is computed from

$$x_c = \frac{\int_{s_0}^{s_p} s^2 I_c ds}{\int_{s_0}^{s_p} s^2 I ds} \left(K(s_0, s_p, D, \bar{f}^2) \right) = \text{const.}$$

where s_0 = function of minimum angle

s_p = function of maximum angle

I = the intensity of coherent X-ray scatter from a specimen

I_c = the part of the intensity at the same point that is concentrated in the crystalline peaks (reciprocal lattice point)

$\left(K(s_0, s_p, D, \bar{f}^2) \right)$ is lost from peaks and appears as diffuse scatter in the background as a result of atomic thermal vibrations and lattice imperfections. K can be found from the empirical chart and can be assume as a constant for each system, because the s is in the range of 0.1-0.3 which all k will gave the value of K in the range of 1.0-1.2. Therefore, in this thesis, the K were assume to be constant at 1.0. More over the back scattering at s equal 0.1-0.3 is extremely low so the total scattering will be assume as the integration of the $s^2 I$ without the deductions.

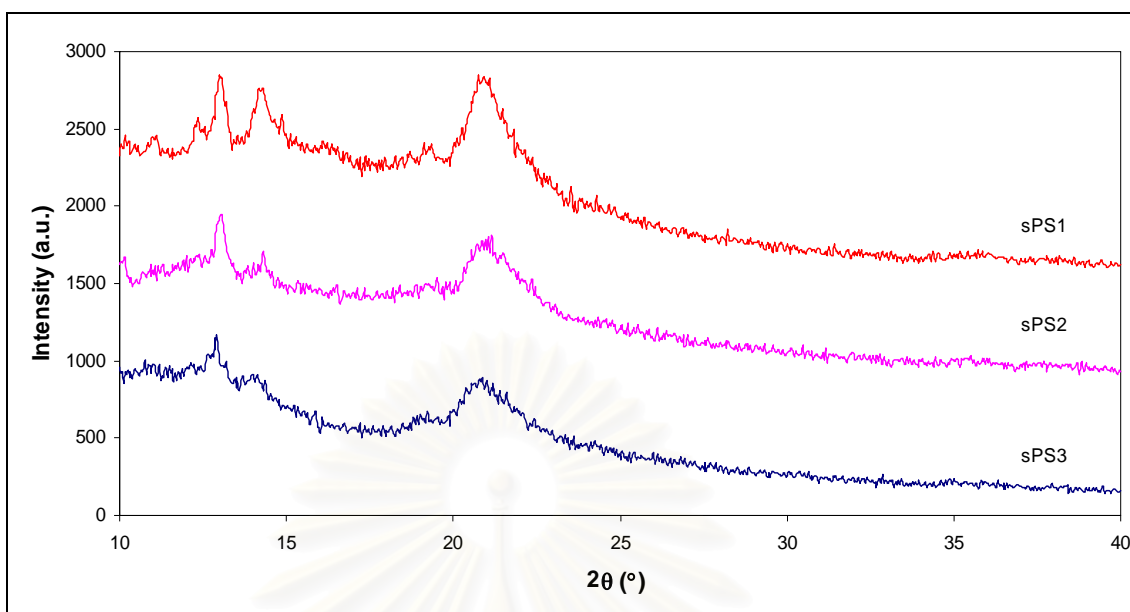


Figure 5.1 X-ray diffractogram of syndiotactic polystyrenes

Table 5.11 % Crystallinity of syndiotactic polystyrenes

Sample	% Crystallinity
sPS1	52.38
sPS2	36.72
sPS3	42.21

From the Table 5.11, syndiotactic polystyrenes has different crystallinity. sPS1 has the highest crystallinity.

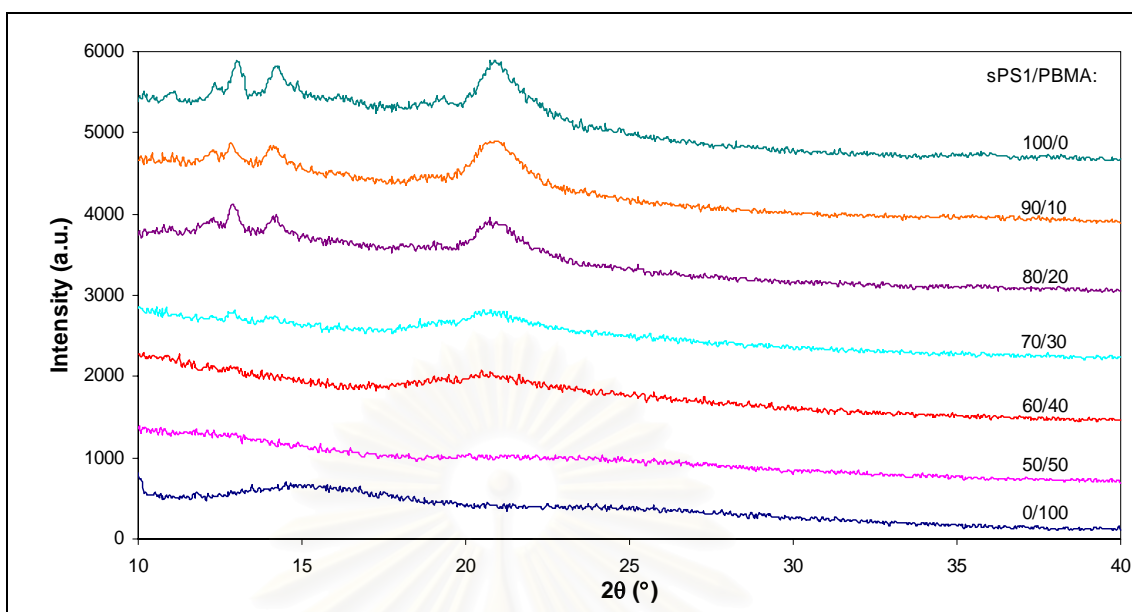


Figure 5.2 X-ray diffractogram of sPS1/PBMA blends at various compositions

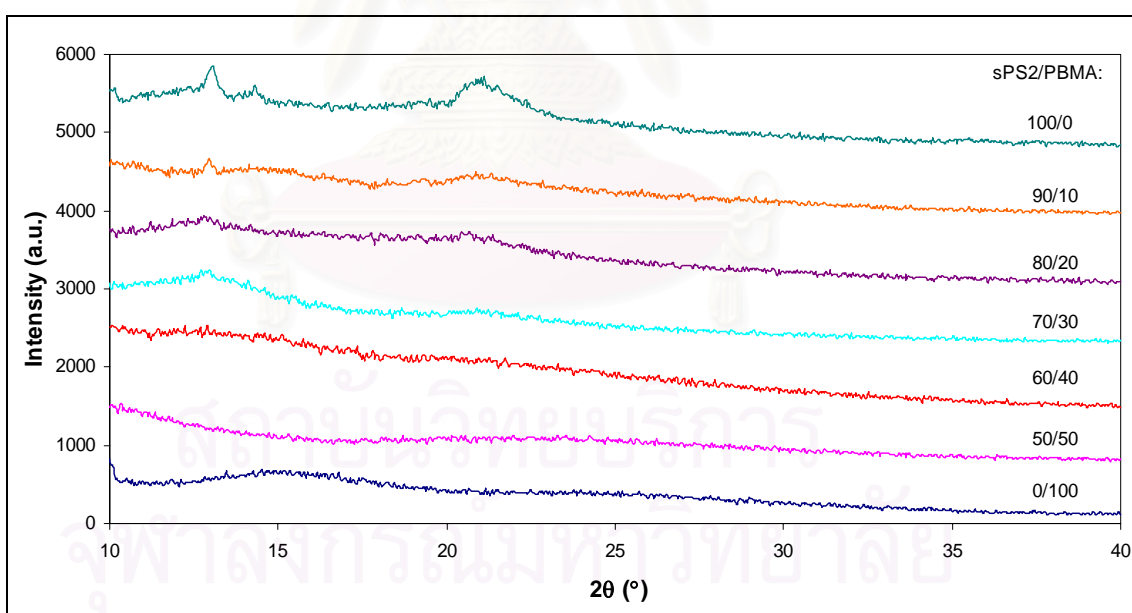


Figure 5.3 X-ray diffractogram of sPS2/PBMA blends at various compositions

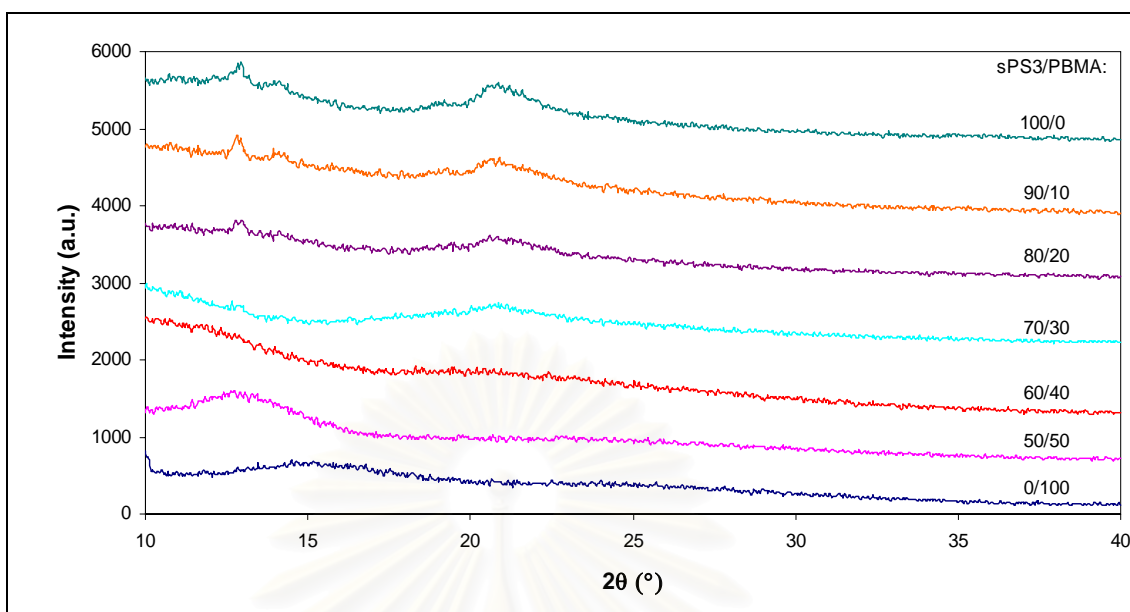


Figure 5.4 X-ray diffractogram of sPS3/PBMA blends at various compositions

Table 5.12 % Crystallinity of sPS/PBMA blends at various compositions

sPS (weight fraction)	% Crystallinity		
	sPS1/PBMA	sPS2/PBMA	sPS3/PBMA
0.5	24.29	32.96	27.02
0.6	24.85	27.31	25.88
0.7	27.08	35.63	31.03
0.8	44.21	34.59	34.78
0.9	44.22	28.05	39.05
1.0	52.38	36.72	42.21

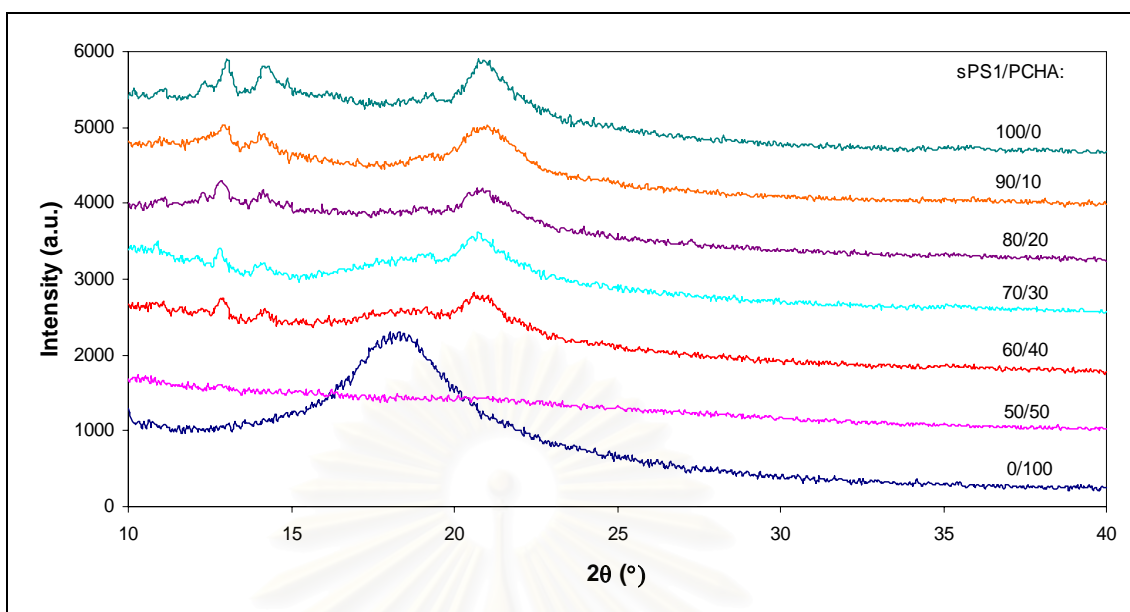


Figure 5.5 X-ray diffractogram of sPS1/PCHA blends at various compositions

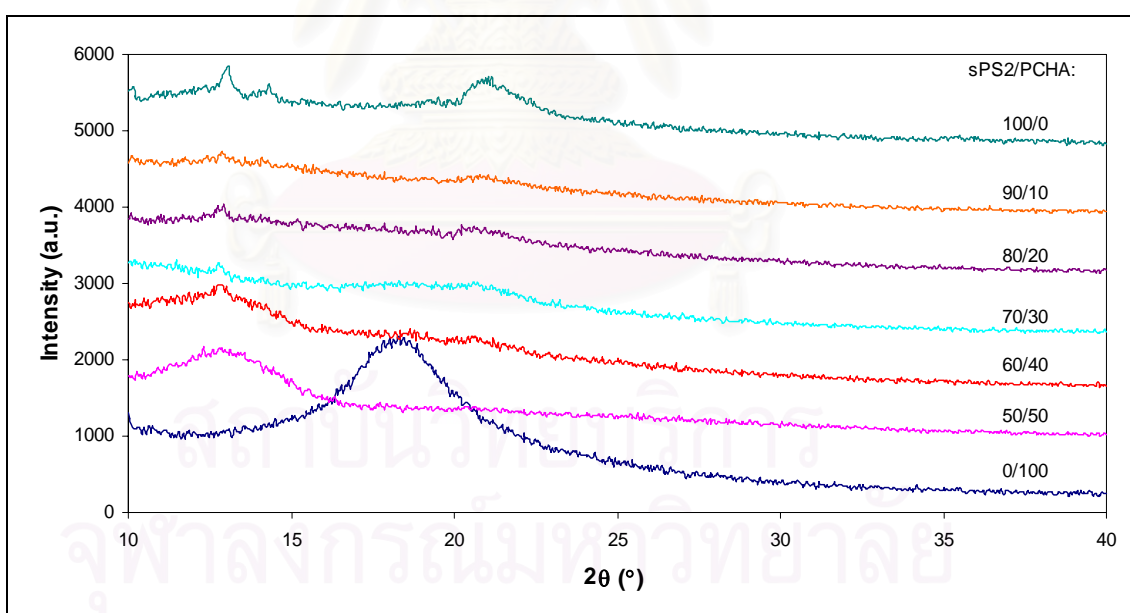


Figure 5.6 X-ray diffractogram of sPS2/PCHA blends at various compositions

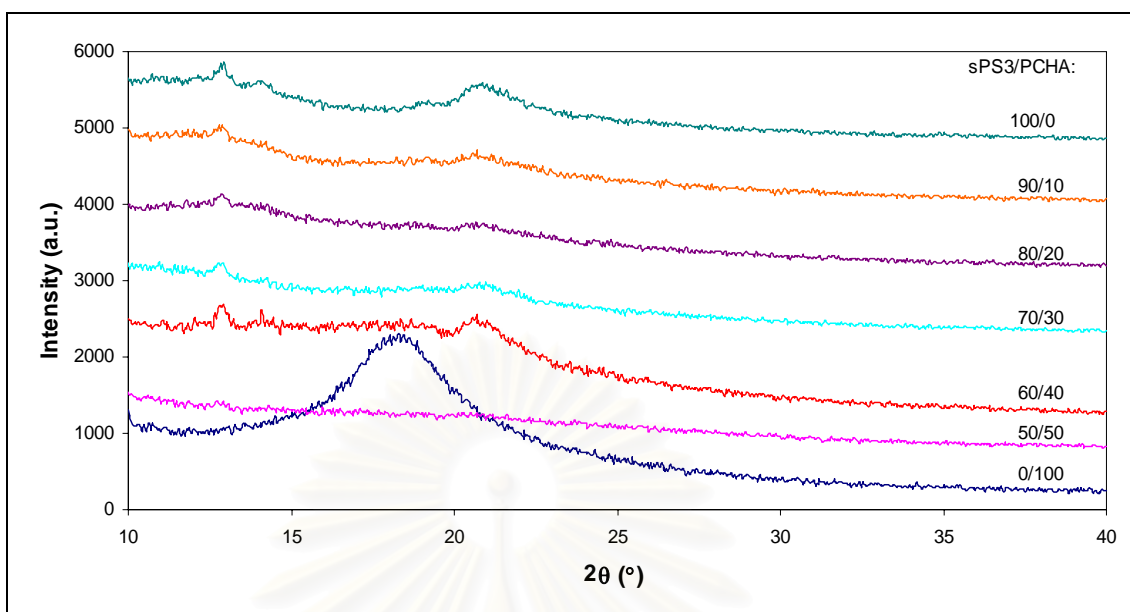


Figure 5.7 X-ray diffractogram of sPS3/PCHA blends at various compositions

Table 5.13 % Crystallinity of sPS/PCHA blends at various compositions

sPS (weight fraction)	% Crystallinity		
	sPS1/PCHA	sPS2/PCHA	sPS3/PCHA
0.5	42.21	35.01	41.93
0.6	35.87	34.94	36.36
0.7	40.77	35.16	40.36
0.8	37.52	34.59	40.42
0.9	38.88	34.80	36.30
1.0	52.38	36.72	42.21

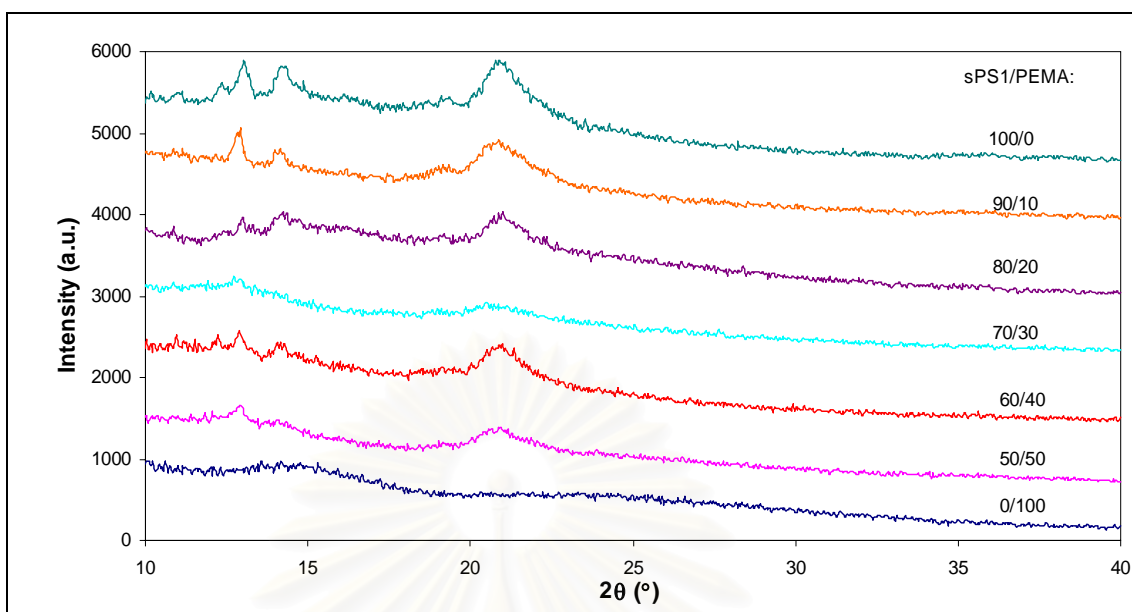


Figure 5.8 X-ray diffractogram of sPS1/PEMA blends at various compositions

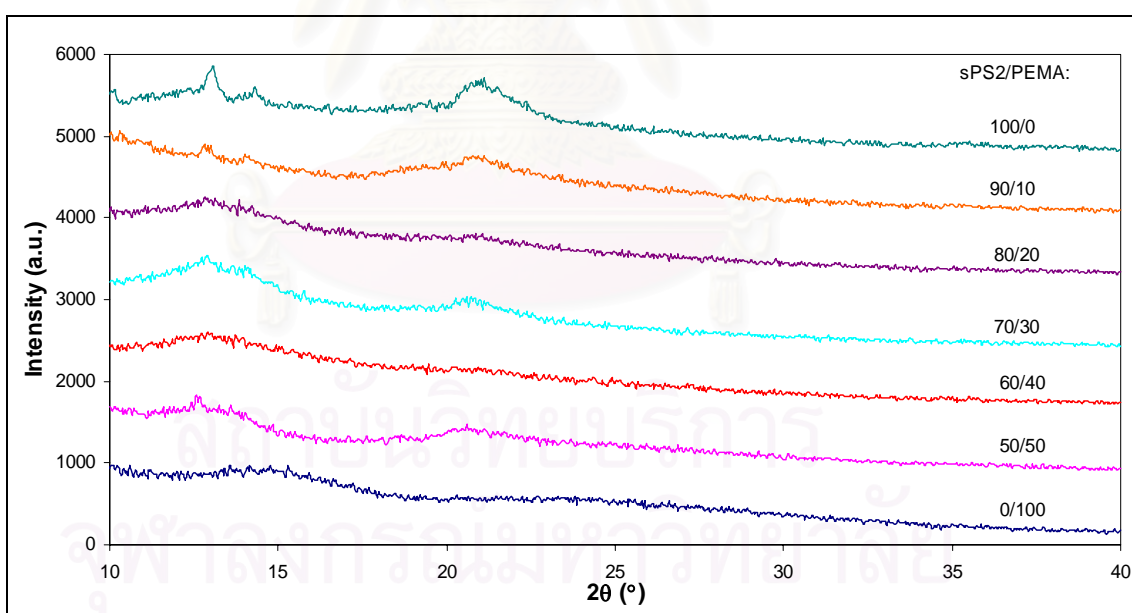


Figure 5.9 X-ray diffractogram of sPS2/PEMA blends at various compositions

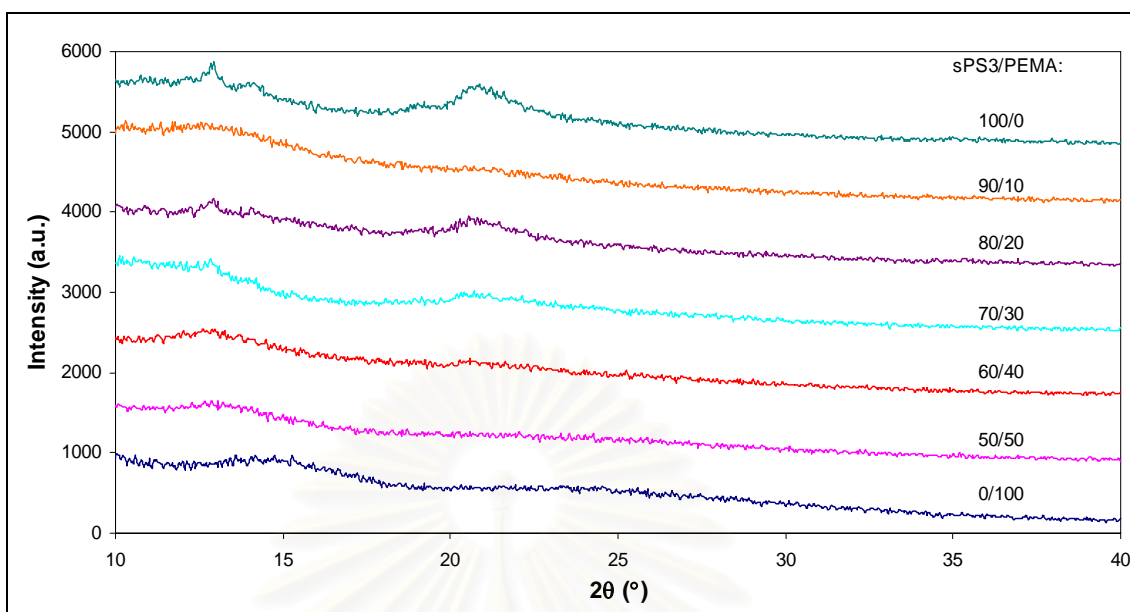


Figure 5.10 X-ray diffractogram of sPS3/PEMA blends at various compositions

Table 5.14 % Crystallinity of sPS/PEMA blends at various compositions

sPS (weight fraction)	% Crystallinity		
	sPS1/PEMA	sPS2/PEMA	sPS3/PEMA
0.5	27.79	29.20	32.72
0.6	32.19	31.55	33.53
0.7	33.58	32.40	32.68
0.8	31.78	34.01	33.01
0.9	42.51	34.87	37.17
1.0	52.38	36.72	42.21

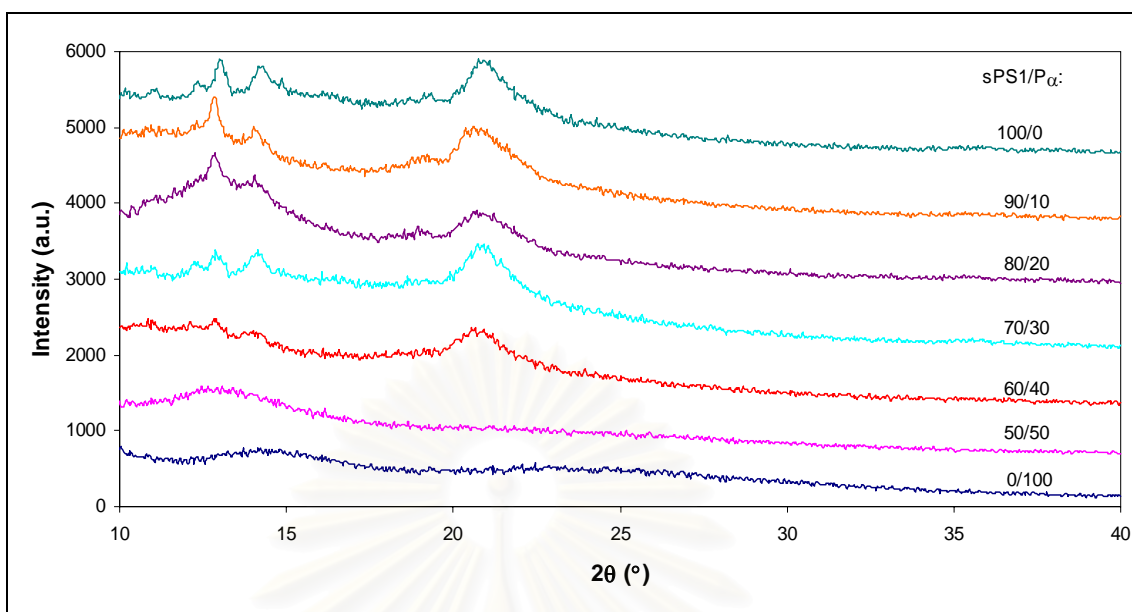


Figure 5.11 X-ray diffractogram of sPS1/Poly(α -methylstyrene) blends at various compositions

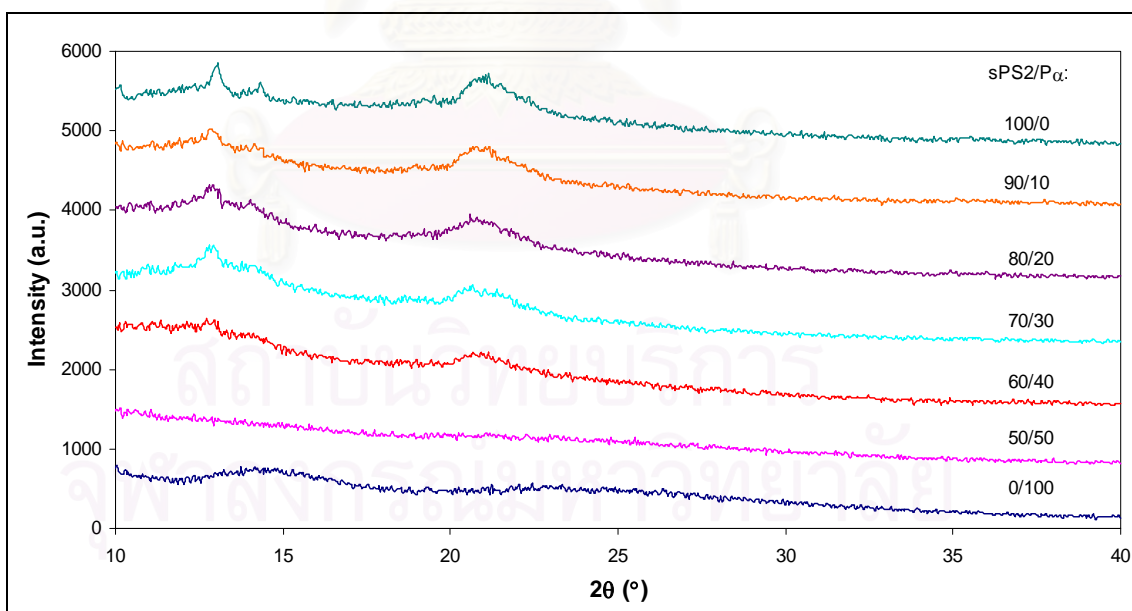


Figure 5.12 X-ray diffractogram of sPS2/Poly(α -methylstyrene) blends at various compositions

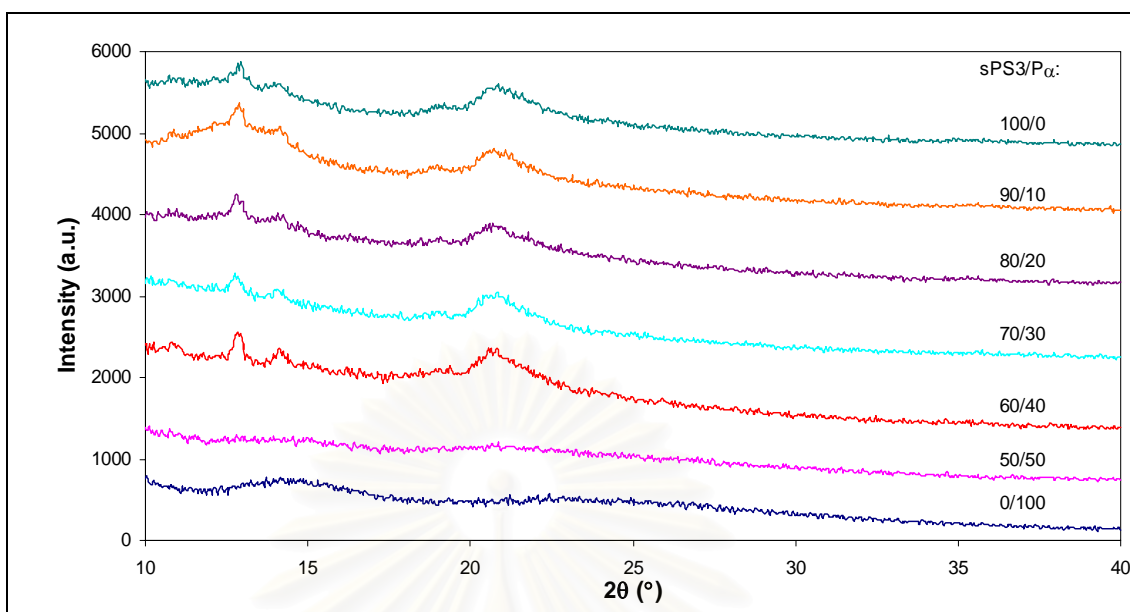


Figure 5.13 X-ray diffractogram of sPS3/Poly(α -methylstyrene) blends at various compositions

Table 5.15 % Crystallinity of sPS/Poly(α -methylstyrene) blends at various compositions

sPS (weight fraction)	% Crystallinity		
	sPS1/P α	sPS2/P α	sPS3/P α
0.5	34.54	24.78	21.01
0.6	41.83	34.10	40.16
0.7	43.91	35.80	39.55
0.8	49.00	36.29	39.71
0.9	49.69	36.44	39.33
1.0	52.38	36.72	42.21

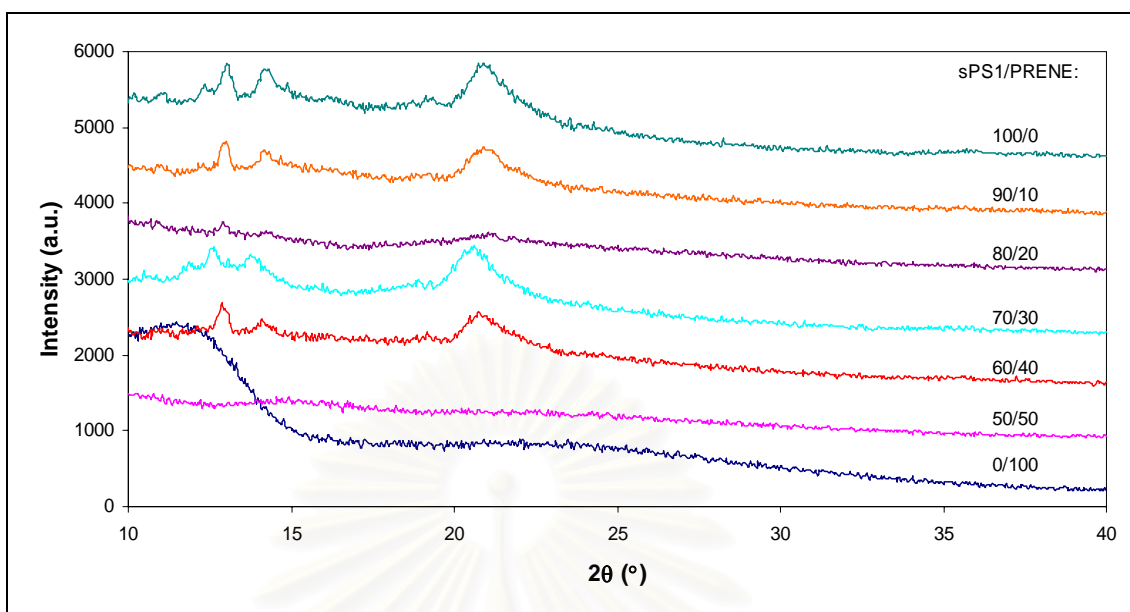


Figure 5.14 X-ray diffractogram of sPS1/Polysoprene blends at various compositions

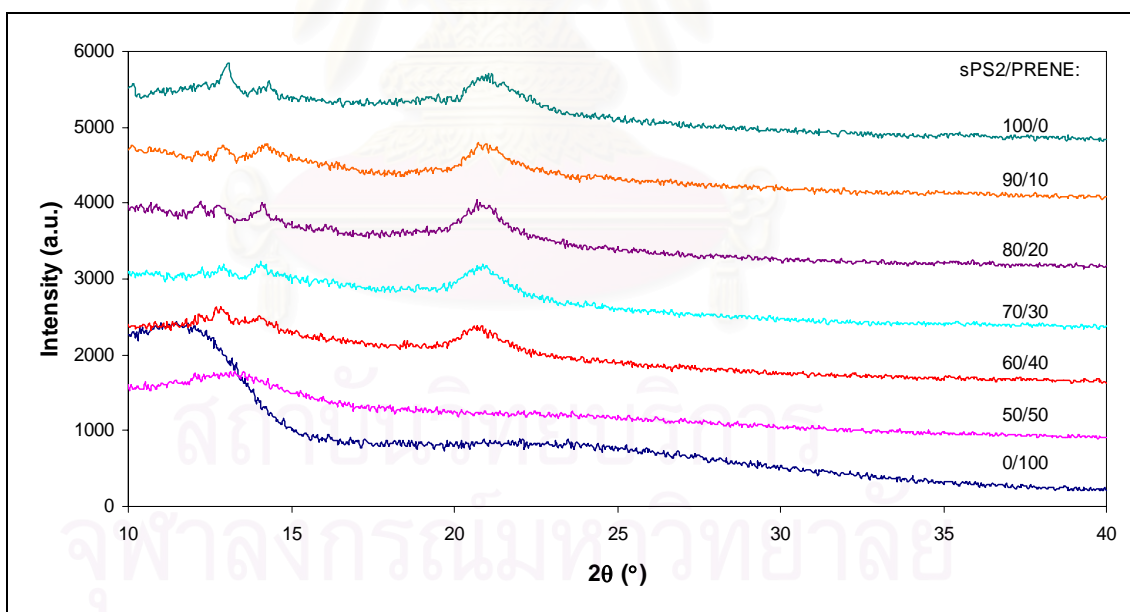


Figure 5.15 X-ray diffractogram of sPS2/Polysoprene blends at various compositions

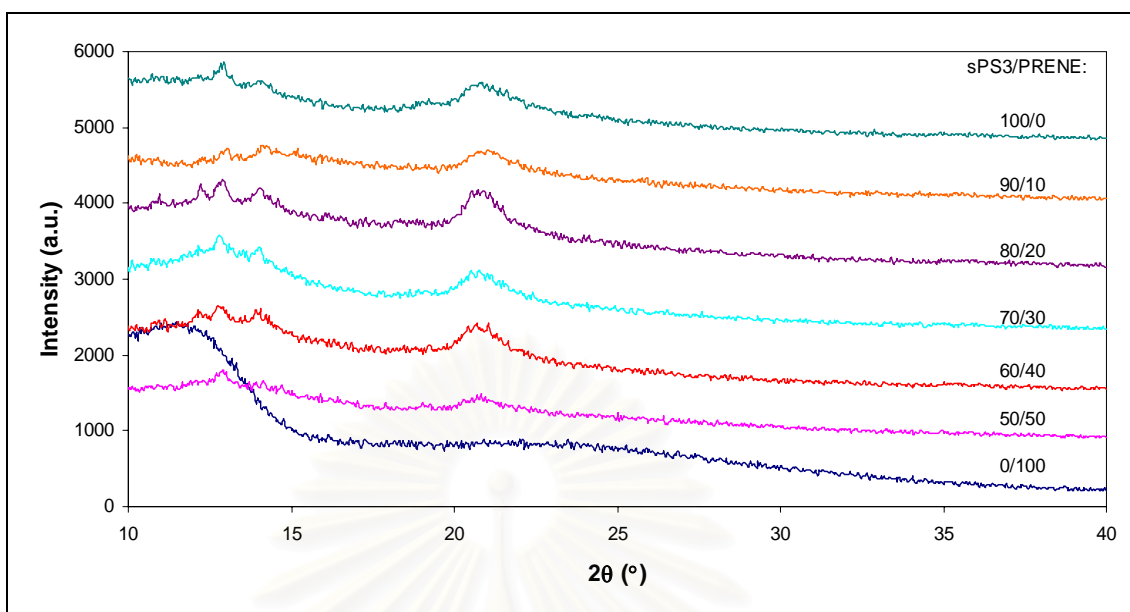


Figure 5.16 X-ray diffractogram of sPS3/Polyisoprene blends at various compositions

Table 5.16 % Crystallinity of sPS/Polyisoprene blends at various compositions

sPS (weight fraction)	% Crystallinity		
	sPS1/Prene	sPS2/Prene	sPS3/Prene
0.5	46.75	28.82	34.60
0.6	42.34	32.64	34.94
0.7	34.19	34.64	35.01
0.8	30.92	35.94	35.11
0.9	33.94	29.48	33.25
1.0	52.38	36.72	42.21

5.4 The Comparison of the DSC and XRD Results

5.4.1 Conformation of DSC and XRD on Crystalline Melting Temperature (T_m), Glass Transition Temperature (T_g) and % Crystallinity of Polymer Blends

The crystalline melting temperature in the first scan (T_{m1}) from the DSC results (see Table 5.5-5.9) correspond to % crystallinity from the XRD results (see Table 5.12-5.16), which have the same trend in all blends. These might be because of T_{m1} and % crystallinity are measured from the similar samples which were isothermal crystallized at 200 °C for 10 minutes after melt the samples at 300 °C, while T_{m2} have the effects from the constant ramp rate at 20 °C/min cooling down in the DSC after the first scan. Both of the first and the second scan were operated up to 300 °C

When the amorphous polymer was added to the pure sPS, the effects of all sPS are the decline of % crystallinity, especially in sPS1. These situations correspond to the decrease of the glass transition temperature (T_g) from the DSC results (see Table 5.5-5.9). The T_g of sPS blends at content of 10 wt% of amorphous polymer (90%wt sPS) obviously decrease. These decrease usually happened except sPS/Poly(α -methylstyrene) blends which might be resulted from the same vicinity of the T_g of both pure polymers.

5.4.2 Conformation of DSC and XRD on Glass Transition Temperature (T_g) and Weight Fraction of sPS in amorphous of Polymer Blends

The weight fraction of sPS in amorphous from XRD and Flory-Fox equation ^a of sPS blends at various compositions are shown in Table 5.17-5.21.

$$^a \text{ Flory-Fox equation : } 1/T_g = w_1/T_{g1} + w_2/T_{g2} ;$$

where 1 and 2 represent sPS and amorphous polymer, respectively; w_i is the weight fraction of component i.

Table 5.21 Weight fraction of sPS in amorphous from XRD and Flory-Fox equation of sPS/Polyisoprene blends at various compositions

sPS (weight fraction)	sPS1/Prene		sPS2/Prene		sPS3/Prene	
	XRD	Fox	XRD	Fox	XRD	Fox
0.5	0.0611	0.8543	0.2976	0.7093	0.2354	0.7048
0.6	0.3063	0.8800	0.4062	0.7995	0.3852	0.7320
0.7	0.5441	0.8923	0.5410	0.8070	0.5384	0.7889
0.8	0.7105	0.8982	0.6878	0.8685	0.6918	0.8167
0.9	0.8486	0.9033	0.8582	0.8877	0.8502	0.8657
1.0	1.0000	1.0000	1.0000	1.0000	1.0000	1.0000

From Table 5.17-5.21, the glass transition temperature (T_g) that measured from the DSC can be calculated back to predict the composition of sPS in the blend according to the Flory-Fox equation. The weight fraction of sPS in amorphous can be calculated from the XRD results. Both methods predicted the increase in the T_g at higher percent of sPS. However, the quantity of the weight percent of sPS in the amorphous predicted by % crystallinity and Flory-Fox equation are not the same.

The weight fraction of sPS in amorphous from Fox equation of sPS/Poly(α -methylstyrene) blends differ from other blends that are some early compositions have minus values due to T_g of blends are lower than both pure polymers. Flory-Fox equation predict the addition of the T_g gradually increase from the lower pure T_g of the polymer to the higher pure T_g of another polymer. So, it cannot predict the synergistic condition of the system.

5.4.3 Conformation of DSC and XRD on Glass Transition Temperature (T_g), % Crystallinity and Number Average Molecular Weight (M_n) of sPS of Polymer Blends

Both T_g and % crystallinity of sPS2 and sPS3 blends have the same quantity (in error limit of less than $\pm 5\%$). These might be because of the M_n of both sPS are in

the same vicinity. Therefore sPS1 and Pichet's sPS (sPS0) that have close M_n should be have the same T_g and % crystallinity in blends. However the T_g of those two set of data are not within the error limit. Those could be because of the different blend preparation methods (melt mixing and solvent casting). The % crystallinities of sPS0 and sPS1 blends at various compositions have the same values (in error limit of less than $\pm 5\%$). However sPS0 blends tended to have higher quantity than sPS1 in the acrylate polymers (PBMA, PCHA and PEMA). These may happen because of the solvent during the mixing condition have some effects in sPS1 blends.

5.5 The Comparison between the Acrylate Polymers

The T_g of sPS/PEMA blends at various composition have the highest T_g due to the highest T_g of pure PEMA. The T_g of sPS/PCHA blends at various composition have the lowest T_g , due to the lowest T_g of pure PCHA (see Table 5.5-5.7).

sPS/PCHA blends at low sPS content have higher % crystallinity than other acrylate blends. Nevertheless, sPS/acrylate blends at high sPS content have the same quantity of % crystallinity.

sPS/acrylate blends tended to have the higher trend of % crystallinity than Poly(α -methylstyrene) and Polyisoprene blends.

5.6 Crystal Structure

From all of the data in this work, we cannot find clearly the intensities of the diffraction peaks located at $2\theta = 11.6$ and 12.2° that are employed to estimate the content of the α form in the crystals. The peak and the area under the peak are not clearly specified which unclear data may result in the interpretation of the systems. However, the peaks around 11.6° are small results in the less likely form α crystals.

CHAPTER VI

CONCLUSIONS AND RECOMMENDATIONS

6.1 Conclusions

The conclusions of this research are summarized as follows :

1. Yield of polystyrene increases as the polymerization temperature increases.
2. The catalytic activity increases as the polymerization temperature increases but it decreases with an increase in polymerization time.
3. The increase in the polymerization temperature affords the polystyrene with slightly increasing syndiotacticity.
4. T_g and T_m of all pure sPS increase with the increase M_n .
5. All of the blends except sPS/PVME blends at various compositions exhibit single T_g which shifts to a higher temperature with increasing the sPS content and the increase M_n .
6. sPS/PVME blends at PVME contents higher than 20 wt% show two T_g , indicates that the sPS/PVME blends are phase separated.
7. T_m of sPS blends are lower than pure sPS.
8. The crystalline melting temperature in the first scan (T_{m1}) correspond to % crystallinity which have the same trend in all blends.
9. When the amorphous polymer were added, they affect to % crystallinity of all pure sPS decrease, especially in sPS1. They correspond to T_g of sPS blends at the

amorphous polymer content 10 wt% obviously decrease except sPS/Poly(α -methylstyrene) blends.

10. T_g accord to the weight fraction of sPS in amorphous from the XRD results and Fox equation which increase as the sPS content.

11. T_g and % crystallinity of sPS2 and sPS3 blends have the close values (in error limit of less than $\pm 5\%$).

12. T_g of sPS/PEMA blends have the highest T_g , they due to pure PEMA has the highest T_g

6.2 Recommendations for Further Studies

The recommendations for further studies are as follows:

1. It should be interested to study the mechanical properties of these blends at sPS content 90 wt% due to T_g at this composition obviously decrease.
2. It should be investigated the M_n of sPS that have much more different M_n that might be seen the clear differences.
3. It should be investigated the M_n of sPS that lower than this work because it might be displayed the differences more than one.
4. It should be investigated the other annealing temperatures that might be affected to % crystallinity.
5. It should be investigated the other cooling rates that might be affected to T_m and % crystallinity.

6. It should be investigated the other equations that use to calculate the weight fraction of sPS in amorphous which give the positive values.



สถาบันวิทยบริการ
จุฬาลงกรณ์มหาวิทยาลัย

REFERENCES

- Alexander Leroy E. *X-ray Diffraction Method in Polymer Science*. John Wiley & Son, Inc., New York, USA, 1969.
- Bhoje Gowd E.; Nair S. S.; and Ramesh C. *Macromolecules*, 2002; 35(22): 8509-8514.
- Chatani Y.; Shimane Y., Inoue Y.; Inagaki T. and Ishioka T. *Polymer*, 1992; 33: 488-492.
- Cimmino S. Di Pace E.; Martuscelli E.; and Silvestre C. *Polymer*, 1993; 34: 214-217.
- Cimmino S.; Di Pace E.; Martuscelli E.; and Silvestre C. *Polymer*, 1993; 34: 2799-2803.
- Fang-Chyou Chiu; and Chi-Gong Peng. *Polymer*, 2002; 43: 4879-4886.
- Fang-Chyou Chiu; and Ming-Te Li. *Polymer*, 2003; 44: 8013-8023.
- Fan R.; Cao K.; Li B., Fan H.; and Li B. G. *European Polymer Journal*, 2001; 37: 2335-2338.
- Giannetti E.; Nicoletti G. M.; and Mazzocchi R. *J Polym Sci Polym Chem Ed*, 1985: 2117.
- Guerra G.; De Rosa C.; Vitagliano V. M.; Petraccone V; and Corradini P. *Polymer Communications*, 1991; 32: 30-32.
- Guerra G.; Vitagliano V. M.; De Rosa C.; Petraccone V.; and Corradini P. *Macromolecules*, 1990; 23(5): 1539-1544.
- Hong B. K.; Jo H. W.; Lee S. C.; and Kim J. *Polymer*, 1998; 39: 1793-1797.
- Ishihara N.; Seimiya T.; Kuramoto M.; and Uoi M. *Macromolecules*, 1986; 19(9): 2464-2465.
- Ishihara N.; Kuramoto M.; and Uoi M. *Macromolecules*, 1988; 21(12): 3356-3360.
- Kaminsky W.; Lenk S.; Scholz V.; Roesky H. W.; Herzog A. *Macromolecules*, (Article), 1997; 30(25): 7647-7650.
- Kim Y.; and Do Y. *Journal of Organometallic Chemistry*, 2002; 655 : 186-191.
- Kim Y.; Koo B. H.; and Do Y. *Journal of Organometallic Chemistry*, 1997; 527 :155-161.
- Kricheldorf Hans R. *Handbook of Polymer Synthesis*, Part A, Marcel Dekker, Inc., New York, 1992.

- Kucht A.; Kucht H.; Barry S.; Chien J. C. W.; and Rausch M. D. *Organometallics*, 1993; 12(8): 3075-3078.
- Lyu Y. Y.; Byun Y.; Yim J. H.; Chang S.; Lee S. Y.; Pu L. S.; and Lee I. K. *European Polymer Journal*, 2004; 40: 1051–1056.
- McCrum N. G. *et al. Principles of Polymer Engineering*. Oxford University Press, New York, 1998.
- Nomura K.; and Fudo A. *Catalysis Communications*, 2003; 4: 269–274.
- Odian G. *Principles of Polymerization*. 3rd ed. John Wiley & Son, 1991.
- Pahupongsab P. *Effects of Low Molar Mass Liquid Crystal Addition on the Miscibility of Syndiotactic Polystyrene Blends*. Master's Degree Thesis, Department of Chemical Engineering, Faculty of Engineering, Graduate School, Chulalongkorn University, 2004.
- PO R.; and Cardi N. *Progress in Polymer Science*, 1996; 21: 47-88.
- Qing Wu; Zhong Ye and Shangan Lin *Macromol. Chem. Phys.*, 1977: 1823-1828.
- Ready T. E.; Chein J. C. W.; and Rausch M. D. *Journal of Organometallic Chemistry*, 1996; 519: 21-28.
- Rosen Stephen L. *Fundamental Principles of Polymeric Materials*. 2nd ed. John Wiley & Son, Inc., 1993.
- Schneider N.; Propenc M. H.; and Brintzinger H. H. *Journal of Organometallic Chemistry*; 545-546 (1997) : 291-295.
- Sperling L. H. *Introduction to Physical Polymer Science*. 3rd ed. New York : John Wiley & Son, 2001.
- Takebe T.; Funaki K., Yamasaki K. in *4th SPSJ International Polymer Conference*, Yokohama, 1992: 175.
- Ulrich H. *Introduction to Industrial Polymers*. 2nd ed. Hanser Publisher, 1993.
- Wang C.; Liao W. P.; Cheng Y. W.; and Lin T. L. *Polymer*, 2004; 45: 961–971.
- Woo E.M.; Sun Y.S.; and Yang C.P. *Progress in Polymer Science*, 2001; 26: 945-983.



APPENDICES

สถาบันวิทยบริการ
จุฬาลงกรณ์มหาวิทยาลัย

Appendix A: The Data of DSC Characterization

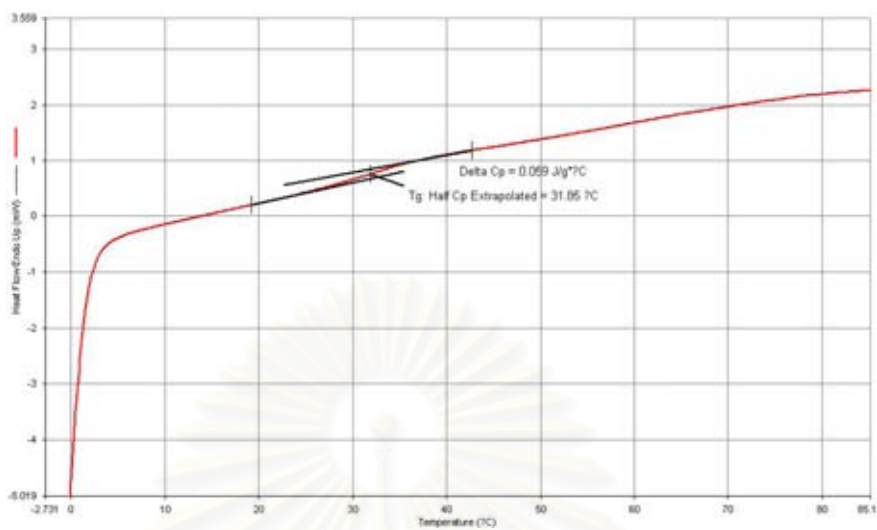


Figure A.1 DSC curve of PBMA

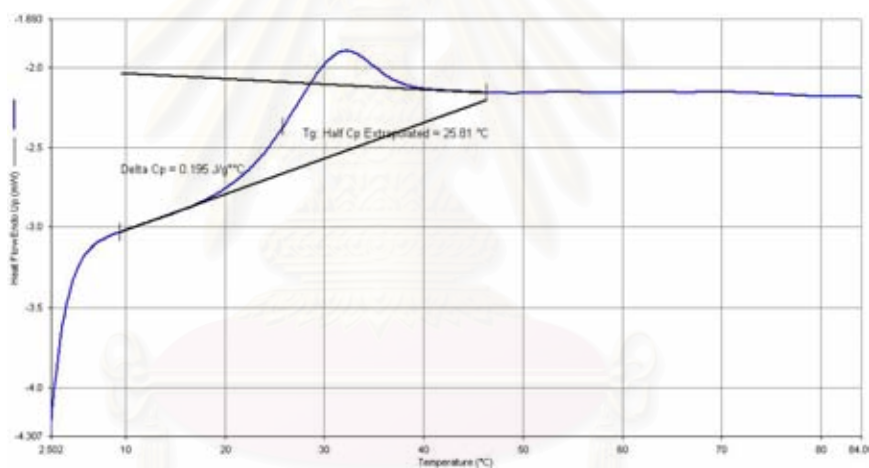


Figure A.2 DSC curve of PCHA

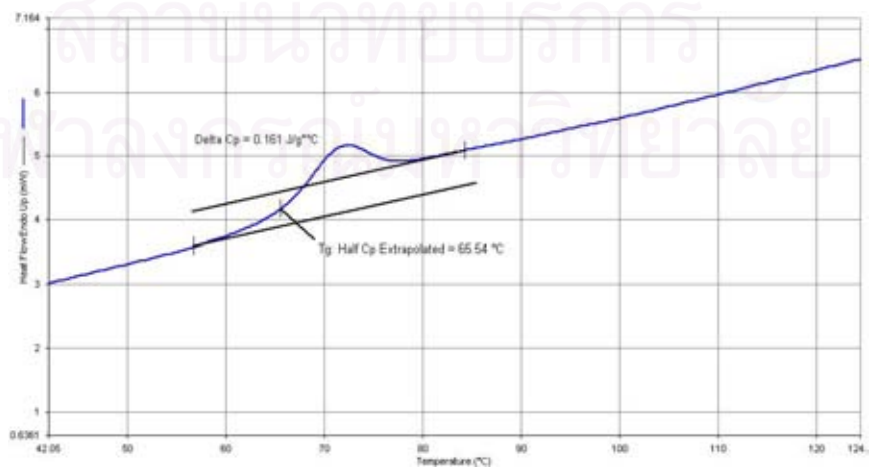


Figure A.3 DSC curve of PEMA

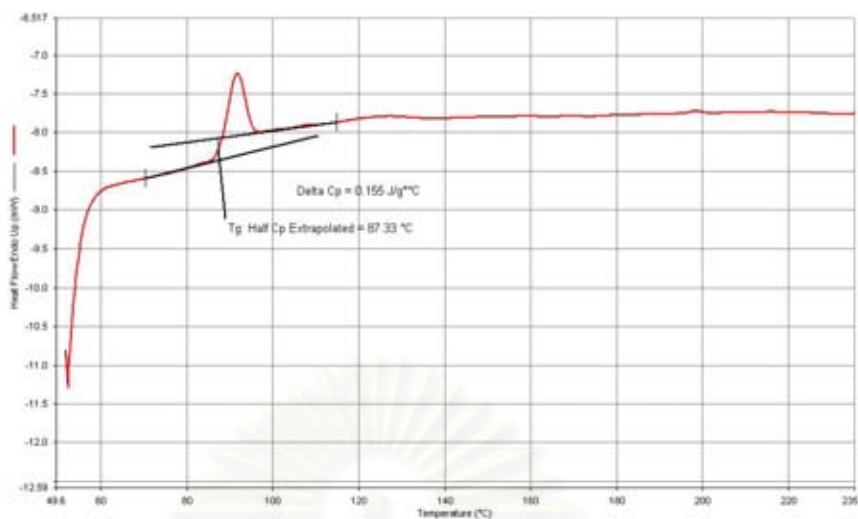


Figure A.4 DSC curve of Poly(α -methylstyrene)

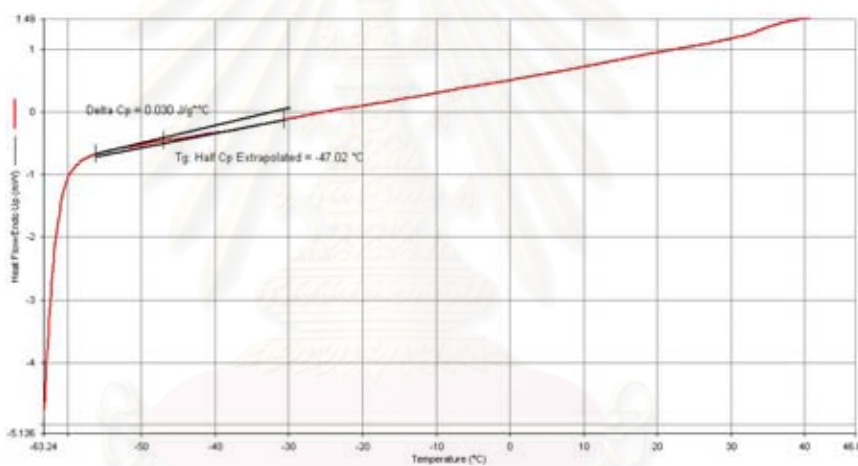


Figure A.5 DSC curve of Polyisoprene

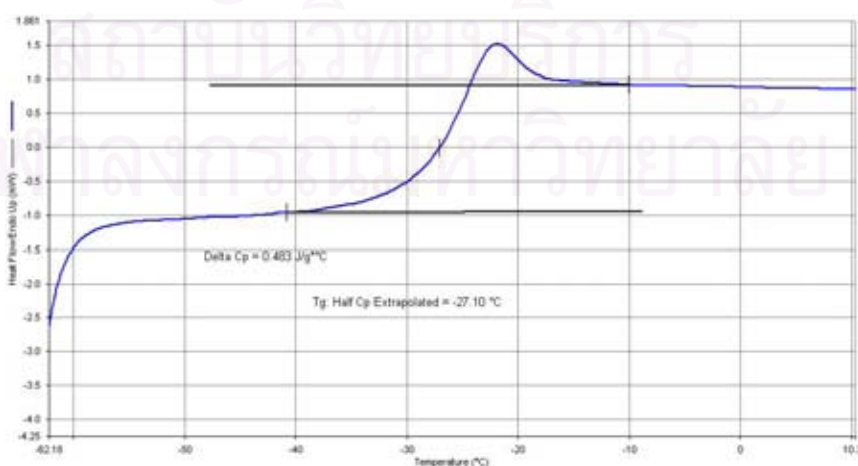


Figure A.6 DSC curve of PVME

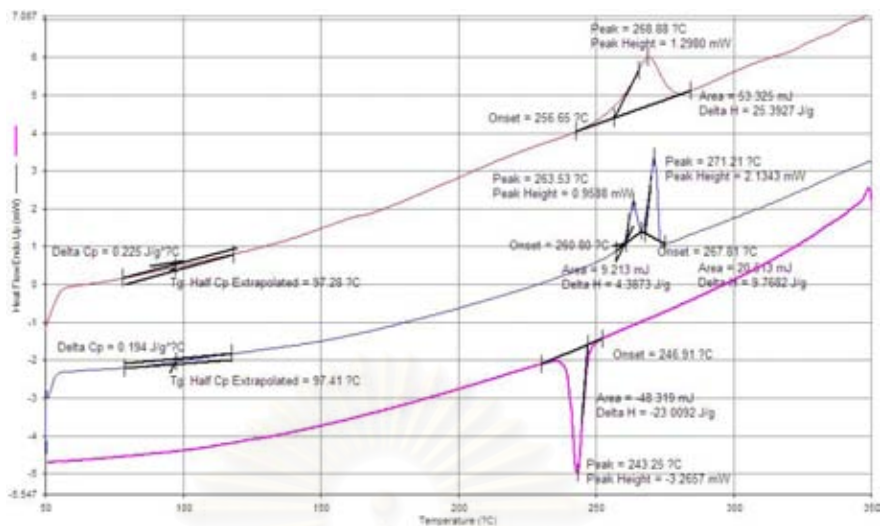


Figure A.7 DSC curve of sPS1

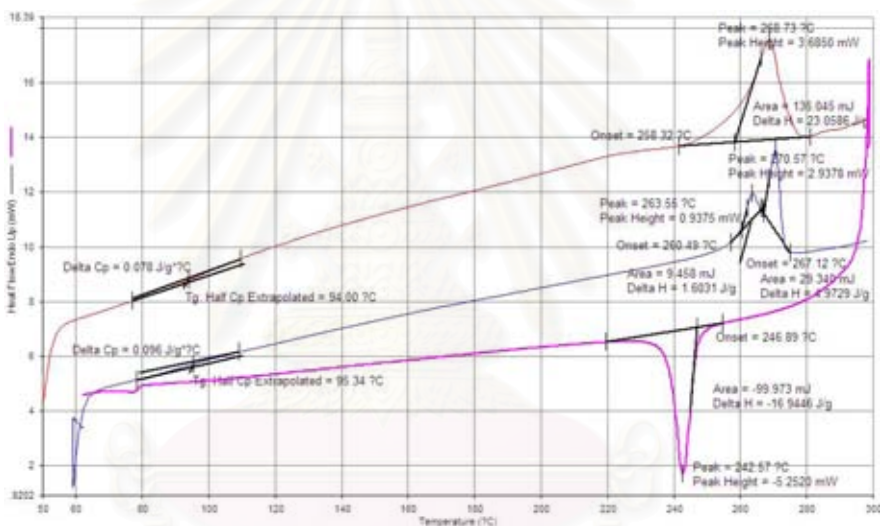


Figure A.8 DSC curve of sPS2

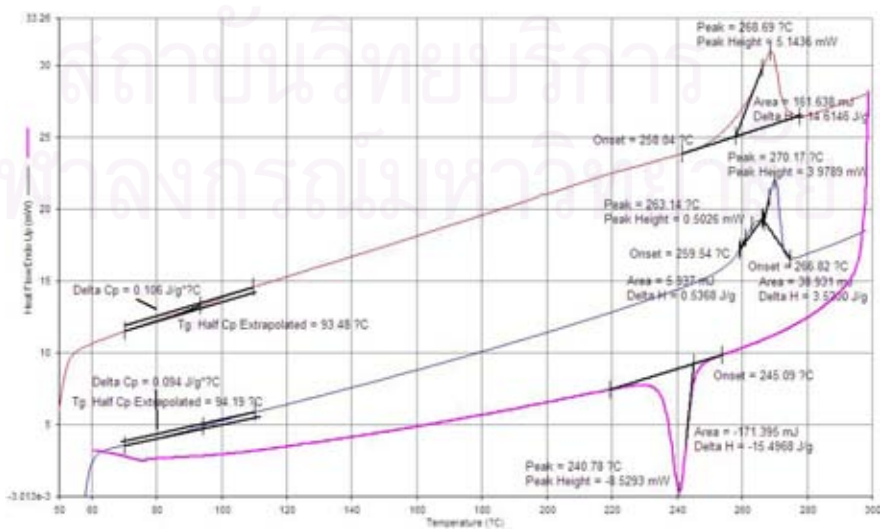


Figure A.9 DSC curve of sPS3

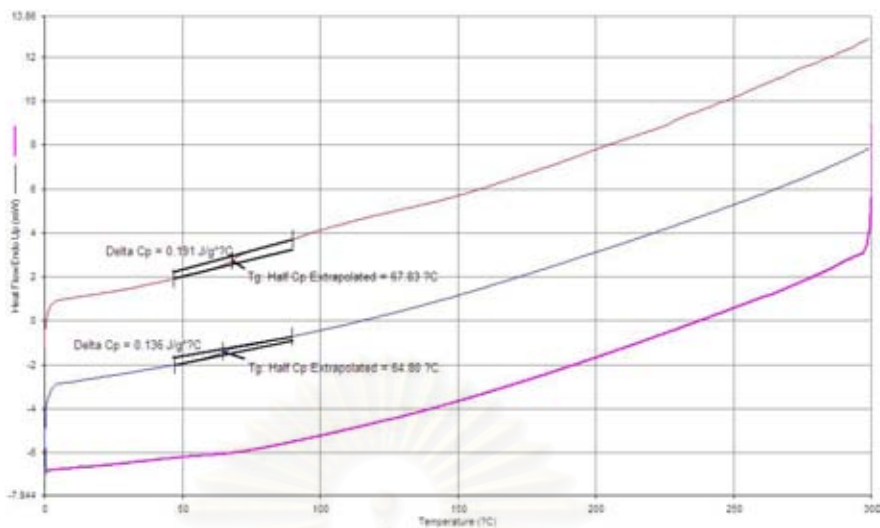


Figure A.10 DSC curve of sPS1 / PBMA blends at composition 50/50 wt%

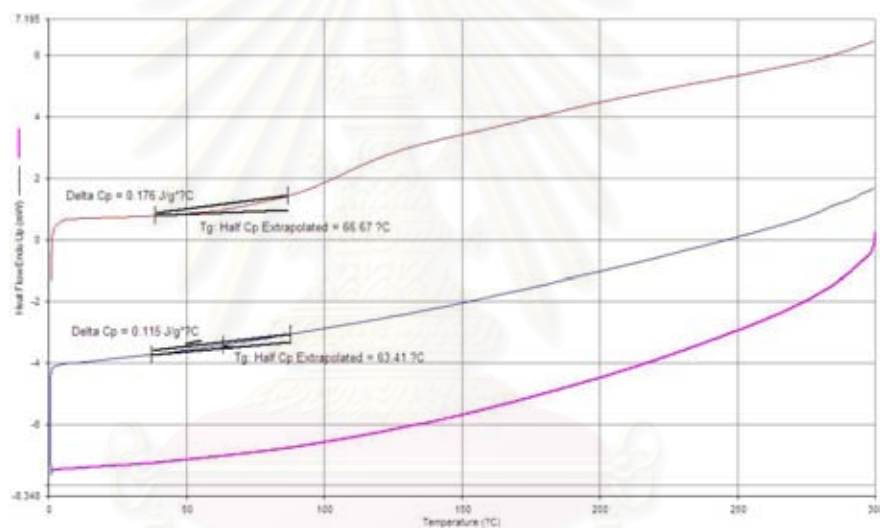


Figure A.11 DSC curve of sPS2 / PBMA blends at composition 50/50 wt%

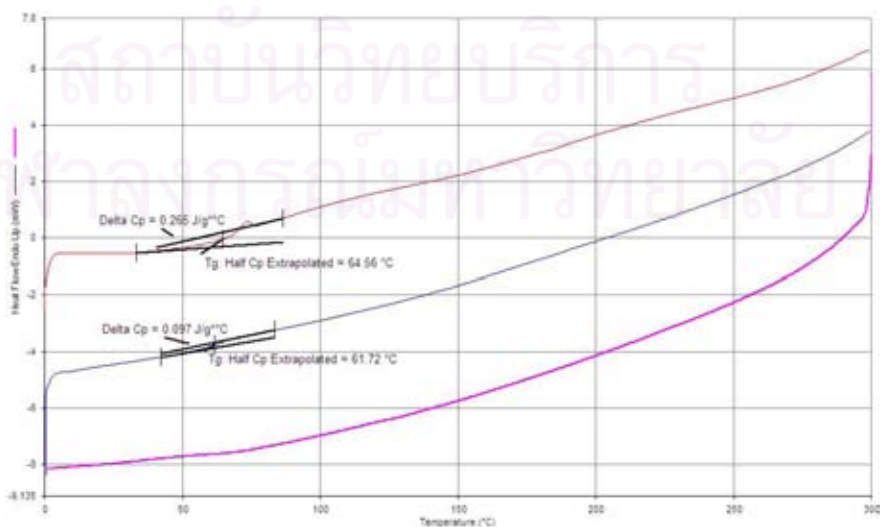


Figure A.12 DSC curve of sPS3 / PBMA blends at composition 50/50 wt%

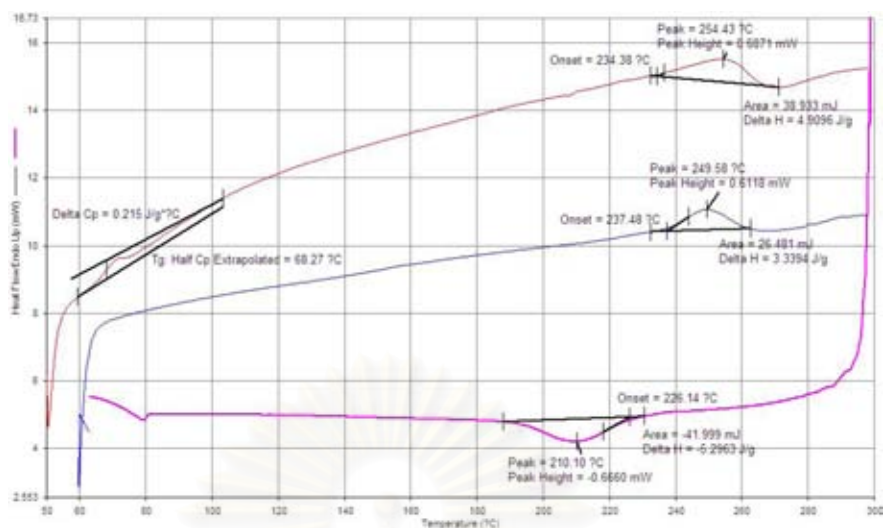


Figure A.13 DSC curve of sPS1 / PBMA blends at composition 60/40 wt%

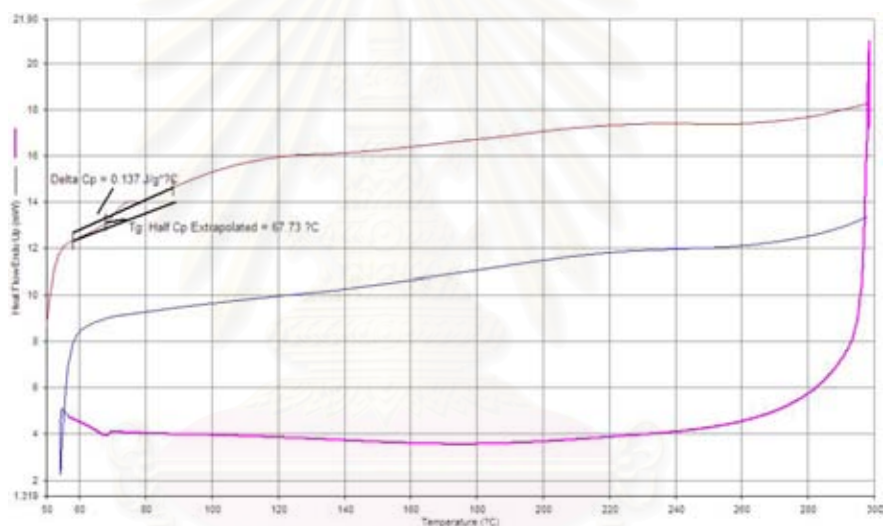


Figure A.14 DSC curve of sPS2 / PBMA blends at composition 60/40 wt%

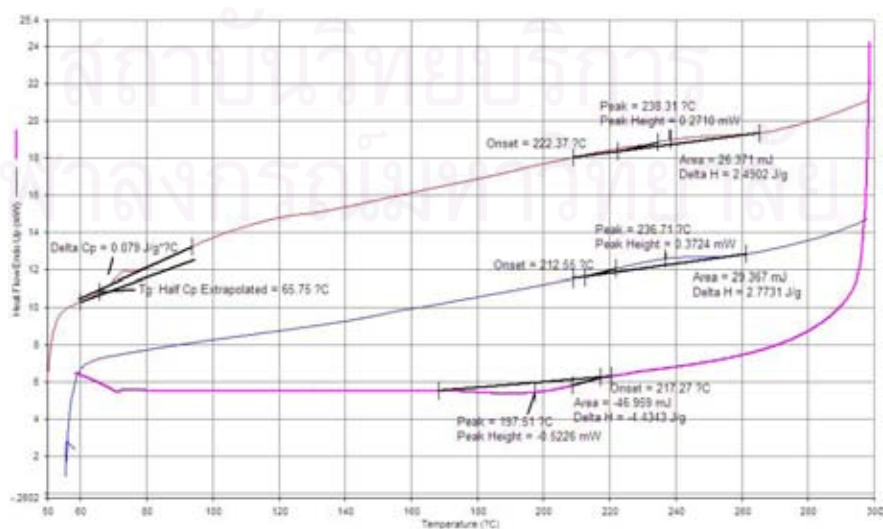


Figure A.15 DSC curve of sPS3 / PBMA blends at composition 60/40 wt%

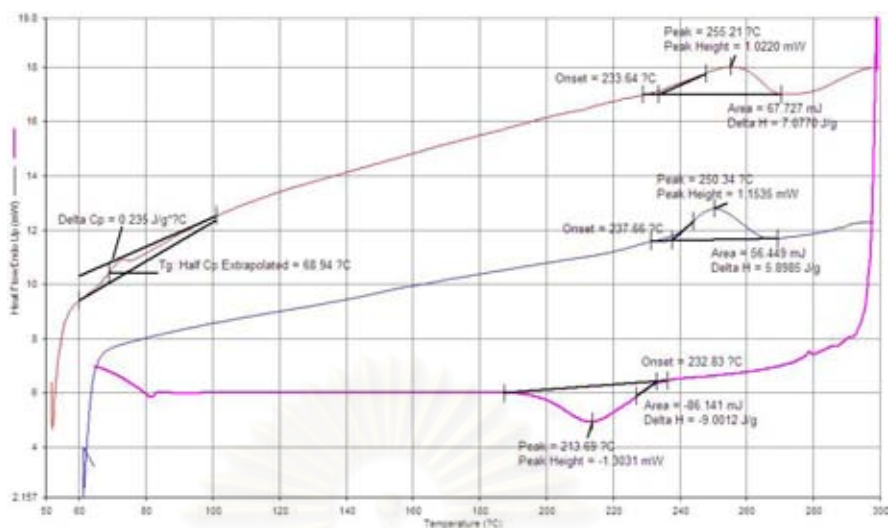


Figure A.16 DSC curve of sPS1 / PBMA blends at composition 70/30 wt%

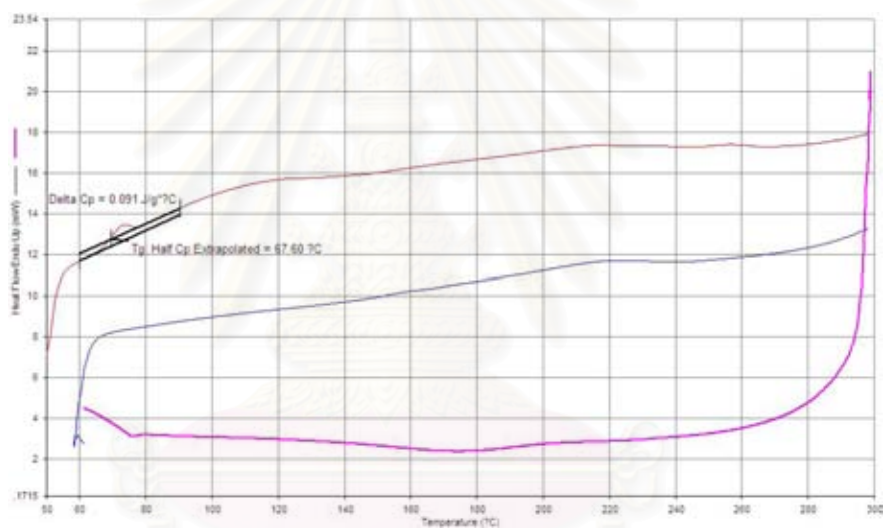


Figure A.17 DSC curve of sPS2 / PBMA blends at composition 70/30 wt%

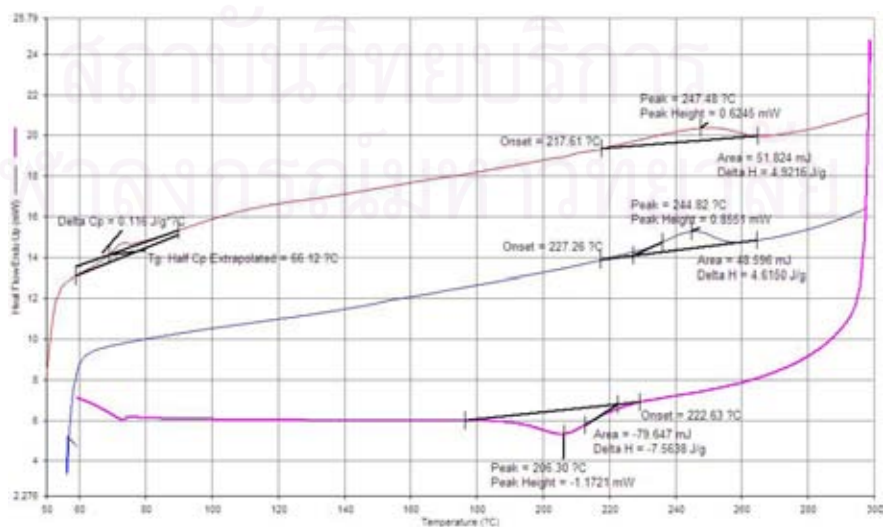


Figure A.18 DSC curve of sPS3 / PBMA blends at composition 70/30 wt%

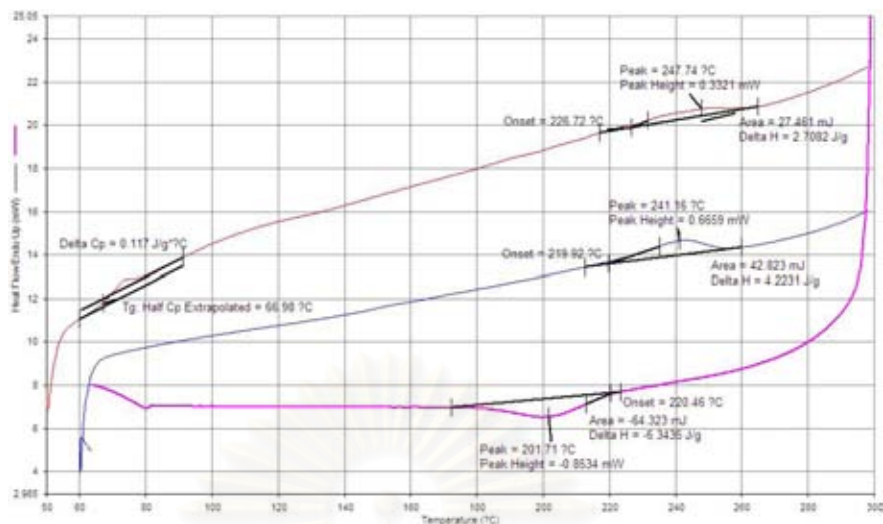


Figure A.19 DSC curve of sPS1 / PBMA blends at composition 80/20 wt%

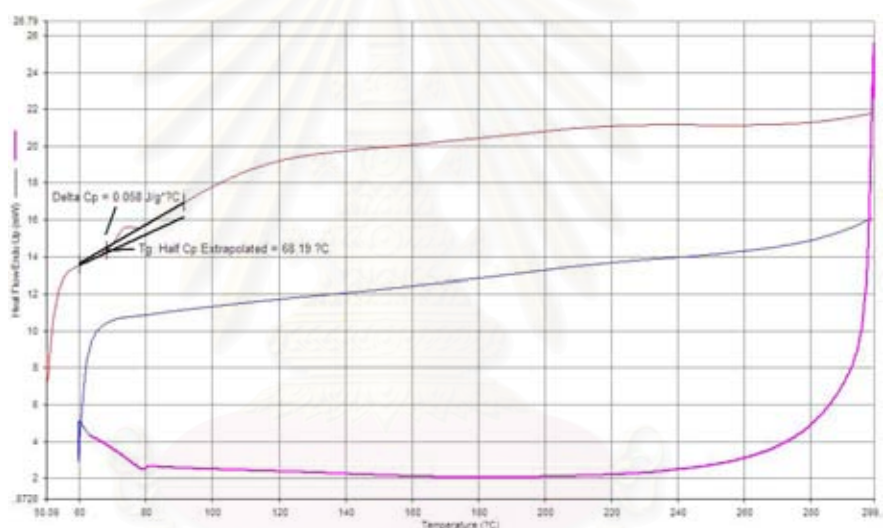


Figure A.20 DSC curve of sPS2 / PBMA blends at composition 80/20 wt%

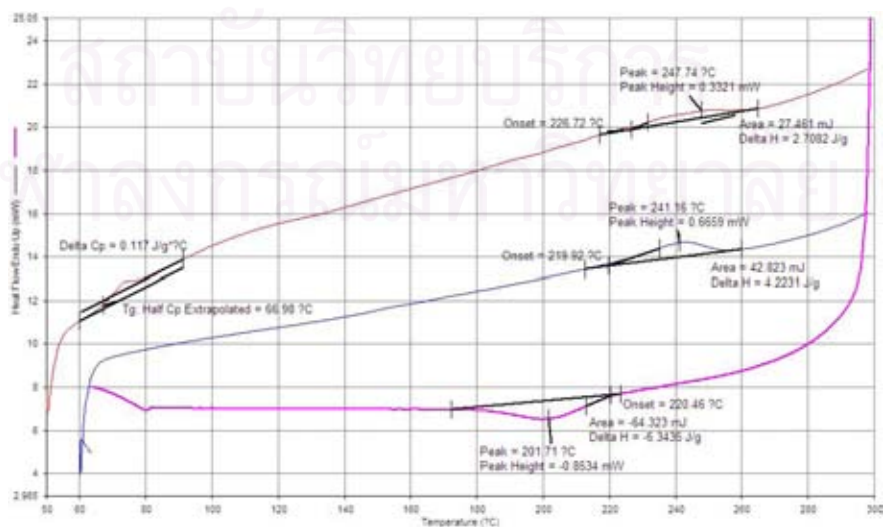


Figure A.21 DSC curve of sPS3 / PBMA blends at composition 80/20 wt%

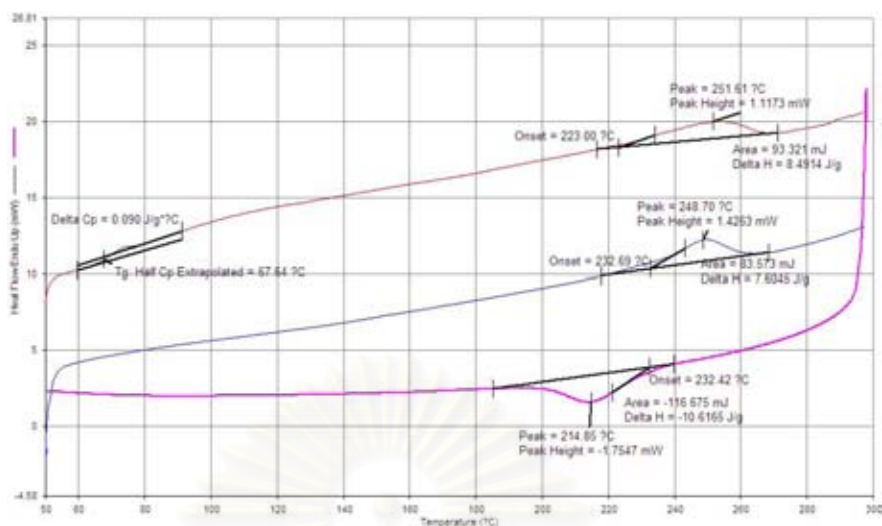


Figure A.22 DSC curve of sPS1 / PBMA blends at composition 90/10 wt%

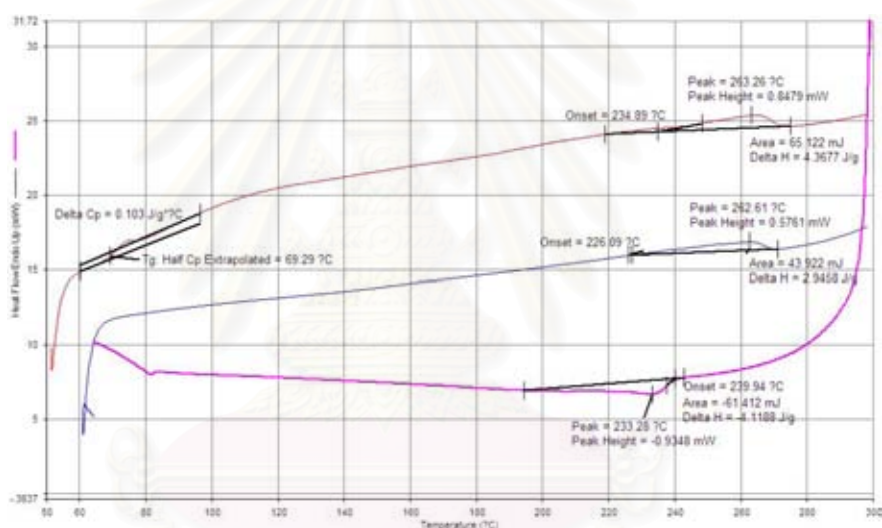


Figure A.23 DSC curve of sPS2 / PBMA blends at composition 90/10 wt%

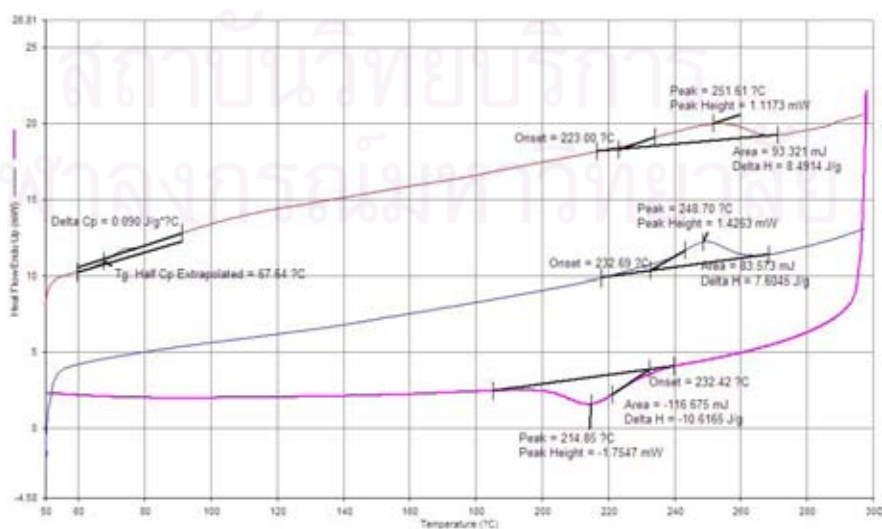


Figure A.24 DSC curve of sPS3 / PBMA blends at composition 90/10 wt%

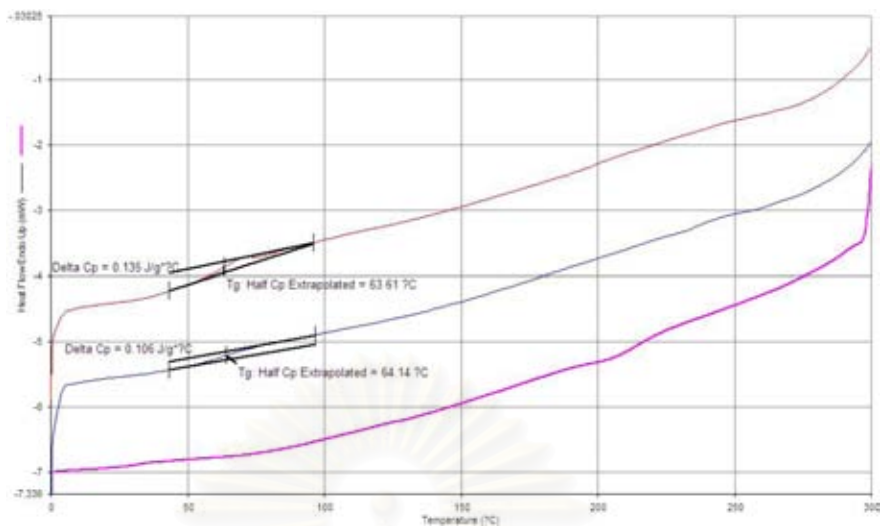


Figure A.25 DSC curve of sPS1 / PCHA blends at composition 50/50 wt%

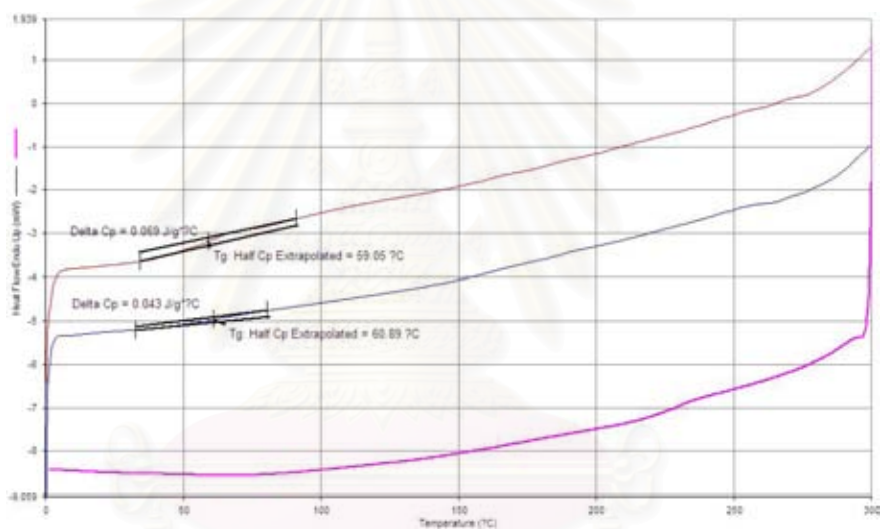


Figure A.26 DSC curve of sPS2 / PCHA blends at composition 50/50 wt%

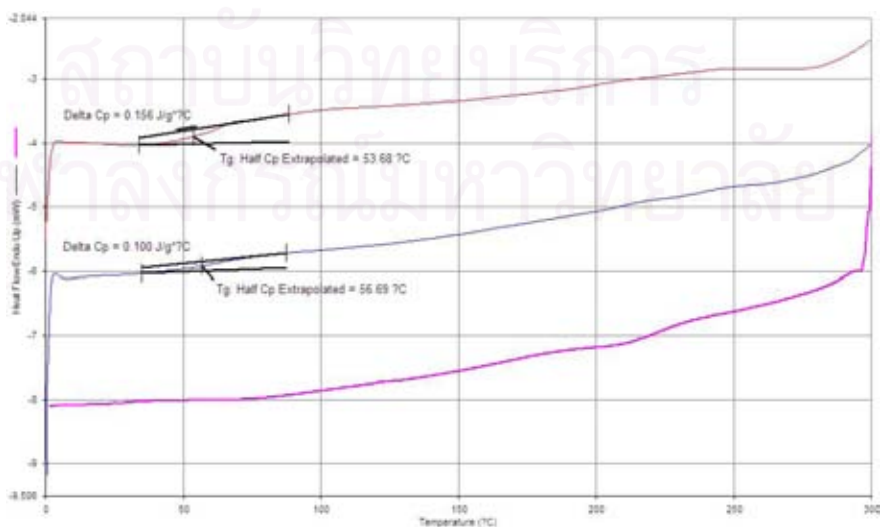


Figure A.27 DSC curve of sPS3 / PCHA blends at composition 50/50 wt%

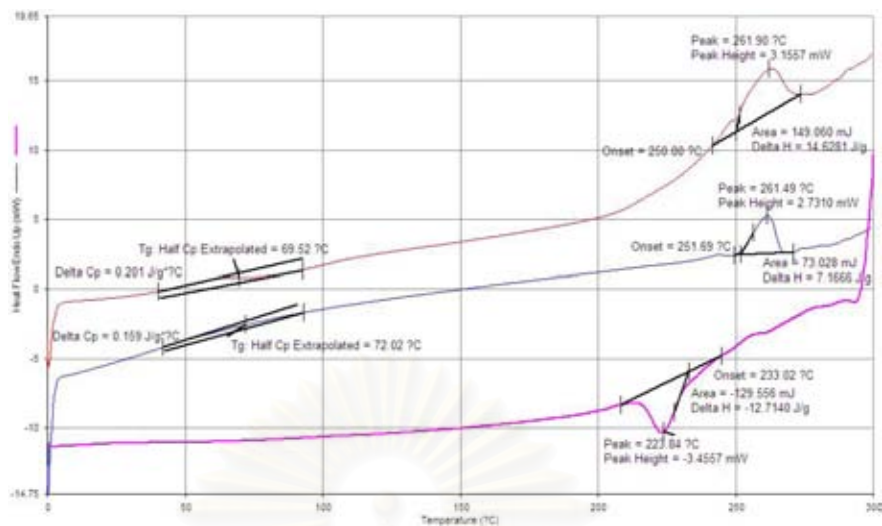


Figure A.28 DSC curve of sPS1 / PCHA blends at composition 60/40 wt%

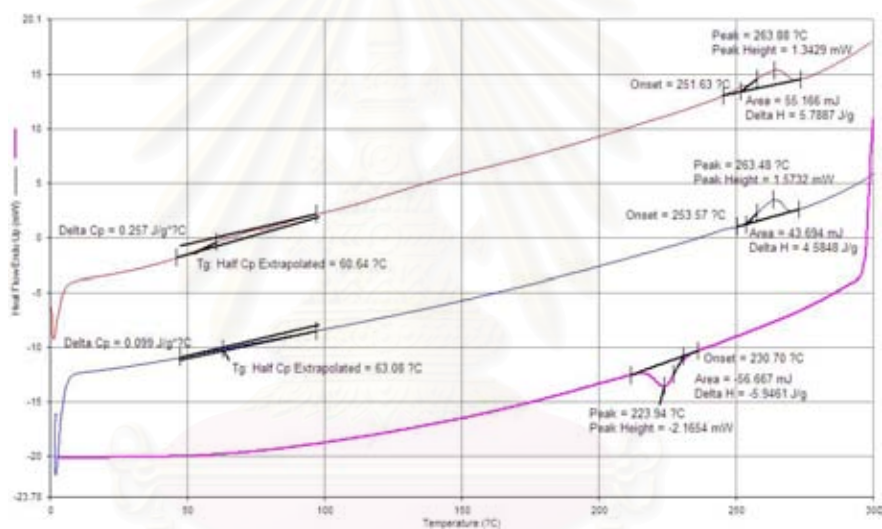


Figure A.29 DSC curve of sPS2 / PCHA blends at composition 60/40 wt%

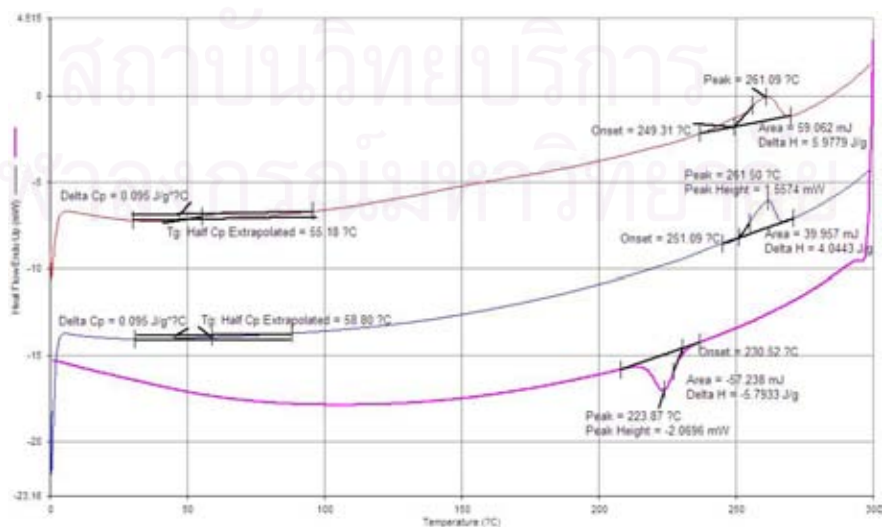


Figure A.30 DSC curve of sPS3 / PCHA blends at composition 60/40 wt%

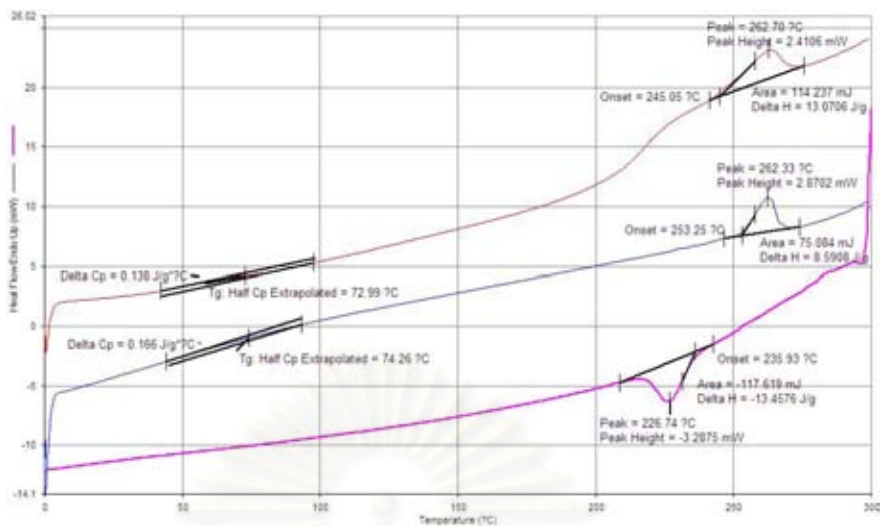


Figure A.31 DSC curve of sPS1 / PCHA blends at composition 70/30 wt%

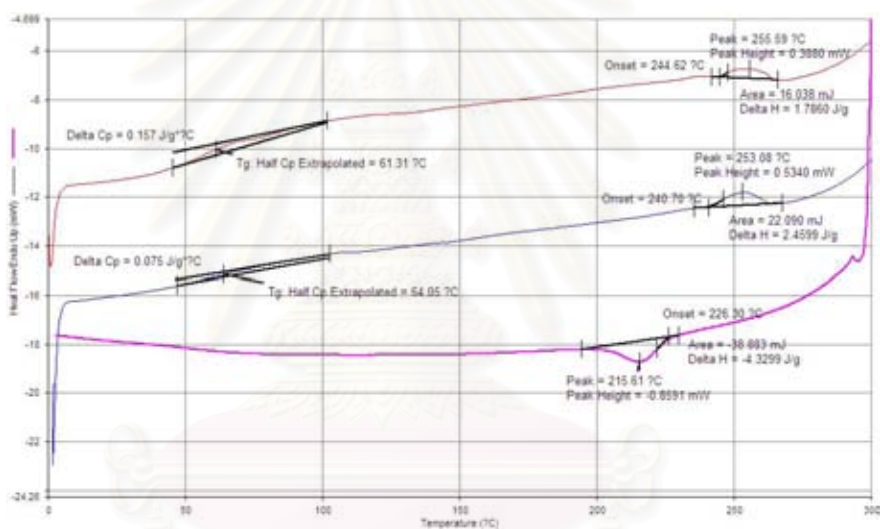


Figure A.32 DSC curve of sPS2 / PCHA blends at composition 70/30 wt%

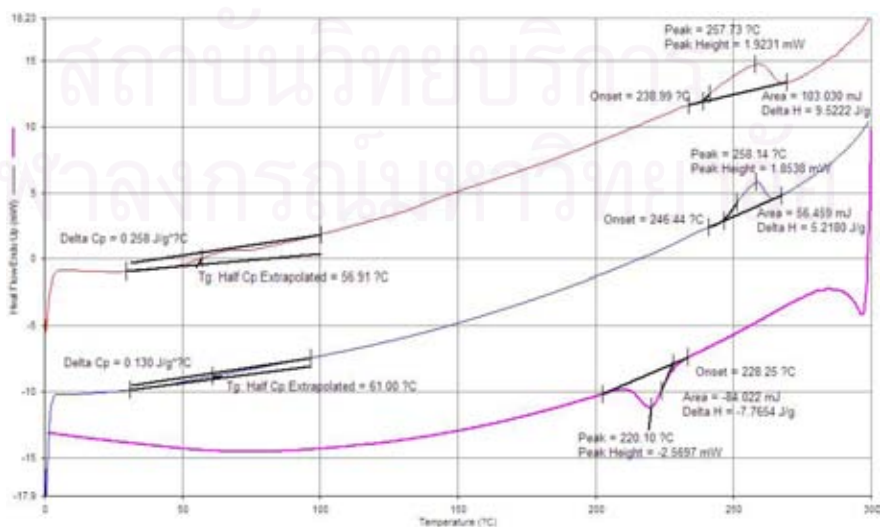


Figure A.33 DSC curve of sPS3 / PCHA blends at composition 70/30 wt%

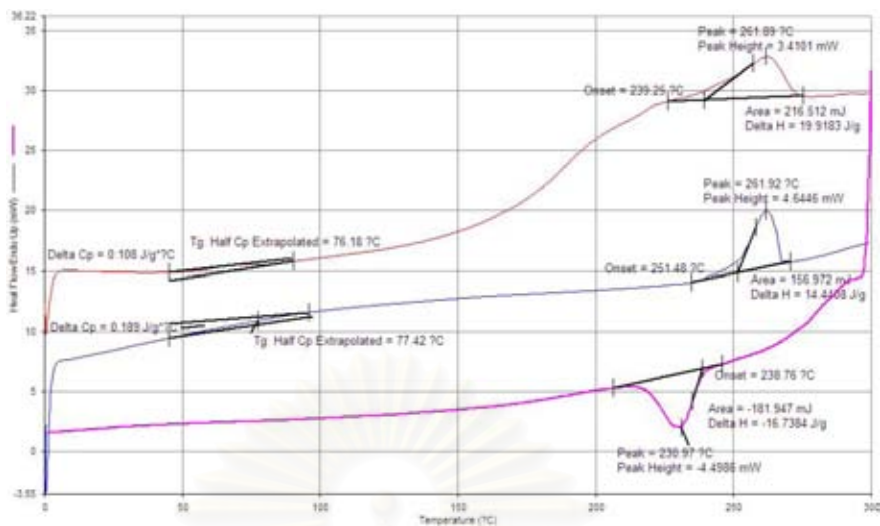


Figure A.34 DSC curve of sPS1 / PCHA blends at composition 80/20 wt%

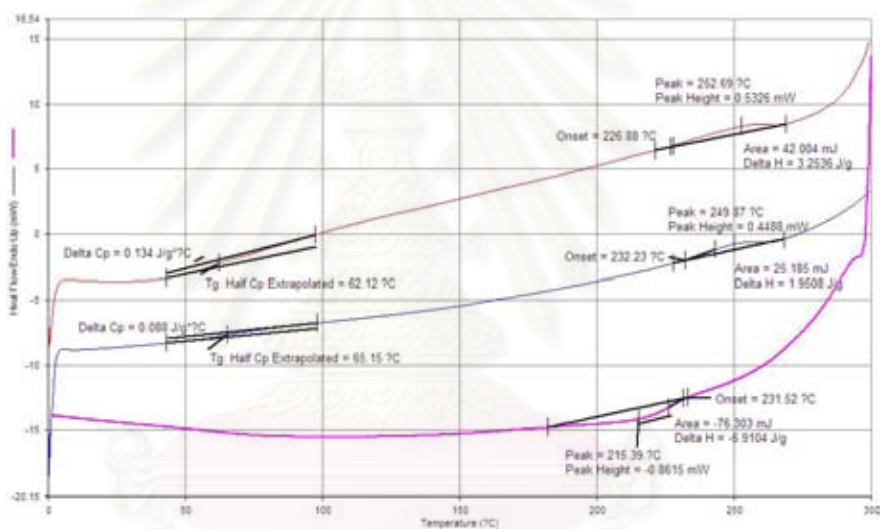


Figure A.35 DSC curve of sPS2 / PCHA blends at composition 80/20 wt%

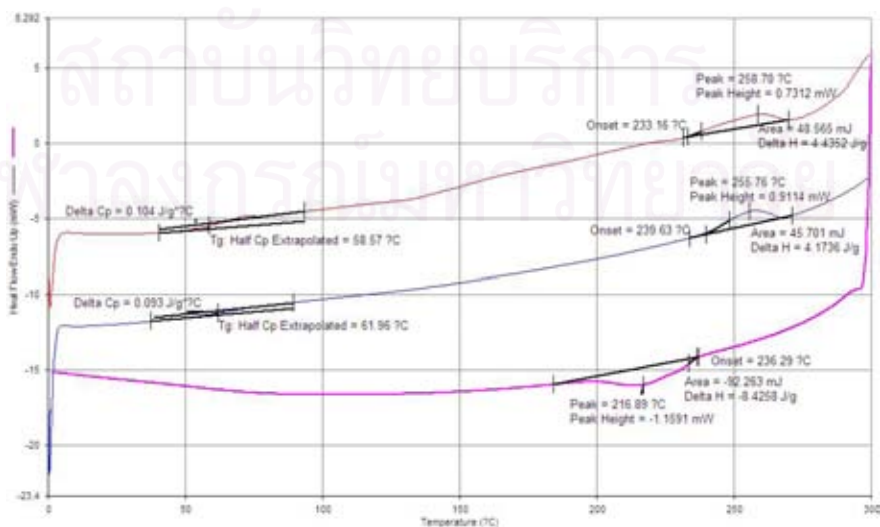


Figure A.36 DSC curve of sPS3 / PCHA blends at composition 80/20 wt%

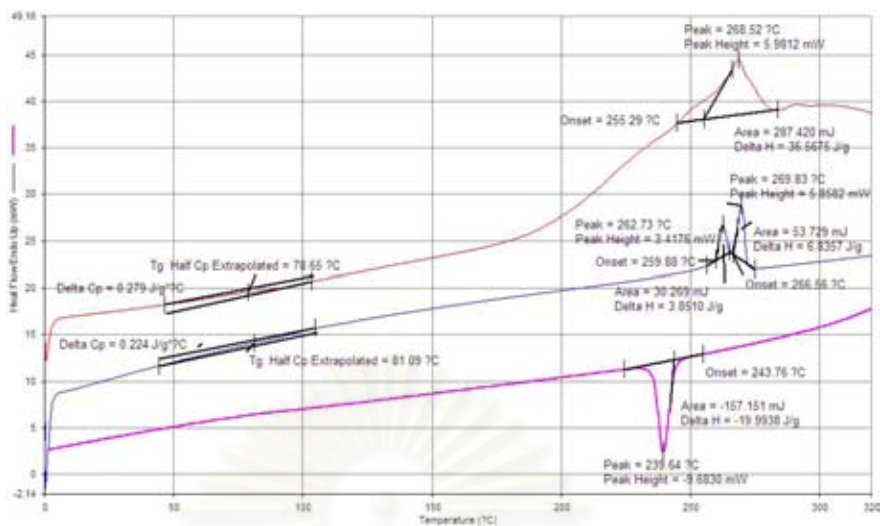


Figure A.37 DSC curve of sPS1 / PCHA blends at composition 90/10 wt%

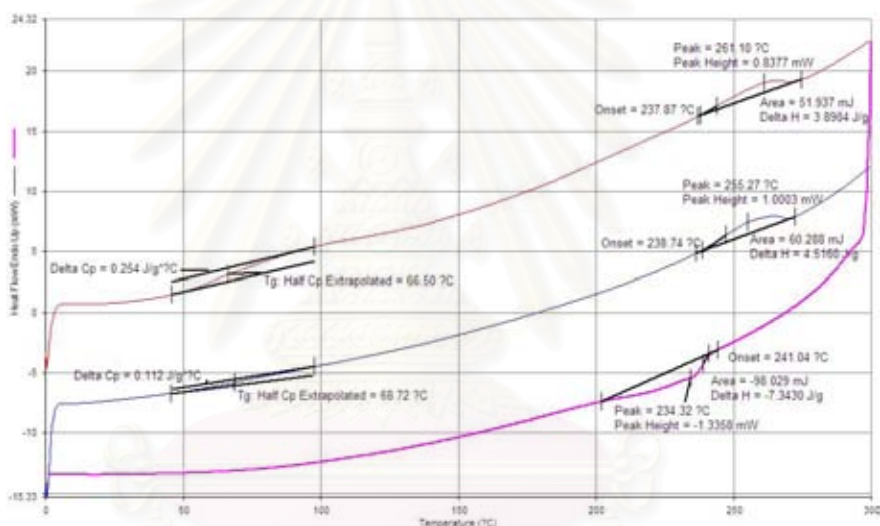


Figure A.38 DSC curve of sPS2 / PCHA blends at composition 90/10 wt%

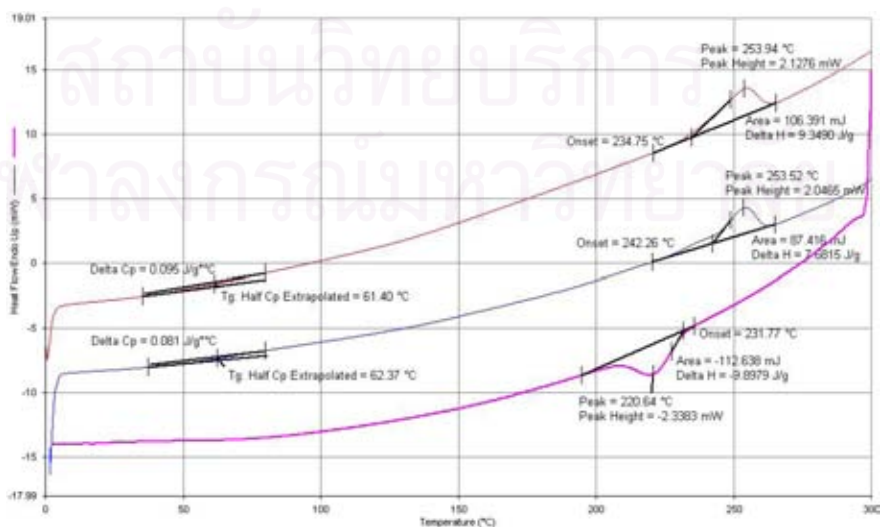


Figure A.39 DSC curve of sPS3 / PCHA blends at composition 90/10 wt%

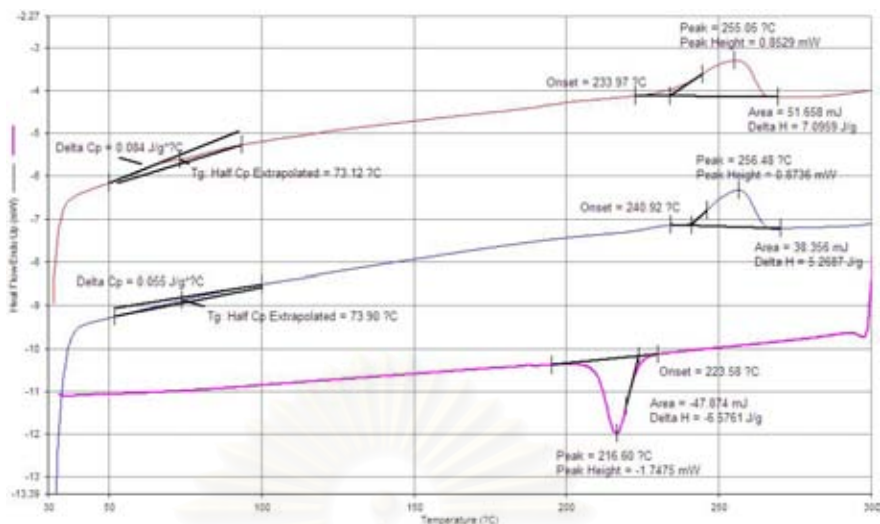


Figure A.40 DSC curve of sPS1 / PEMA blends at composition 50/50 wt%

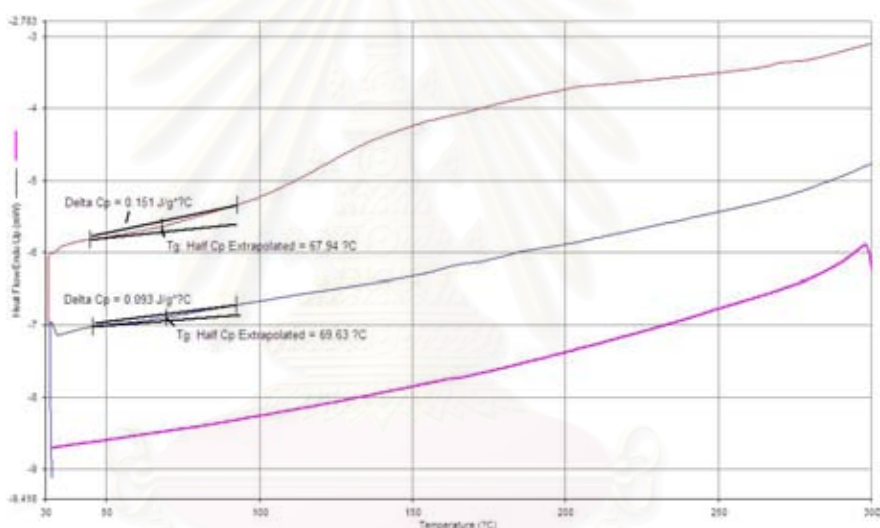


Figure A.41 DSC curve of sPS2 / PEMA blends at composition 50/50 wt%

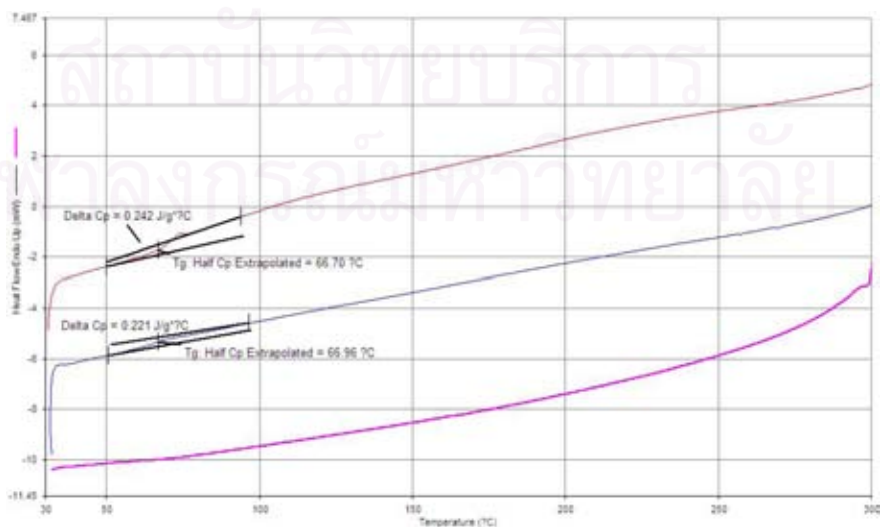


Figure A.42 DSC curve of sPS3 / PEMA blends at composition 50/50 wt%

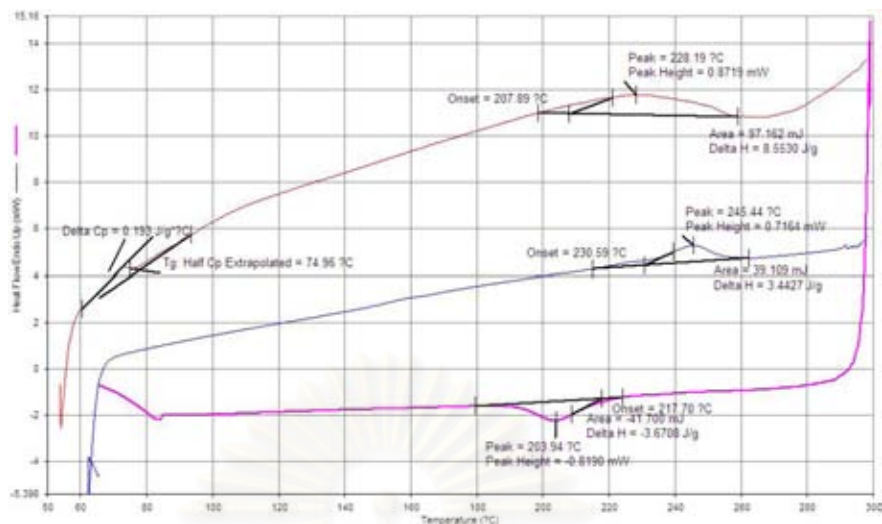


Figure A.43 DSC curve of sPS1 / PEMA blends at composition 60/40 wt%

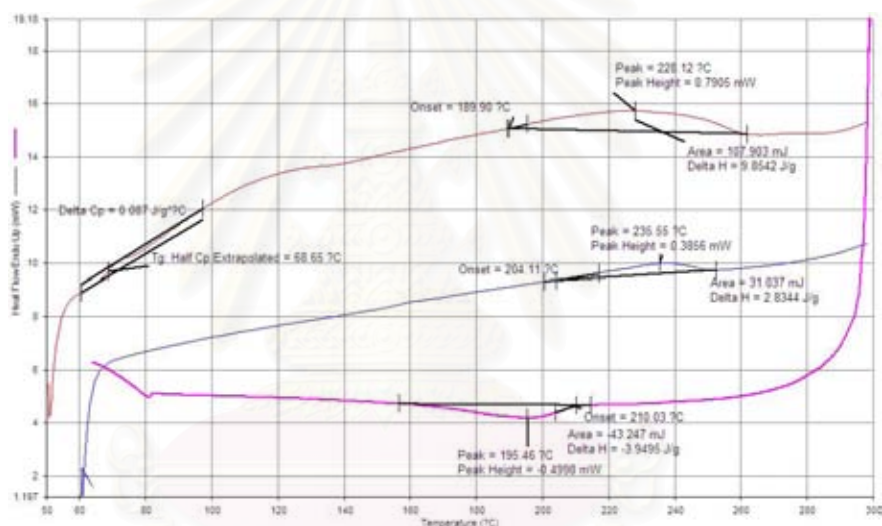


Figure A.44 DSC curve of sPS2 / PEMA blends at composition 60/40 wt%

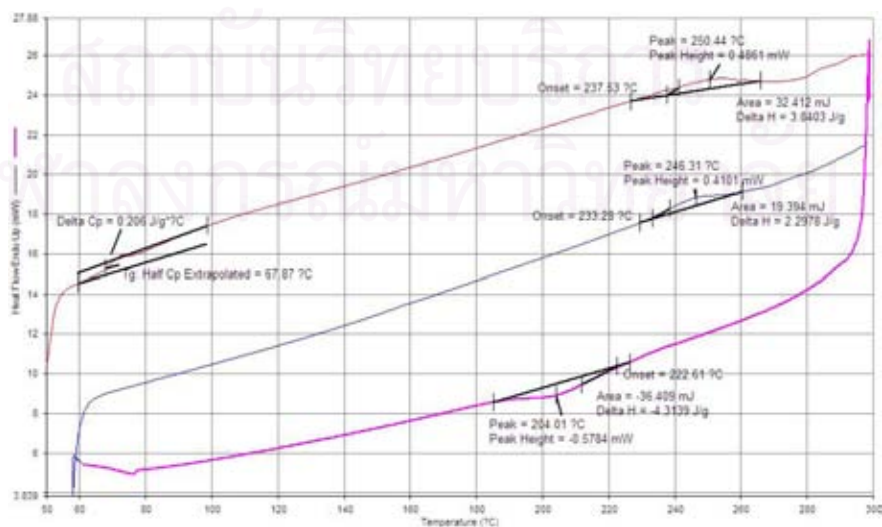


Figure A.45 DSC curve of sPS3 / PEMA blends at composition 60/40 wt%

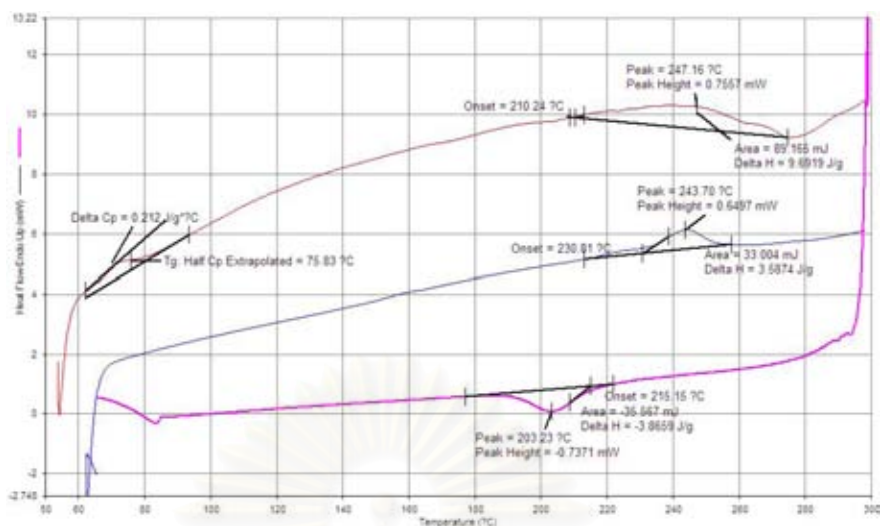


Figure A.46 DSC curve of sPS1 / PEMA blends at composition 70/30 wt%

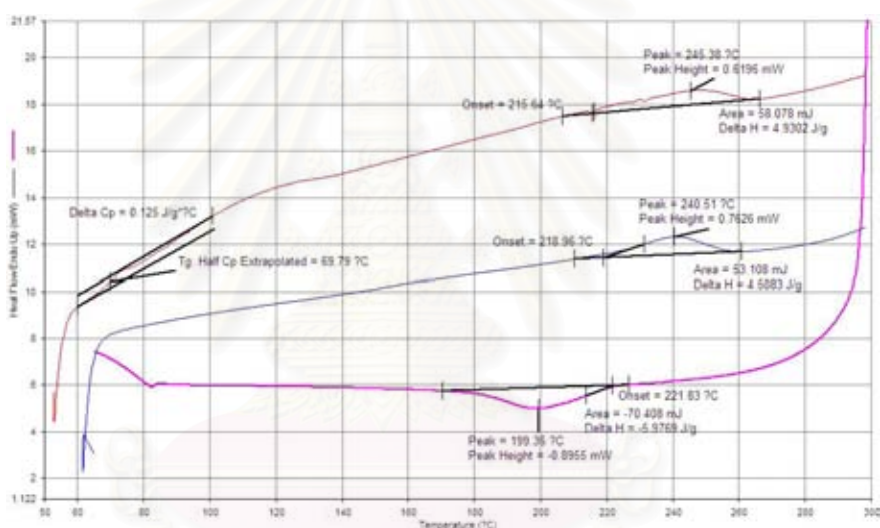


Figure A.47 DSC curve of sPS2 / PEMA blends at composition 70/30 wt%

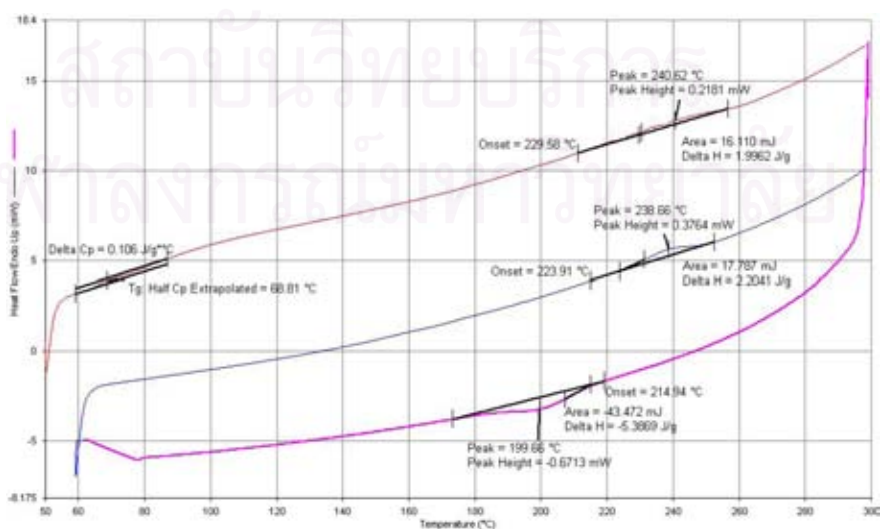


Figure A.48 DSC curve of sPS3 / PEMA blends at composition 70/30 wt%

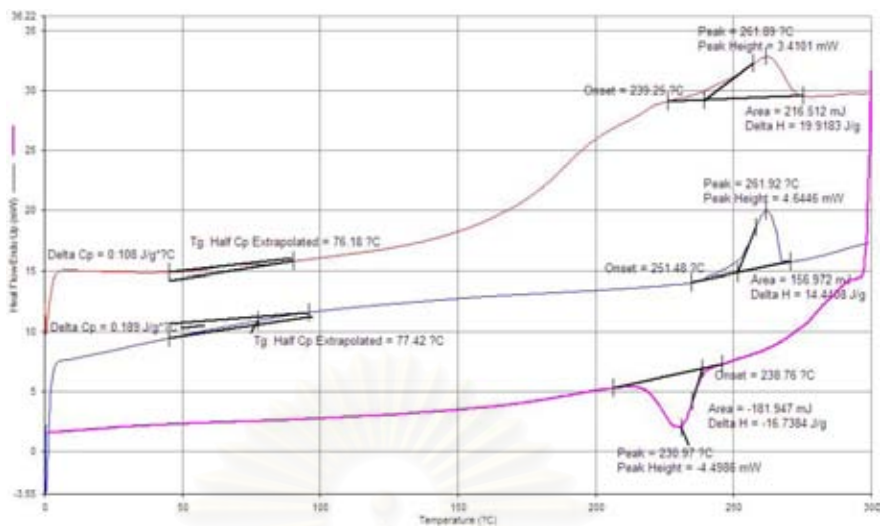


Figure A.49 DSC curve of sPS1 / PEMA blends at composition 80/20 wt%

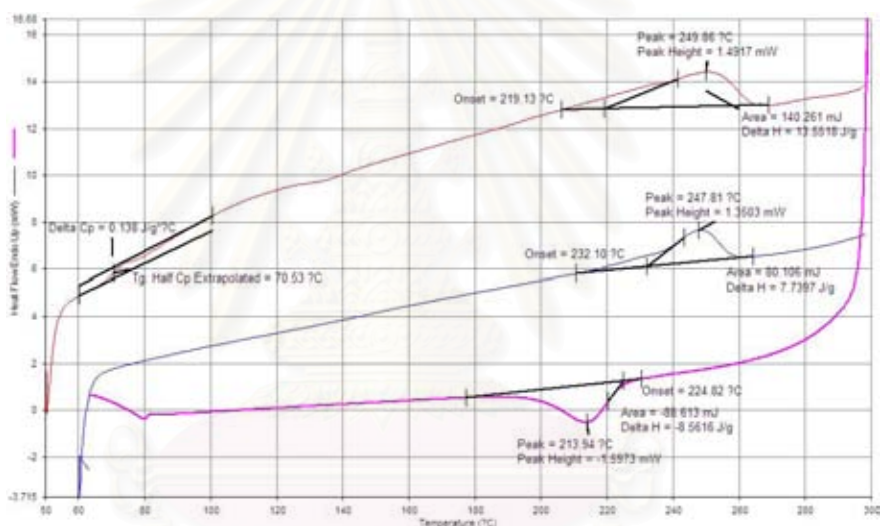


Figure A.50 DSC curve of sPS2 / PEMA blends at composition 80/20 wt%

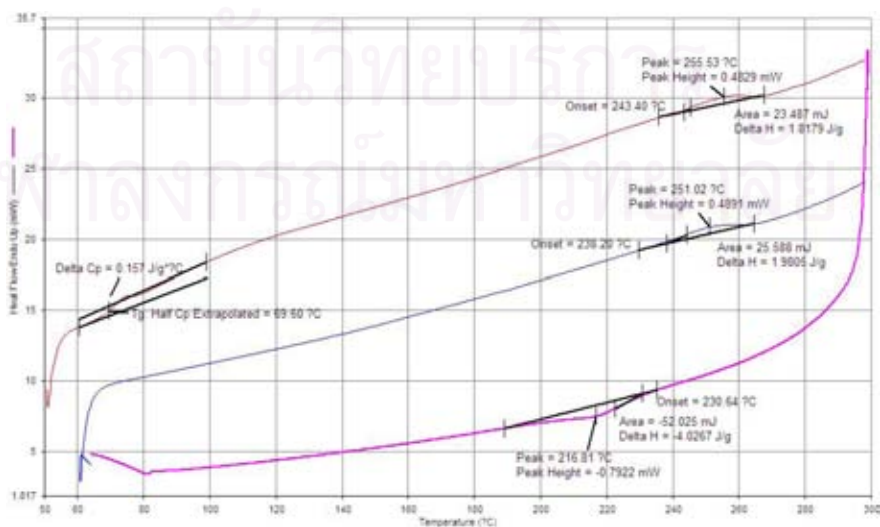


Figure A.51 DSC curve of sPS3 / PEMA blends at composition 80/20 wt%

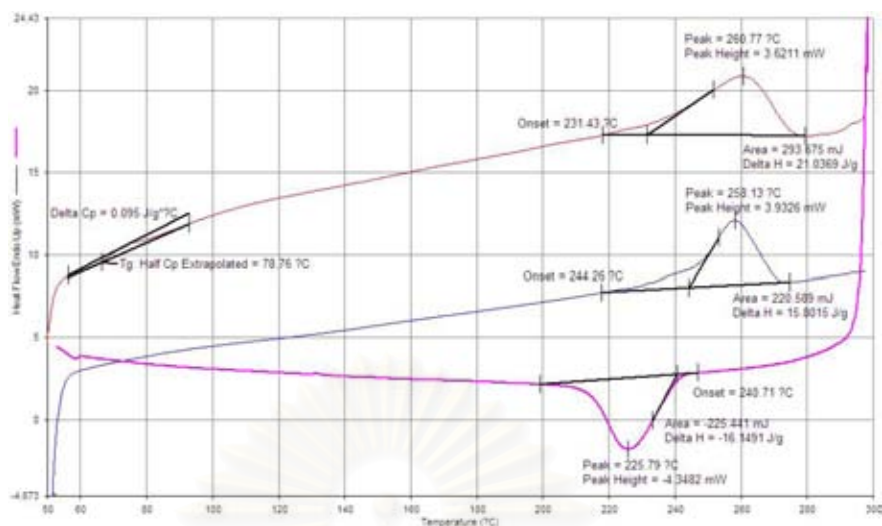


Figure A.52 DSC curve of sPS1 / PEMA blends at composition 90/10 wt%

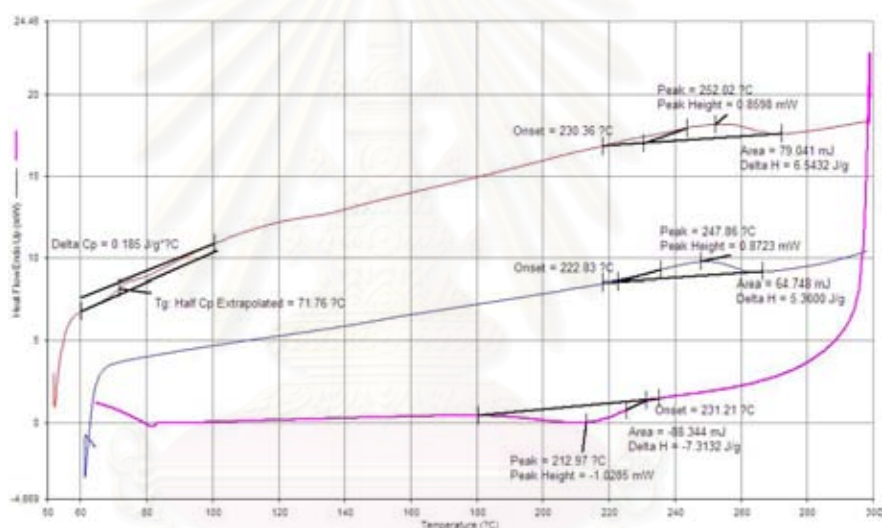


Figure A.53 DSC curve of sPS2 / PEMA blends at composition 90/10 wt%

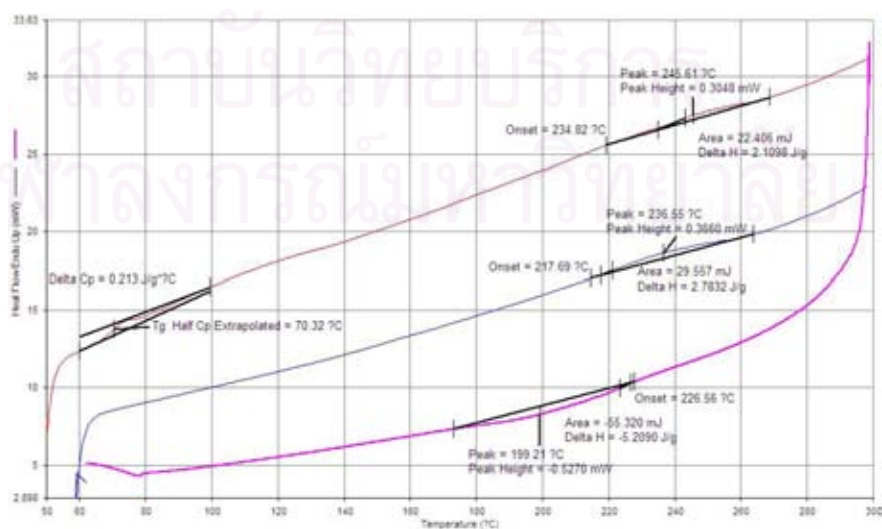


Figure A.54 DSC curve of sPS3 / PEMA blends at composition 90/10 wt%

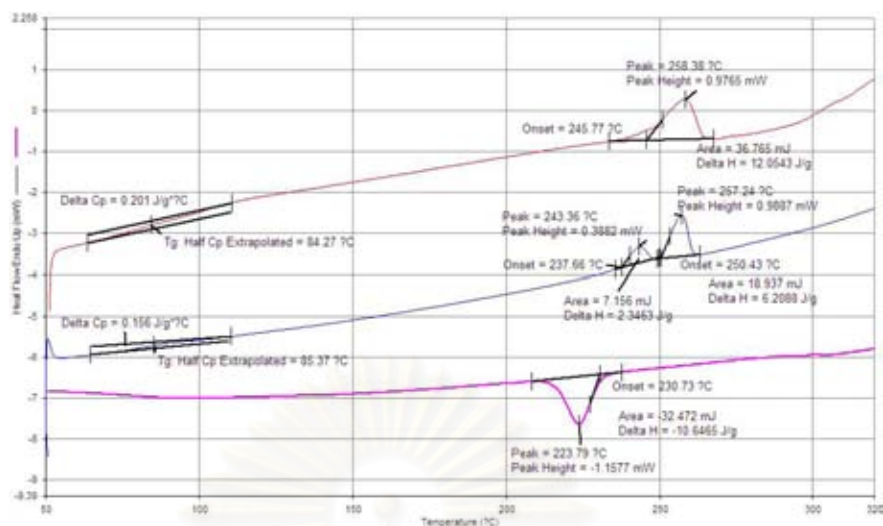


Figure A.55 DSC curve of sPS1 / Poly(α -methylstyrene) blends at composition 50/50 wt%

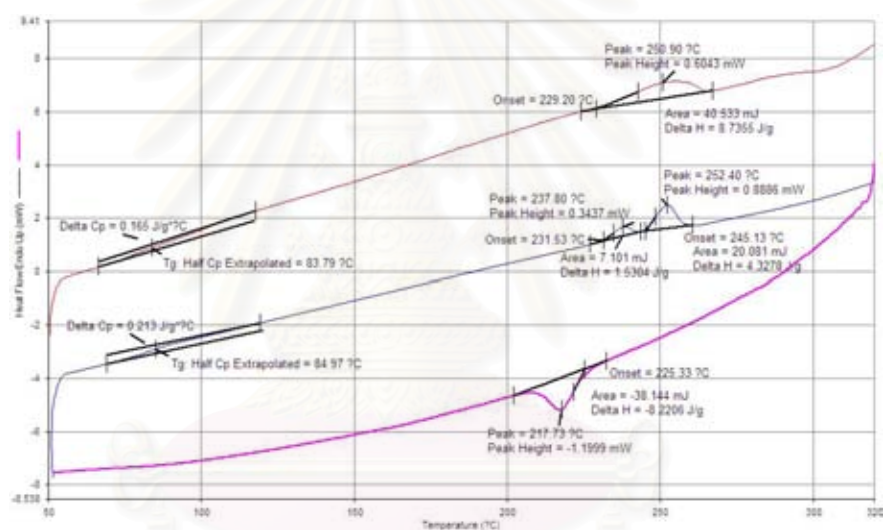


Figure A.56 DSC curve of sPS2 / Poly(α -methylstyrene) blends at composition 50/50 wt%

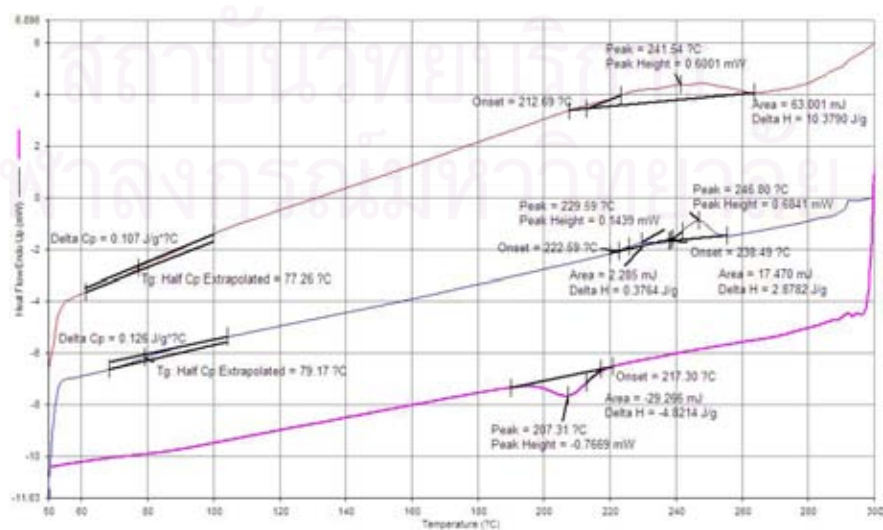


Figure A.57 DSC curve of sPS3 / Poly(α -methylstyrene) blends at composition 50/50 wt%

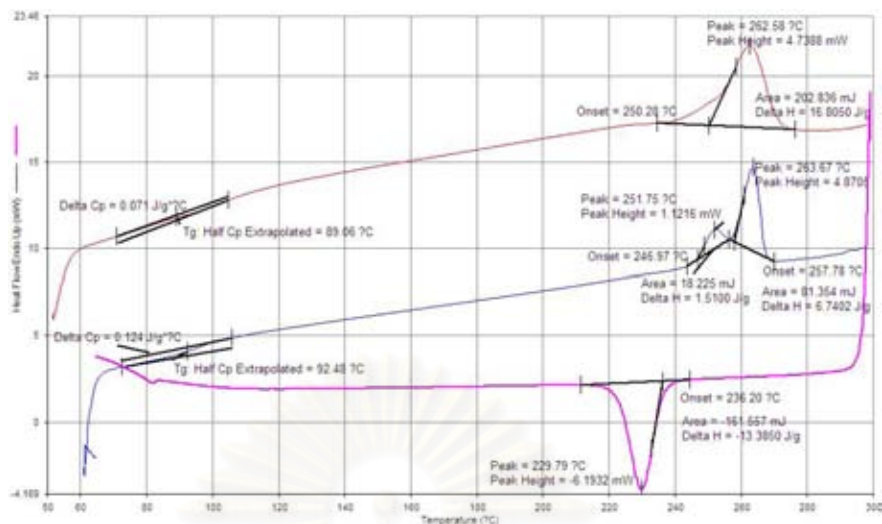


Figure A.58 DSC curve of sPS1 / Poly(α -methylstyrene) blends at composition 60/40 wt%

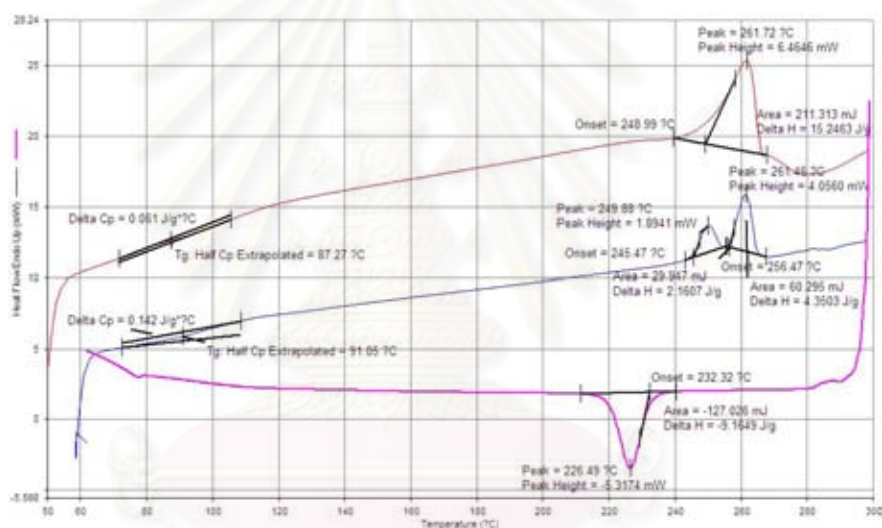


Figure A.59 DSC curve of sPS2 / Poly(α -methylstyrene) blends at composition 60/40 wt%

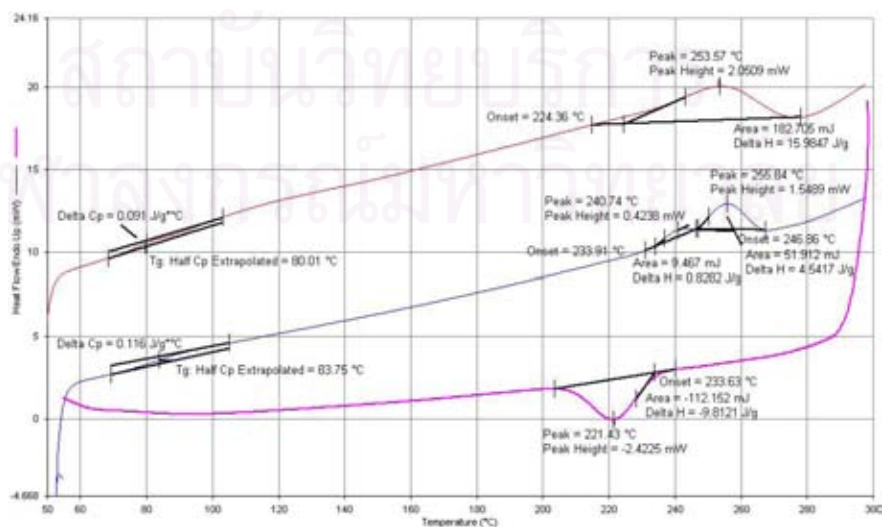


Figure A.60 DSC curve of sPS3 / Poly(α -methylstyrene) blends at composition 60/40 wt%

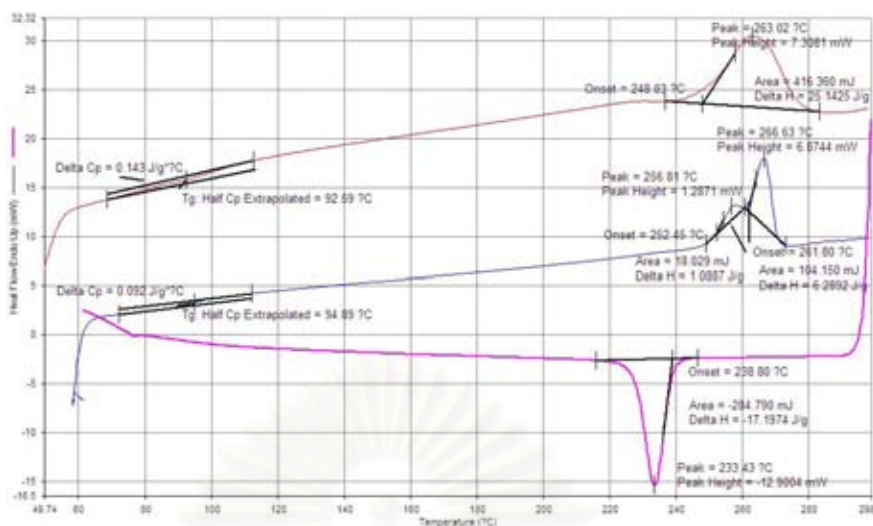


Figure A.61 DSC curve of sPS1 / Poly(α -methylstyrene) blends at composition 70/30 wt%

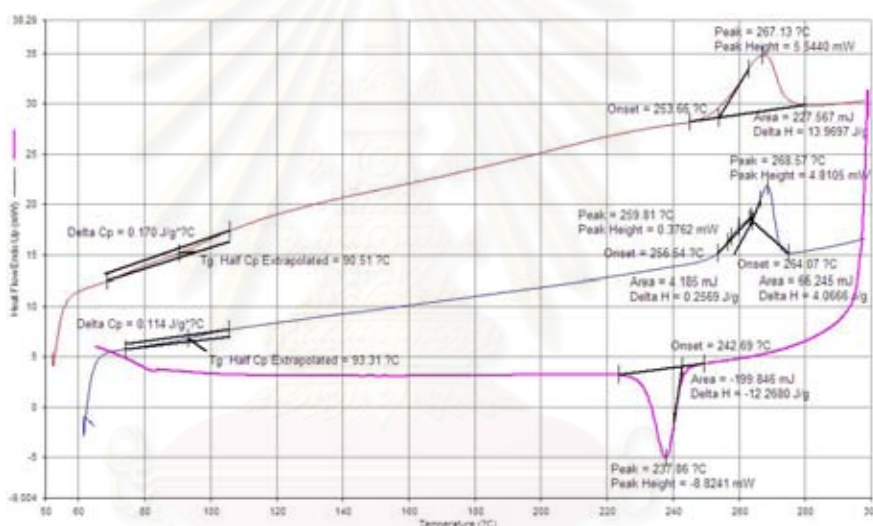


Figure A.62 DSC curve of sPS2 / Poly(α -methylstyrene) blends at composition 70/30 wt%

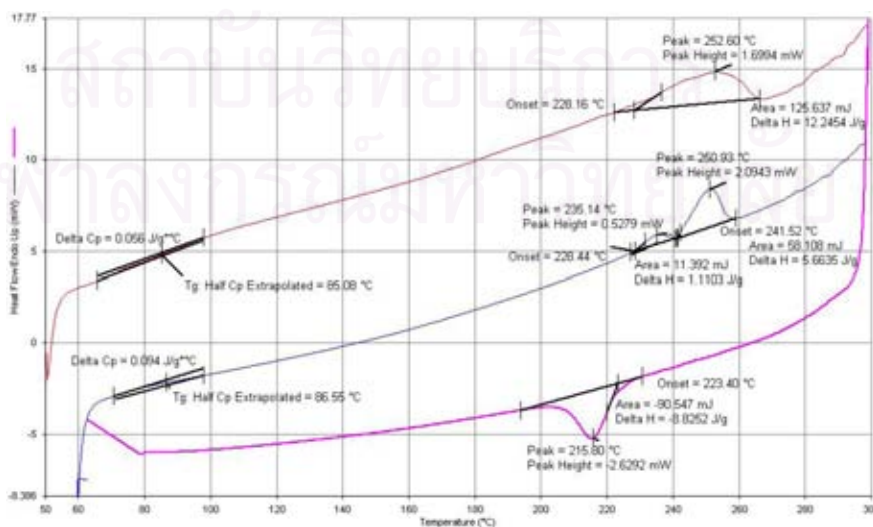


Figure A.63 DSC curve of sPS3 / Poly(α -methylstyrene) blends at composition 70/30 wt%

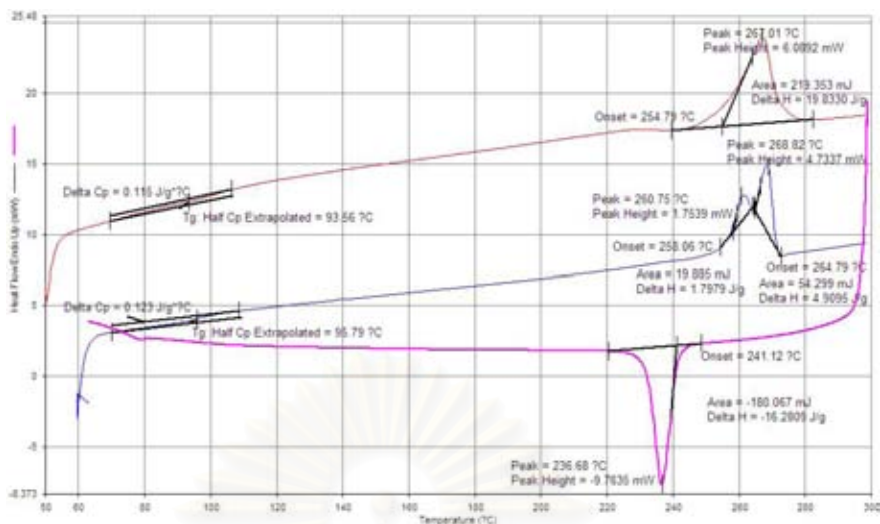


Figure A.64 DSC curve of sPS1 / Poly(α -methylstyrene) blends at composition 80/20 wt%

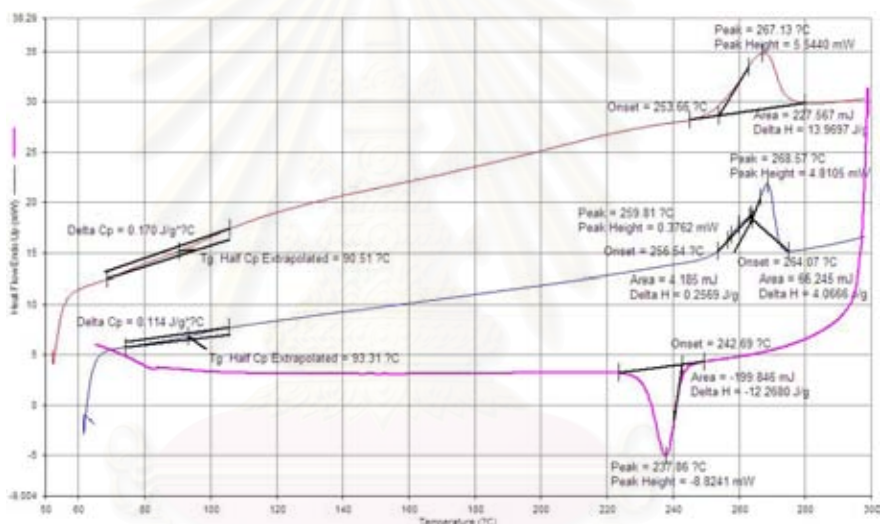


Figure A.65 DSC curve of sPS2 / Poly(α -methylstyrene) blends at composition 80/20 wt%

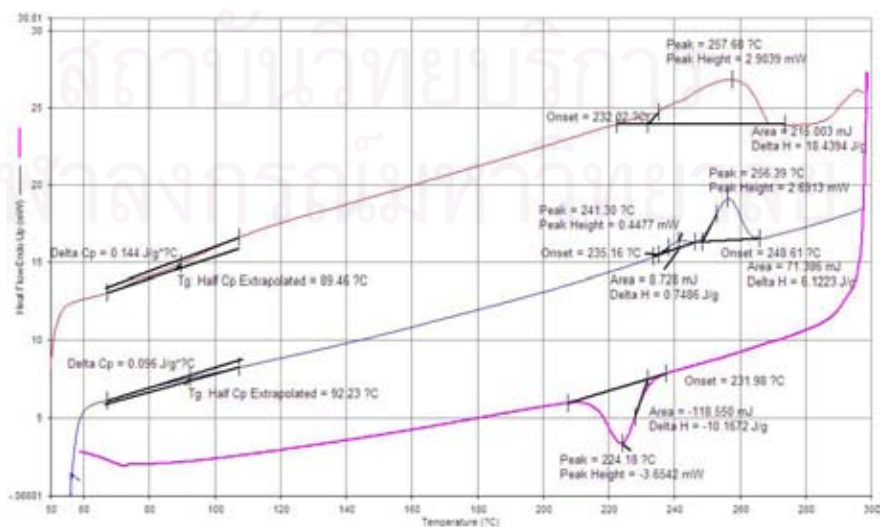


Figure A.66 DSC curve of sPS3 / Poly(α -methylstyrene) blends at composition 80/20 wt%

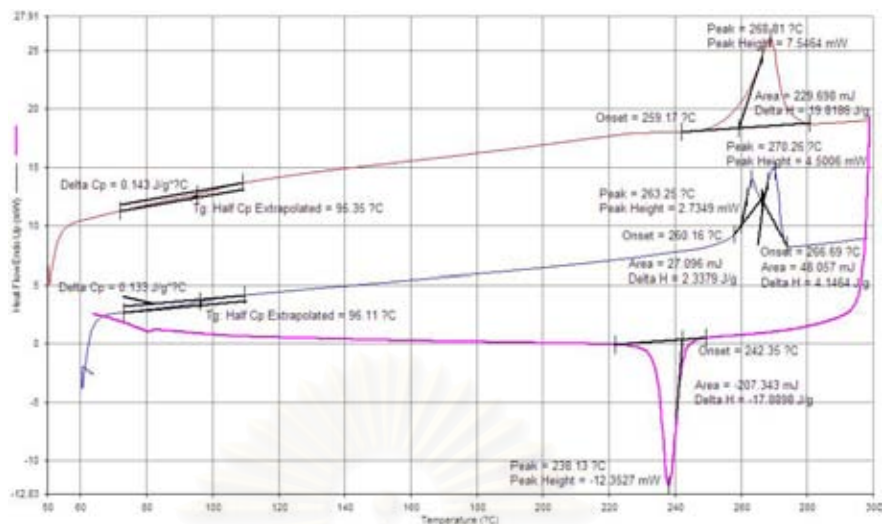


Figure A.67 DSC curve of sPS1 / Poly(α -methylstyrene) blends at composition 90/10 wt%

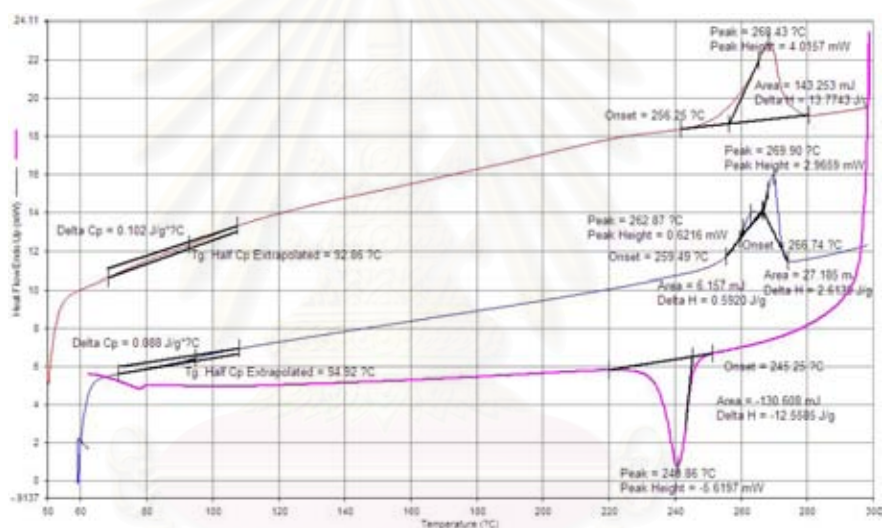


Figure A.68 DSC curve of sPS2 / Poly(α -methylstyrene) blends at composition 90/10 wt%

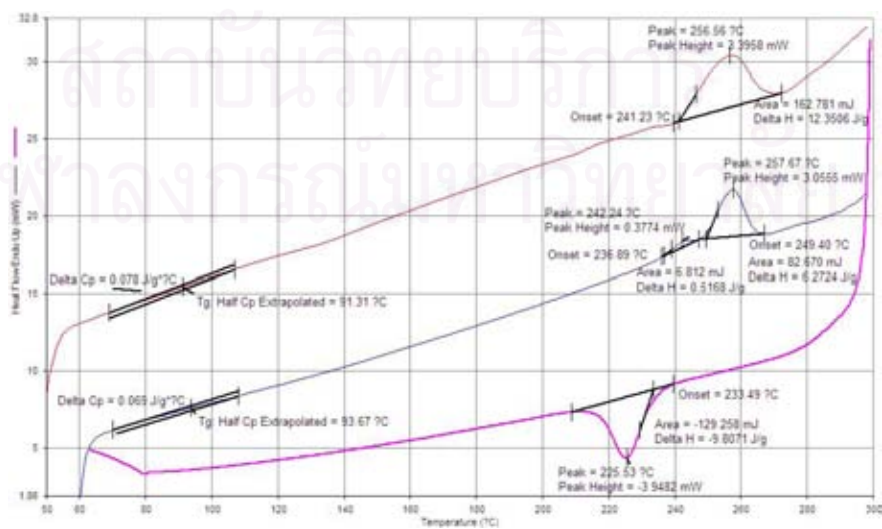


Figure A.69 DSC curve of sPS3 / Poly(α -methylstyrene) blends at composition 90/10 wt%

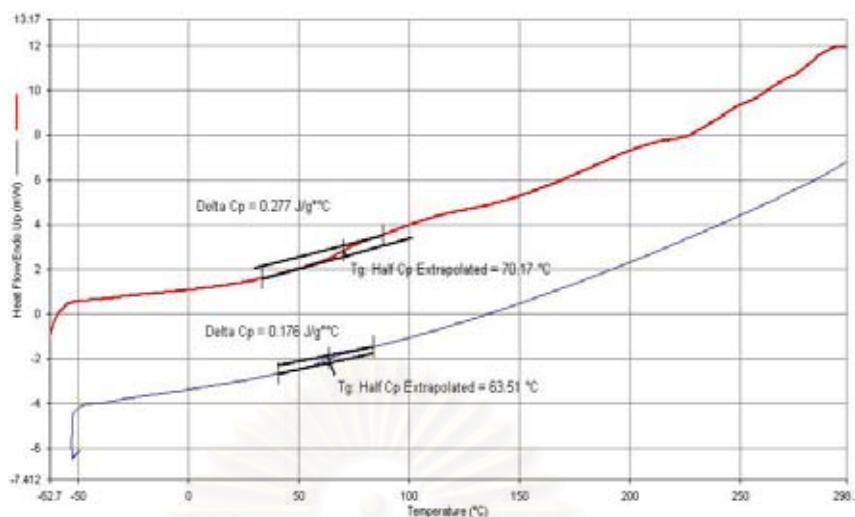


Figure A.70 DSC curve of sPS1 / Polyisoprene blends at composition 50/50 wt%

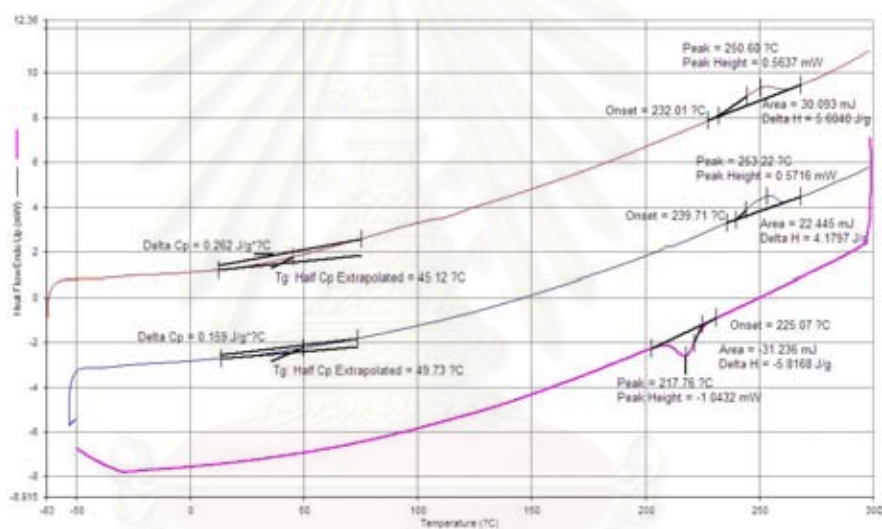


Figure A.71 DSC curve of sPS2 / Polyisoprene blends at composition 50/50 wt%

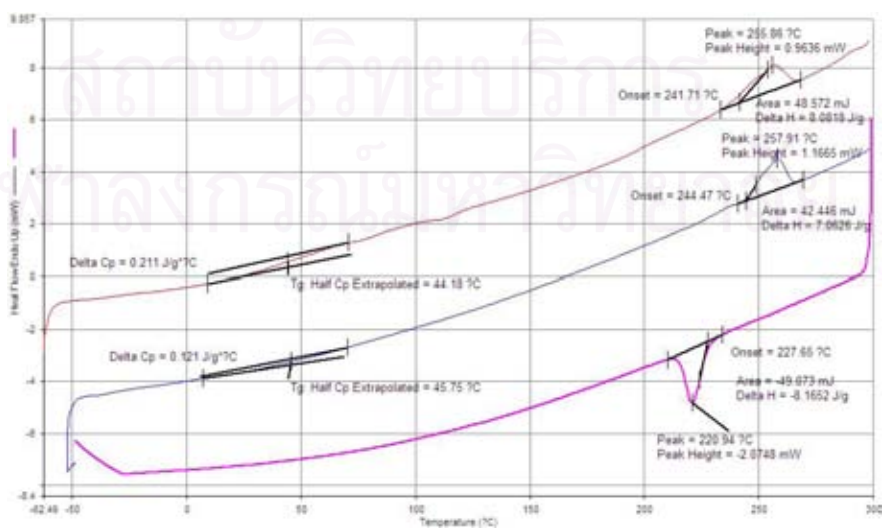


Figure A.72 DSC curve of sPS3 / Polyisoprene blends at composition 50/50 wt%

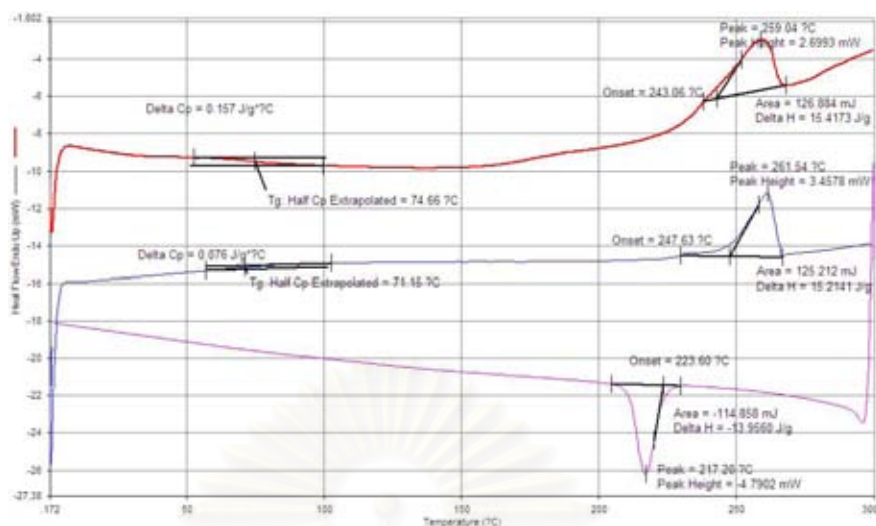


Figure A.73 DSC curve of sPS1 / Polyisoprene blends at composition 60/40 wt%

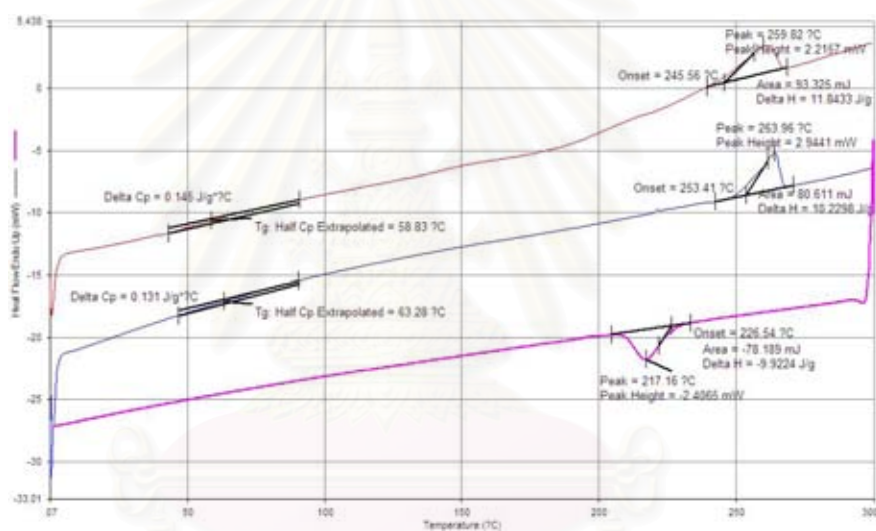


Figure A.74 DSC curve of sPS2 / Polyisoprene blends at composition 60/40 wt%

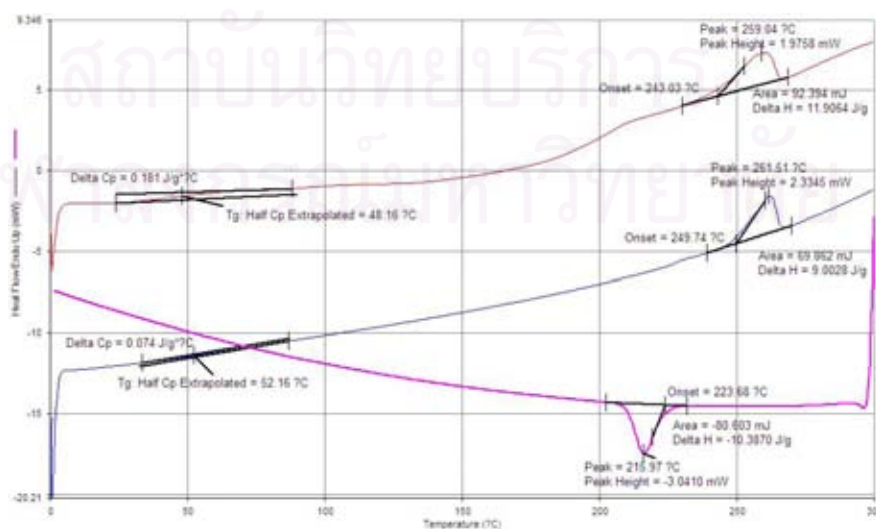


Figure A.75 DSC curve of sPS3 / Polyisoprene blends at composition 60/40 wt%

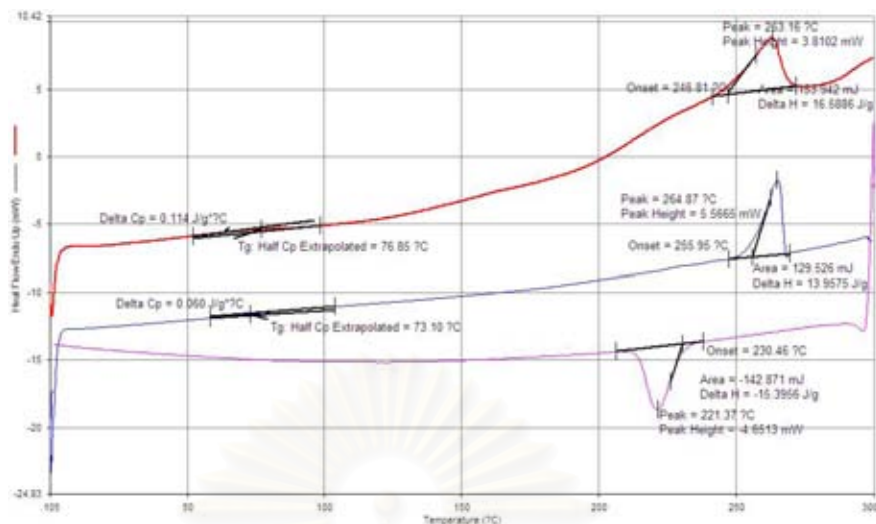


Figure A.76 DSC curve of sPS1 / Polyisoprene blends at composition 70/30 wt%

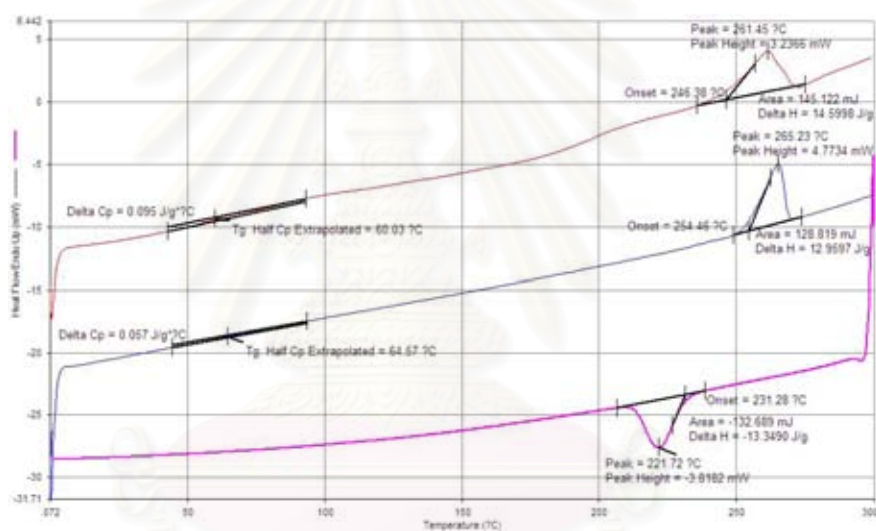


Figure A.77 DSC curve of sPS2 / Polyisoprene blends at composition 70/30 wt%

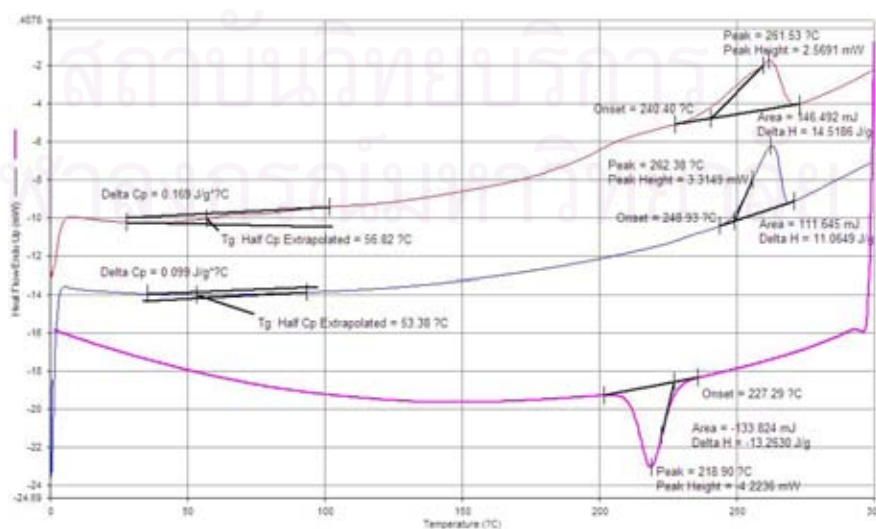


Figure A.78 DSC curve of sPS3 / Polyisoprene blends at composition 70/30 wt%

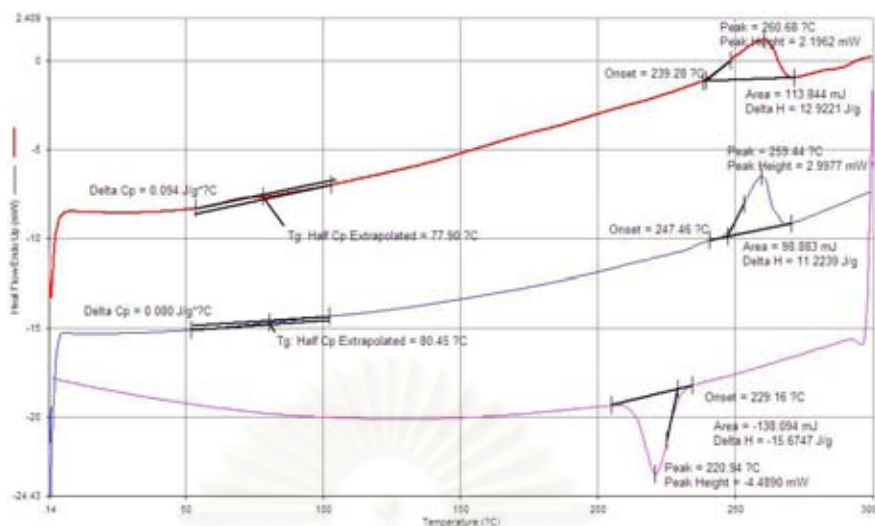


Figure A.79 DSC curve of sPS1 / Polyisoprene blends at composition 80/20 wt%

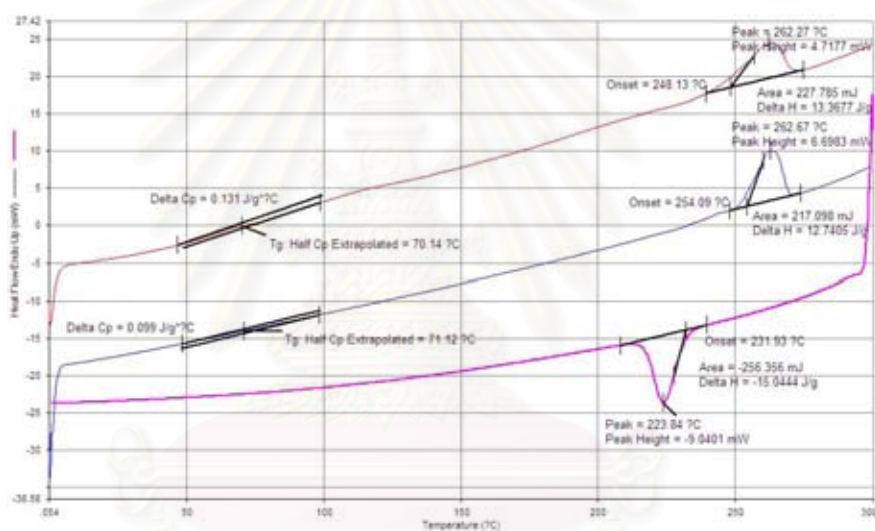


Figure A.80 DSC curve of sPS2 / Polyisoprene blends at composition 80/20 wt%

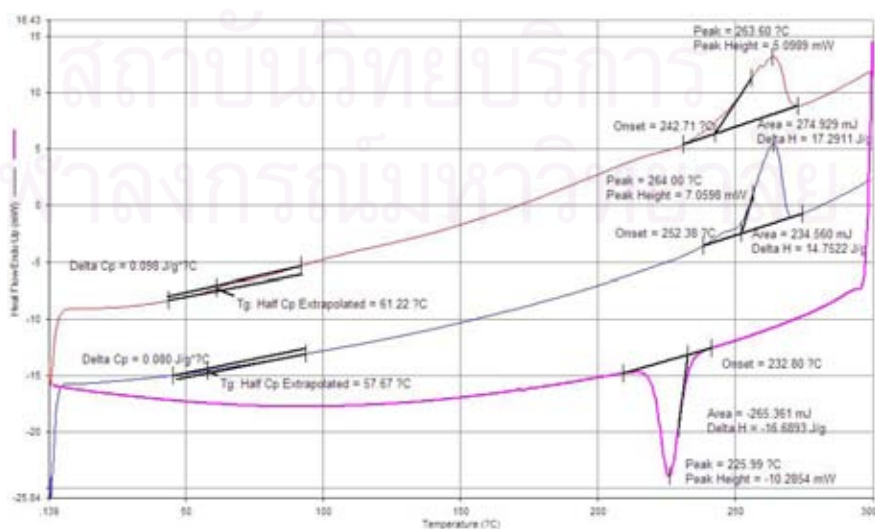


Figure A.81 DSC curve of sPS3 / Polyisoprene blends at composition 80/20 wt%

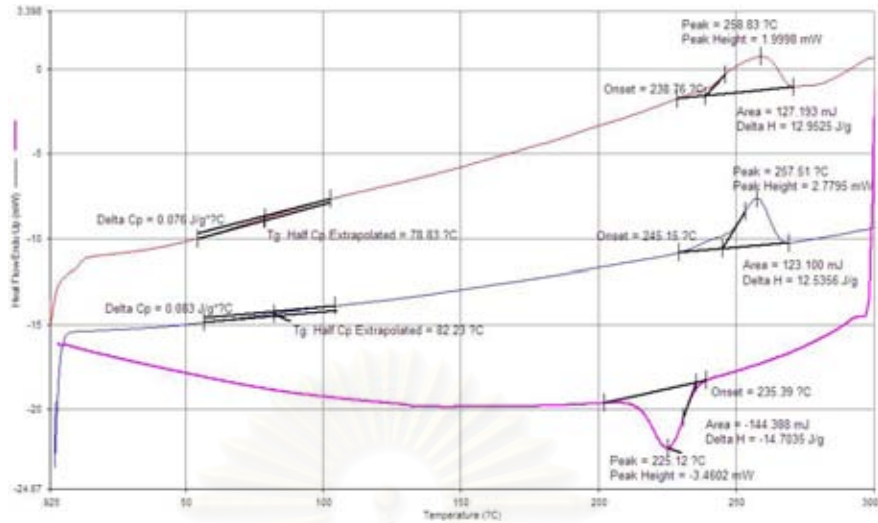


Figure A.82 DSC curve of sPS1 / Polyisoprene blends at composition 90/10 wt%

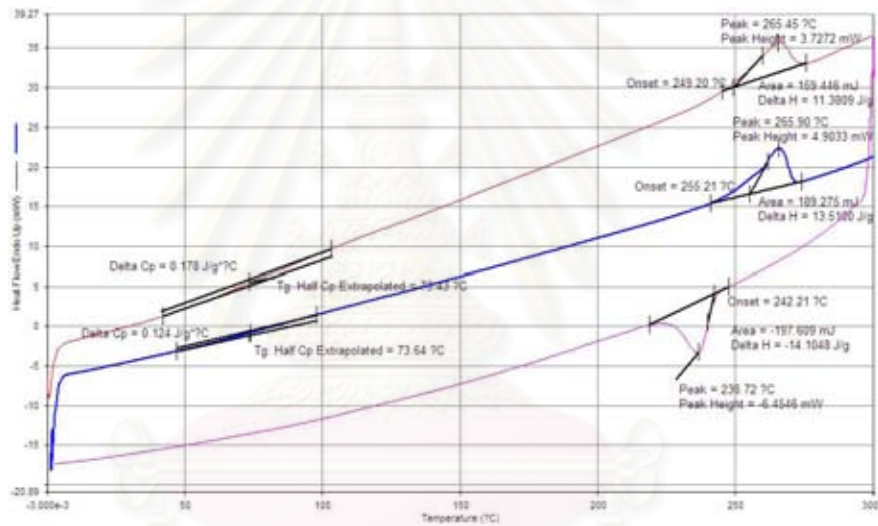


Figure A.83 DSC curve of sPS2 / Polyisoprene blends at composition 90/10 wt%

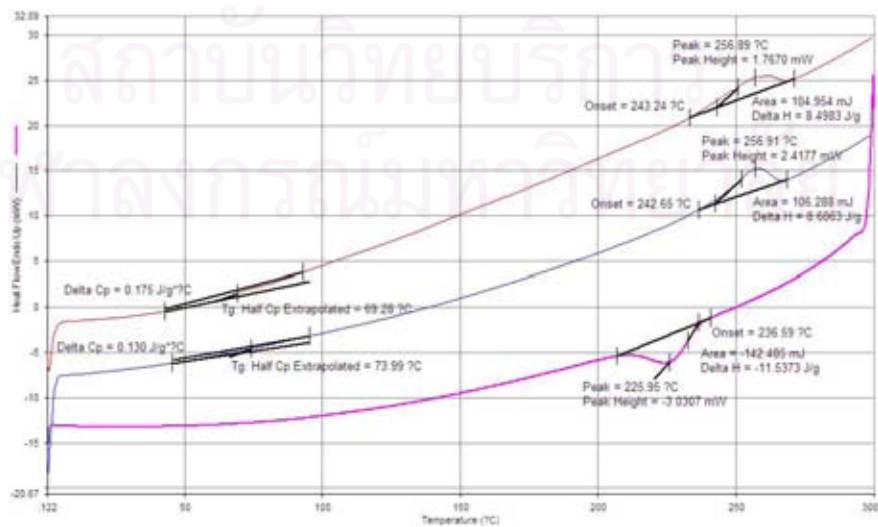


Figure A.84 DSC curve of sPS3 / Polyisoprene blends at composition 90/10 wt%

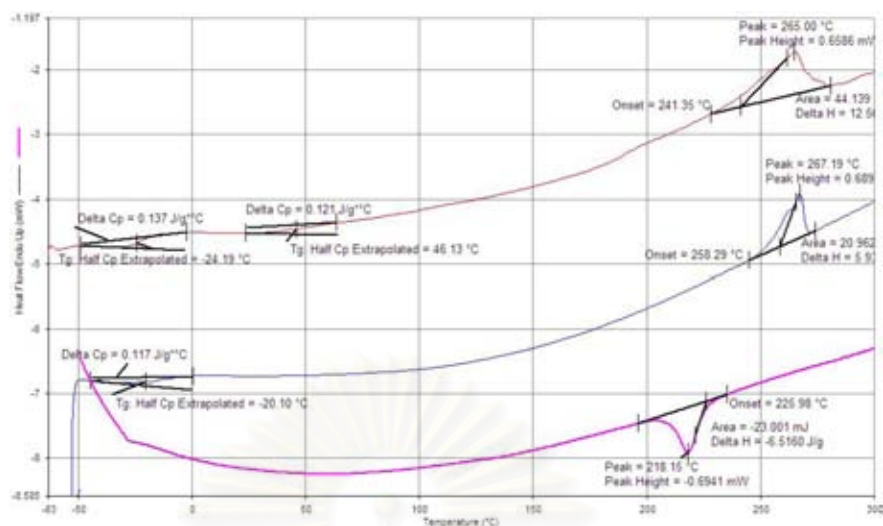


Figure A.85 DSC curve of sPS1 / PVME blends at composition 50/50 wt%

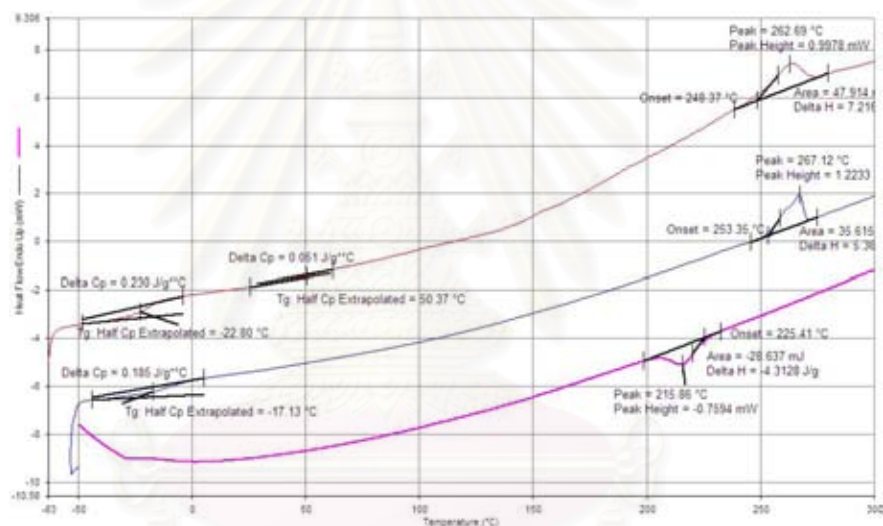


Figure A.86 DSC curve of sPS2 / PVME blends at composition 50/50 wt%

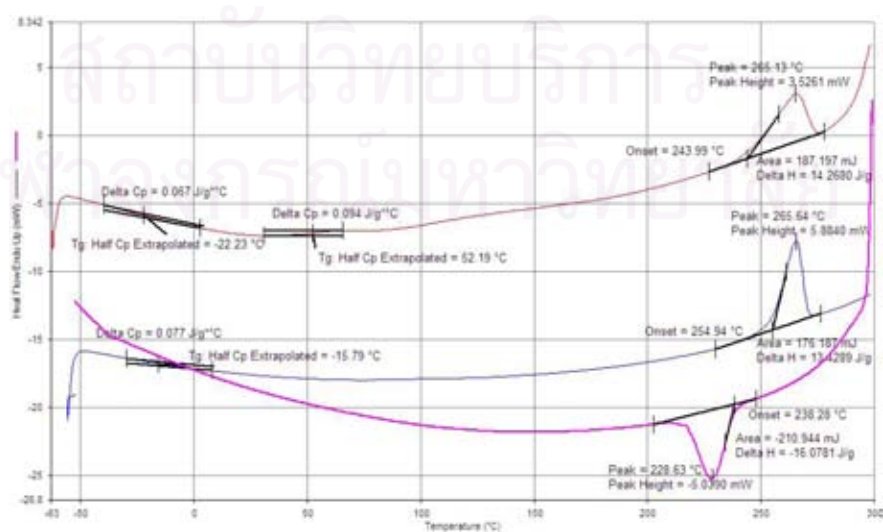


Figure A.87 DSC curve of sPS3 / PVME blends at composition 50/50 wt%

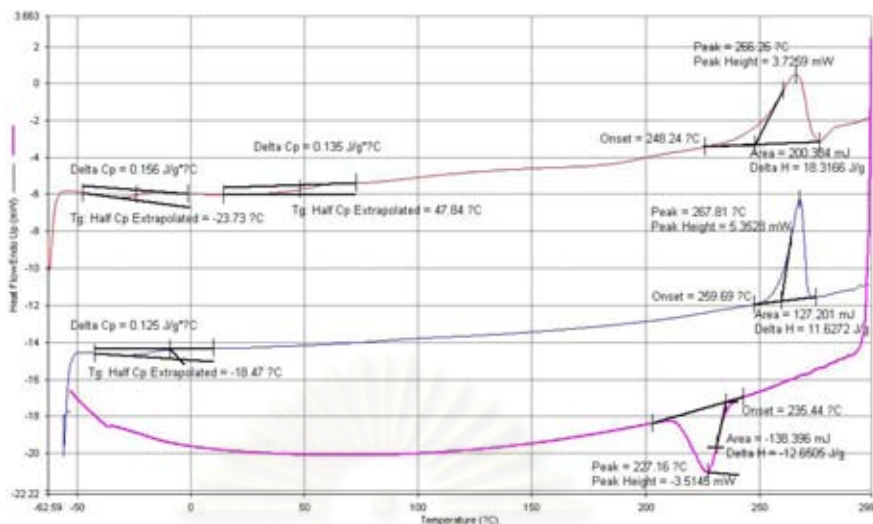


Figure A.88 DSC curve of sPS1 / PVME blends at composition 60/40 wt%

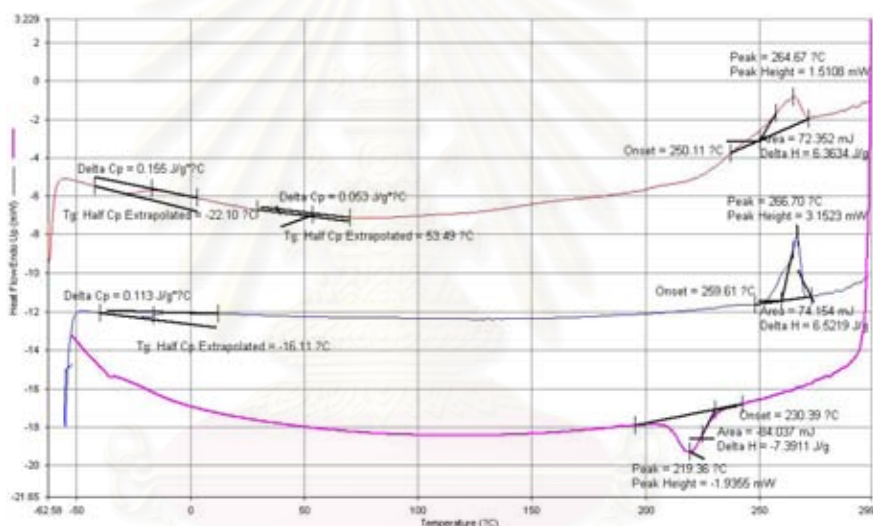


Figure A.89 DSC curve of sPS2 / PVME blends at composition 60/40 wt%

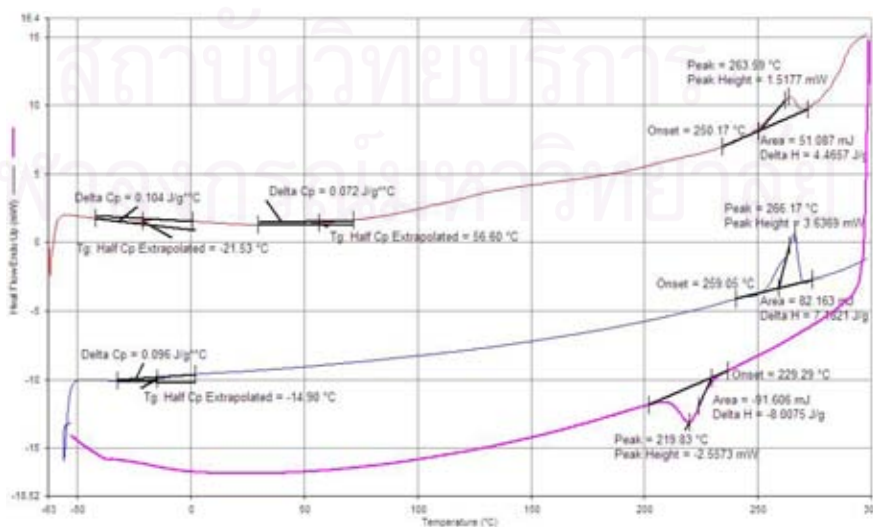


Figure A.90 DSC curve of sPS3 / PVME blends at composition 60/40 wt%

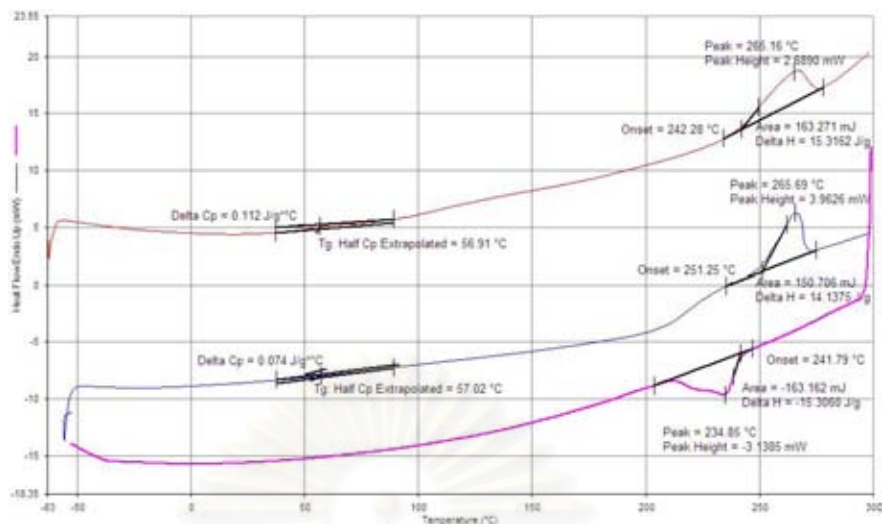


Figure A.91 DSC curve of sPS1 / Polyisoprene blends at composition 70/30 wt%

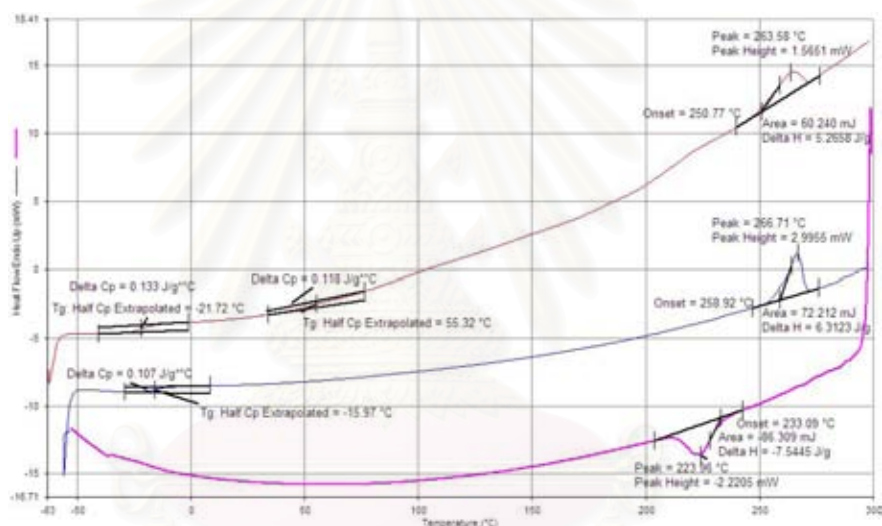


Figure A.92 DSC curve of sPS2 / PVME blends at composition 70/30 wt%

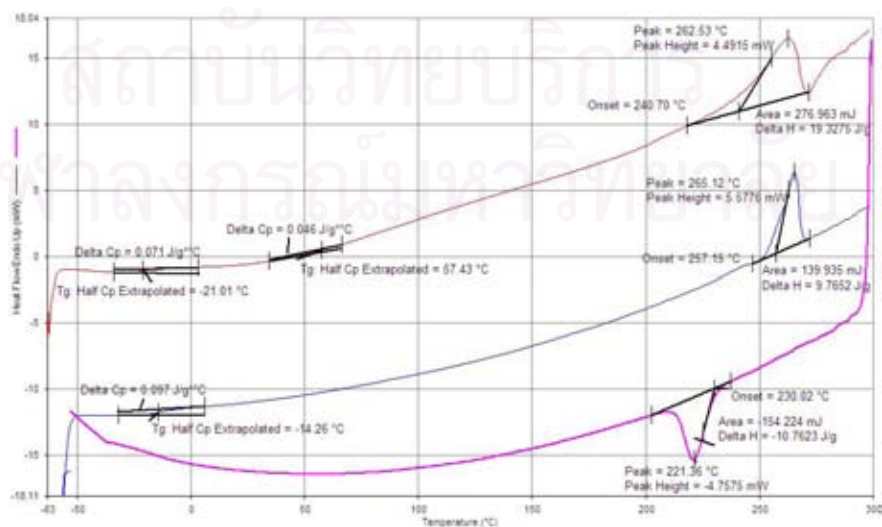


Figure A.93 DSC curve of sPS3 / PVME blends at composition 70/30 wt%

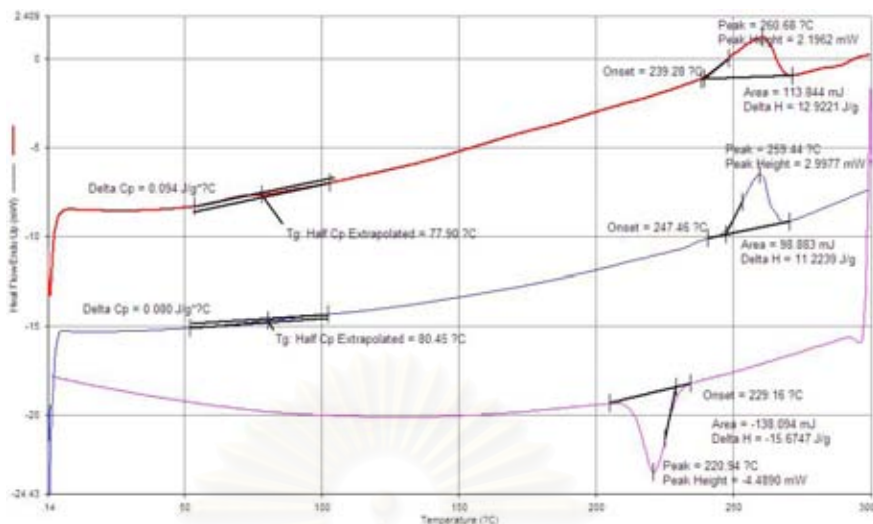


Figure A.94 DSC curve of sPS1 / PVME blends at composition 80/20 wt%

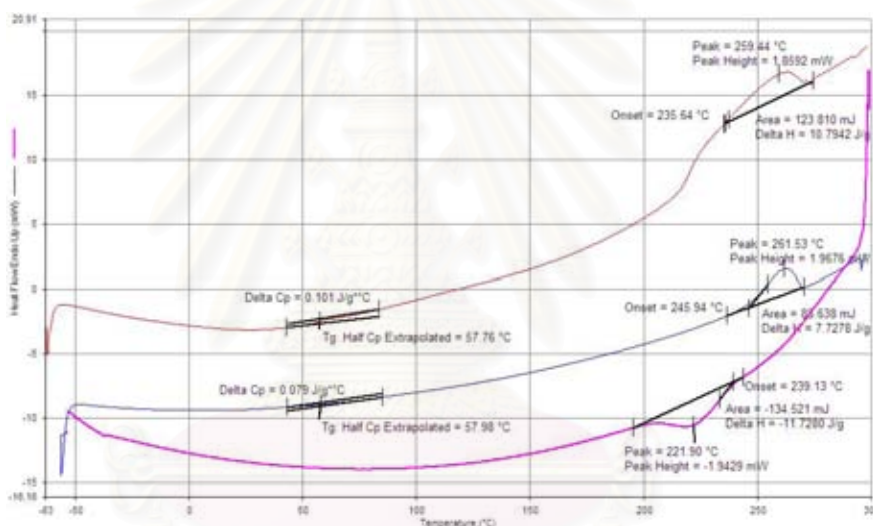


Figure A.95 DSC curve of sPS2 / PVME blends at composition 80/20 wt%

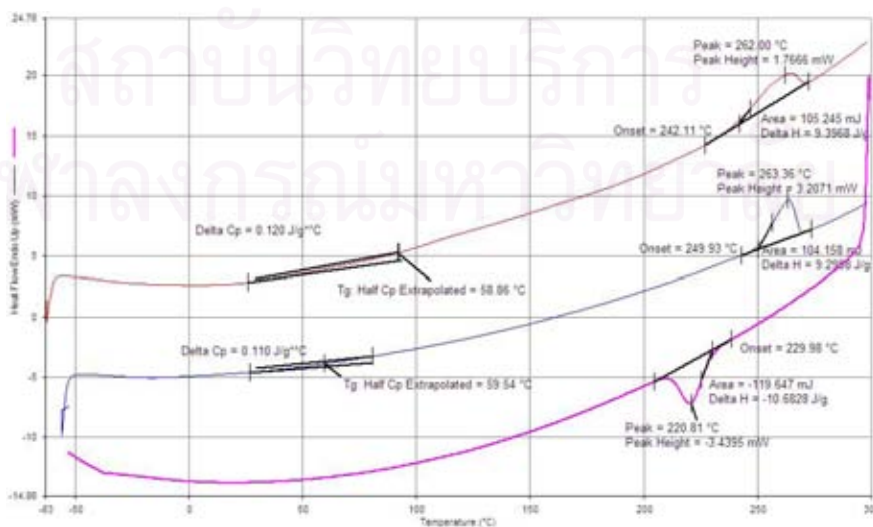


Figure A.96 DSC curve of sPS3 / Polyisoprene blends at composition 80/20 wt%

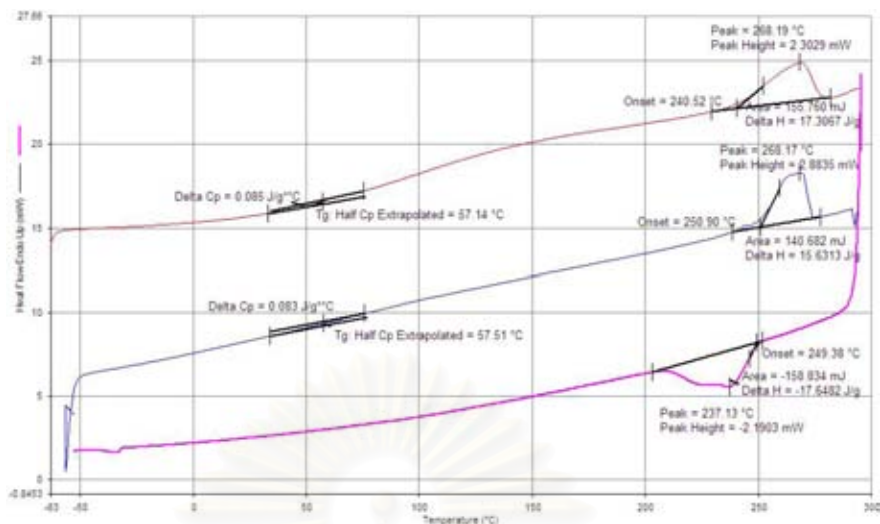


Figure A.97 DSC curve of sPS1 / PVME blends at composition 90/10 wt%

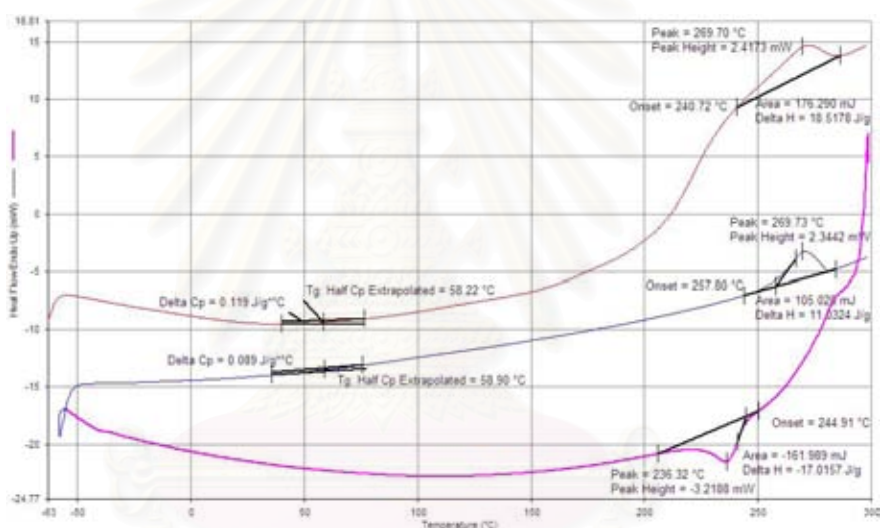


Figure A.98 DSC curve of sPS2 / PVME blends at composition 90/10 wt%

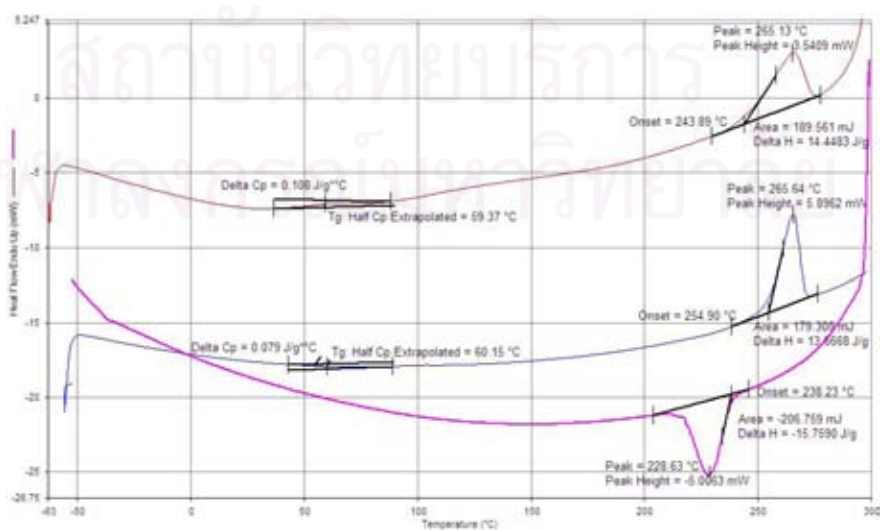


Figure A.99 DSC curve of sPS3 / PVME blends at composition 90/10 wt%

Appendix B: The Data of GPC Characterization

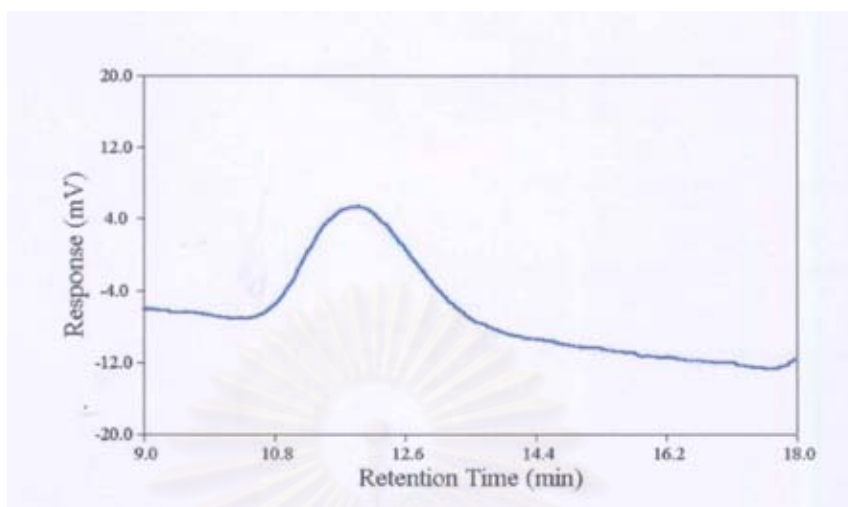


Figure B.1 The chromatogram of sPS1

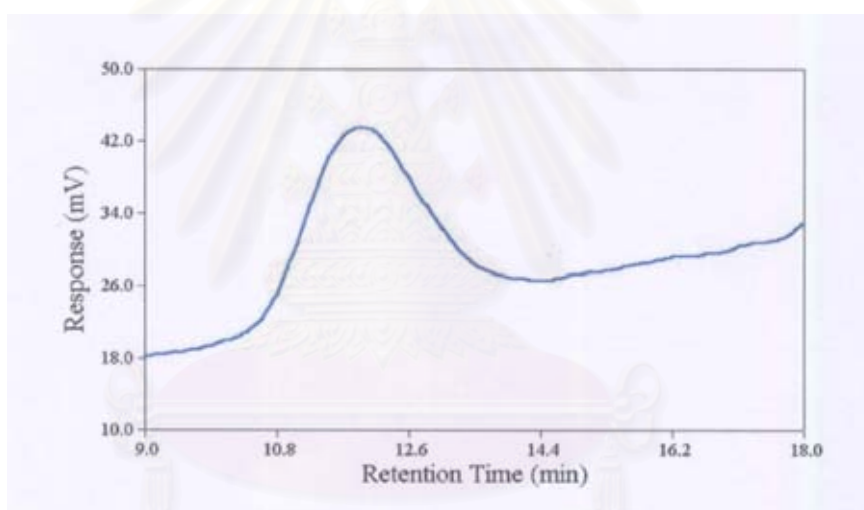


Figure B.2 The chromatogram of sPS2

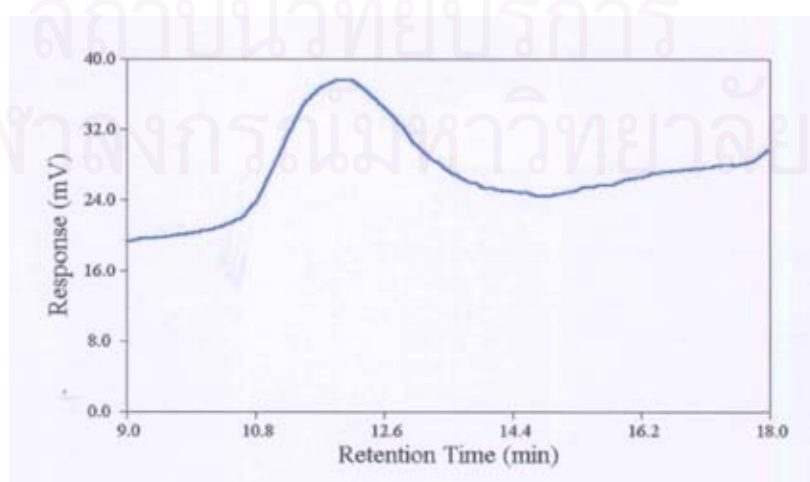


Figure B.3 The chromatogram of sPS3

VITA

Miss Ampaipun Sivavichchakij was born in Phuket, Thailand on May 31, 1981. She received the Bachelor's Degree of Engineering in Chemical Engineering from Department of Chemical Engineering, Faculty of Engineering, Kasetsart University in 2002. She entered the Master of Engineering in Chemical Engineering Program at Chulalongkorn University in 2003.



สถาบันวิทยบริการ
จุฬาลงกรณ์มหาวิทยาลัย